University of Nevada, Reno

Characteristics of extreme precipitation in southern California and applications to post-fire debris flows, shallow landslides, and water resources

A dissertation submitted in partial fulfillment of the requirements for the degree of Doctor of Philosophy in Atmospheric Science

by

Nina S. Oakley

Dr. Timothy J. Brown/Dissertation Advisor

May, 2018

THE GRADUATE SCHOOL

We recommend that the dissertation
prepared under our supervision by

NINA S. OAKLEY

Entitled

Characteristics Of Extreme Precipitation In Southern California And Applications To Post-Fire Debris Flows, Shallow Landslides, And Water Resources

be accepted in partial fulfillment of the
requirements for the degree of

DOCTOR OF PHILOSOPHY

Timothy J. Brown, Ph.D., Advisor

Eric Wilcox, Ph.D., Committee Member

Craig Smith, Ph.D., Committee Member

F. Martin Ralph, Ph.D., Committee Member

Tom Bullard, Ph.D., Graduate School Representative

David W. Zeh, Ph. D., Dean, Graduate School
May, 2018

Abstract

Shallow landslides and post-fire debris flows in southern California can result in loss of life and millions of dollars in damage to property and infrastructure. Persistent drought conditions reduce southern California's local water resources and have severe socioeconomic impacts. Shallow landslides, post-fire debris flows, and water resources operate on distinct timescales, but in this region share the common theme of extreme precipitation as a driver. I use in-situ observations and atmospheric reanalysis datasets to address the question: What are the characteristics of extreme precipitation associated with mass movements and impacts to water resources in southern California? I explore the spatial and temporal variability of precipitation extremes as well as characterize atmospheric conditions associated with these events.

I find that approximately 70% of post-fire debris flow events assessed in the Transverse Ranges of Southern California are associated with atmospheric rivers. Narrow cold frontal rain bands (and other squall lines) are also commonly associated with post-fire debris flow events. I examine 147 hourly precipitation gauges throughout California and find precipitation intensities that have historically triggered shallow landslides (OTPE; over threshold precipitation events) are most frequently observed in south-facing terrain in the Coast Ranges and Transverse Ranges, as well as in the northern Sierra Nevada. Depending on location, 60-90% of OTPE are associated with atmospheric rivers and multiple OTPE may occur within a

storm event. Last, I show that the difference between a wet and dry year in the Santa Ynez River Basin is typically two to three >90th percentile precipitation events. While there are often more >90th percentile events in El Niño years, there is considerable variability in the record analyzed. Synoptic to mesoscale conditions producing precipitation extremes are also described in this work. These results provide quantitative documentation of previously qualitative observations such that they can serve as a building block for future research, e.g., how these processes might be influenced by a changing climate. Additionally, my results improve situational awareness of the hazards addressed for weather forecasters, emergency managers, and water resource managers, as well as inform natural hazards-related communication and outreach efforts.

Dedication

This dissertation is dedicated to the memory of Dr. Kelly Redmond. Thank you for introducing me to the world of applied climatology and sharing your knowledge.

Acknowledgements

This work was supported by the California Department of Water Resources, California Natural Resources Agency contract 4600010378 and, in part, by the National Oceanic and Atmospheric Administration's Climate Program Office through grant NA11OAR4310150 with the California Nevada Applications Program. This work was also supported by a fellowship from Nevada NASA Space Grant #NNX10AN23H.

Thank you to my dissertation committee, Dr. Tim Brown, Dr. Craig Smith, Dr. Eric Wilcox, Dr. Tom Bullard, and Dr. Marty Ralph for your time and support.

Dr. Chris Funk at UCSB inspired me to pursue further education in weather and climate during my undergraduate studies. Excellent teaching by Chris Dyer at Cabrillo College provided me with mathematics skills that were essential in my MS and Ph.D. courses and research.

I would like to acknowledge my co-authors on the manuscripts that were produced as part of this dissertation: Jeremy Lancaster, Dr. Marty Ralph, Dr. Michael Kaplan, Dr. Forest Cannon, Dr. Benjamin Hatchett, Dr. Jonathan Stock, Stefani Lukashov, Shawn Roj, John Dumas, and Eric Boldt. It has been a pleasure to learn from all of you. I would also like to thank to the National Weather Service Oxnard office, Dennis Staley at USGS, Shawn Johnson at Santa Barbara County Public Works

Department, Ryan Drake at Goleta Water District, Dr. Hugo Loaiciga at UCSB, and Dr. Scotty Strachan at UNR for providing data, information, and useful conversations in support of my research.

I appreciate the support of everyone in the Western Regional Climate Center, California-Nevada Applications Program during my studies. I would also like to thank everyone in the Center for Western Water Extremes at Scripps Institution of Oceanography for providing a friendly and stimulating environment during my visits to San Diego. Thank you to Becky Sox for providing accommodations and motivation on numerous visits to San Diego. I could not have completed this challenging endeavor without the support of my husband, Dr. Benjamin Hatchett, friends, and family.

Table of Contents

List of Tables

List of Figures

Introduction

California experiences extreme precipitation events on par with the hurricanes and thunderstorms occurring in other parts of the country (Ralph and Dettinger 2012). These precipitation extremes can result in damaging floods, landslides, and debris flows (e.g. Ralph et al. 2006; Cannon et al. 2010; Dettinger et al. 2011; Stock and Bellugi 2011; Santi et al. 2011; Young et al. 2017). Precipitation is also highly variable from year to year, especially in southern California (Dettinger 2016). This makes the area prone to impactful drought episodes (Latousek 1995; Loáiciga 2001; Dettinger et al. 2011; US Drought Monitor 2018), creating challenges for water resource management.

The threats of debris flows, landslides, and drought span multiple timescales. For post-fire debris flows, the hourly to sub-hourly precipitation interval is most important (e.g., Staley et al. 2016). For shallow landslides, antecedent rainfall on a seasonal scale is necessary to increase pore pressures (e.g., Godt et al. 2008), plus the occurrence of a triggering high intensity event, which is typically described at the one to multiple hour timescales (Guzzetti et al. 2008). Water resource issues in southern California typically fall in the annual to multi-annual time scale. A single year of drought may cause increased demand and instatement of water restrictions, but multi-year droughts result in significant reductions in reservoir storage. In the chapters of this manuscript, we discuss each of these three hazards in detail and examine their driving atmospheric features.

A common thread across these types of events is the role of atmospheric rivers (ARs), which have been widely recognized as the driver of many hydrologically critical storms in California (e.g., Ralph et al. 2006; Dettinger et al. 2011). These narrow corridors of high water vapor transport occur in the warm sector of a mid-latitude cyclone (AMS 2017) and are frequently associated with flood events in California (e.g., Ralph et al. 2006; Young et al. 2017) and play an important role in generating water resources for the state (Dettinger et al. 2011). Closed low-pressure systems have also been shown to have an impact on California precipitation (e.g., Oakley and Redmond 2014; Abatzoglou 2016), though their ties to floods and other hazards have not previously been explored in as much detail. Mesoscale features such as the presence of a low-level jet associated with ARs (Ralph et al. 2005), orographic processes (Lin et al. 2001) and convection along a cold front (e.g. Hobbs and Persson 1982; Jorgensen 2003) are also critical to understanding the atmospheric conditions driving these hazards.

In three subsequent chapters, we explore post-fire debris flows, shallow landslides, and inter-annual precipitation variability at their respective temporal scales. The spatial focus ranges from a single river basin to a geomorphic province to California statewide. The goal of each chapter is to understand how the event in question varies over the historic record examined, as well as the atmospheric conditions associated with each event. Many of the results presented quantify observations that are commonly discussed in the meteorology, geology, or water resource communities but had not previously appeared in peer-reviewed literature.

By documenting and publishing these observations, we provide a basis for future research. Each study produces results that support operational decision-making in meteorology, geology, or water resource management.

As this research spans three connected but distinct topics, each chapter features an introduction pertinent to the literature reviewed for its topic. A brief summary of the background and motivations for each chapter is provided here.

Chapter 1: Atmospheric conditions associated with post-fire debris flows in the Transverse Ranges

Wildfire has profound effects on storm runoff and sedimentation in the Transverse Ranges. For several years following a fire, runoff rates can more than double due to alteration or removal of the vegetation and litter cover, soil-sealing, translocation of minerals and ash, fire-induced degradation of soil and rock, and the development of water repellant soil conditions (DeBano 1981; Parise and Cannon 2012). Post-fire debris flows tend to occur in steep watershed areas burned at moderate to high severity, with the largest events often triggered by the first significant rainstorm (Cannon et al. 2008; Parise and Cannon 2012). Since the early 1900s urbanization on alluvial fans and floodplains within and adjacent to the Transverse Ranges has resulted in loss of life and property associated with post-fire debris flowss. On New Year's Day 1934, post-fire debris flows issued on to alluvial fans from the Pickens Fire burn area in the San Gabriel Mountains, resulting in 39 fatalities and 597 damaged homes in La Crescenta, La Cañada, and Montrose

(Chawner 1935). On Christmas Day 2003, post-fire debris flows from the Grand Prix and Old burn areas killed 16 people at two locations in the western San Bernardino Mountains (Cannon et al. 2010).

Debris flows are a type of landslide that occurs in response short duration, high intensity rainfall events (e.g. Cannon et al. 2008; Staley et al. 2016). Due to fire induced changes in the watershed, debris flows often result from runoff-dominated processes- the erosion and entrainment of rock and soil from hillslopes and channels, and the progressive bulking of runoff with sediment (Santi et al. 2008). This fire-related process is different from shallow landslides initiated by infiltration-dominated processes, which are less common in a post-fire setting (Cannon and Gartner 2005).

Previous studies on post-fire debris flows typically cite "intense convection" as the cause of rainfall intensities sufficient to trigger debris flows, but do not provide the context for the development of intense convection (e.g. Cannon et al. 2008, 2010; Sidman et al. 2016). In this chapter, we describe both qualitatively and quantitatively the atmospheric conditions associated with 19 cool season storm events producing post-fire debris flows in the Transverse Ranges during the period 1980-2014. These conditions are investigated using both observations and reanalysis data at the synoptic to meso-alpha scales.

The results of this work support operations and further research related to post-fire debris flows in several ways. First, we develop a catalog of historic debris flow events that can be used by National Weather Service personnel to

communicate to emergency managers how a forecast event may compare to one in recent history. Second, for the geology and natural hazards community, we have produced descriptions of events that give significantly more information than the existing "intense convection" concept. This can allow them to decide which types of events to focus instrumentation on and when to check field measurements, as well as improve modeling efforts by using more realistic storm conditions. Lastly, We observed that the features driving post-fire debris flows in the Transverse Ranges are often at the mesoscale, which suggests that future research should focus on this spatial and temporal scale.

Chapter 2: A 22-year climatology of cool season hourly precipitation thresholds conducive to shallow landslides in California

Landslides are common hazards in the Transverse, North Coast, and South Coast Ranges of California (Radbruch-Hall et al. 1982, Wills et al. 2017). In a landslide, cohesive blocks of material move on a well-defined surface of sliding, and no internal shearing takes place concurrently within the sliding block. Landslides can occur when the sum of shear stresses (gravity, addition of mass through precipitation, weathering, joints within rocks) exceed the sum of shear strength of the slope materials (Ritter et al. 1995). The most recent occurrence of widespread landsliding in California was during the intense storms of January 1969 (Stock and Bellugi 2011), though other tragic events such as the La Conchita slide that occurred on 10 January 2005 and claimed 10 lives (Jibson 2006) have impacted the region

since. In the wet winter for Northern California of 2016-2017, no deaths were associated with shallow landslides, but homes were damaged in the Oakland area (Harris 2017) and roads were blocked or damaged in various parts of northern California, impacting travel (e.g., Herhold 2017). The USGS and California Geological Survey have used measurements of rock strength, soil type, slope, and landslide occurrence to develop landslide susceptibility maps for California (Radbruch and Crowther 1973; Wills et al. 2011).

In addition to favorable geologic conditions, susceptibility to landslides is based on precipitation intensity-duration (ID) thresholds. These types of thresholds were first established by Caine (1980) who developed a power law of the form $I=\alpha D^{\beta}$ where I is rainfall intensity (mm h^{-1}), D is duration in hours, and α and β are empirically derived quantities. While ID thresholds are useful in hazard awareness and other applications, they have limitations in predicting shallow landslide occurrence and abundance in that they do not account for exact location, antecedent moisture conditions, soil property, and other factors (Stock and Bellugi 2011).

Antecedent conditions play a major role in the occurrence of shallow landslides in California. As water pressure builds up in the soil, it reduces the friction stress between the soil particles. When friction is reduced sufficiently, the gravitational force can overcome the frictional forces and failure occurs. In the Transverse Range area, it is estimated that 254-381 mm of precipitation is needed in a season before shallow landslides will occur (Campbell 1975; Stock and Bellugi 2011). In northern California, the values are slightly higher, estimated at 300-500

mm (Wieczorek 1987; *J. Stock, 2016, personal communication*). Once these accumulations have been achieved in the season, rainfall intensities help determine when failure will occur by changing groundwater pressure heads (Iverson 2000).

While ID and antecedent precipitation thresholds have been developed for various locations in California, there is no existing work that shows where and when in the state these thresholds are most frequently exceeded. Additionally, there is no existing evaluation of any of the meteorological conditions tied to landslide triggering events beyond a case study scale. In this analysis, we evaluate the spatial and temporal frequency of six thresholds developed in studies across California (5 mm h^{-1}, 10 mm h^{-1}, 15 mm h^{-1}, 20 mm h^{-1}, 7.5 mm h^{-1} for 3h, and 5 mm h^{-1} for 6h) for the period of 1995-2016. A minimum estimate of antecedent seasonal precipitation of 250 mm is also evaluated. We use Remote Automated Weather Stations (RAWS) as they are located in complex terrain.

This work offers many benefits to research and monitoring of landslide activity in California. The precipitation intensity data can be used as an input to shallow landslide loss estimation modeling studies (e.g., Papathoma-Köhle et al. 2015). Permanent soil moisture sensors are limited in California, yet are a necessary tool for forecasting landslide activity (e.g. Baum and Godt 2010). Our results elucidate where triggering rainfall is more likely to occur and, as a supplement to geological information, can inform where siting of new soil moisture sensors provides the greatest benefit. For historic shallow landslide identification activity observed in areal photos or lidar where a trigger time is unknown, the over

threshold events captured in this study can assist in estimation of event timing. The precipitation intensity data developed here can also facilitate the development of a null shallow landslide map by indicating where high intensity precipitation during the cool season is unlikely in California.

Chapter 3: Origins and variability of extreme precipitation in the Santa Ynez River Basin of Southern California.

The Santa Ynez River Basin is a semi-arid region characterized by high precipitation variability and has a long history of impactful multi-year droughts (Upson and Thomas 1951; Latousek 1995; Loáiciga 2001). It serves as a great example to explore and quantify precipitation variability in a southern California watershed.

It is commonly noted that the difference between a wet and a dry year in southern California is “just a couple of storms”, (e.g. Burns 2017) but that statement has not been quantified in existing literature. Dettinger (2016) shows that the top 5% of wet days account for most of the inter-annual variability in southern California, but these results do not give an indication of how many precipitation events are required to produce those wet days. Additionally, there is little published information on the synoptic conditions associated with extreme rainfall events beyond a few case studies or unpublished analyses (e.g., Haynes 2001).

Following a multi-year drought, in early January 2017 Cachuma storage stood at 8% of capacity, nearly shutting off agricultural deliveries and prompting

water agencies to utilize other resources in their portfolios (such as purchasing water from other agencies). Two atmospheric river storms in late January and mid-February 2017 raised the lake level to nearly 50% of capacity. Without these two large storms, those who depend on Cachuma for water resources would have been facing dire circumstances. This event led us to explore the difference in storm events between what we defined as wet, dry, and normal years.

We used daily rainfall data from NWS Cooperative Observer stations in the region as well as stations operated by the Santa Barbara County Public Works Department. Data were divided into "storm events" through various criteria, and we established that 90th percentile precipitation events had a strong relationship with inter-annual precipitation variability. A median-quartile approach was used to define wet, normal and dry years and the frequency of storms associated with each category was determined. We also explored, using NASA's Modern-Era Retrospective Analysis (MERRA), the synoptic conditions associated with these extreme events.

The results of this analysis provide quantitative knowledge that can be used by local agencies to communicate regional precipitation variability and impacts to their stakeholders. These materials provide a broad understanding of regional drought mechanisms and risk, give insight to the challenges of seasonal prediction, and augment water managers' abilities to understand and plan for impactful events. Additionally, the novel investigation of regional precipitation variability may inspire

new insights in ecological, geological, and hydrologic studies in Santa Barbara County, and serve as a baseline for evaluating change in the future.

Chapter 1

Synoptic conditions associated with cool season post-fire debris flows in the Transverse Ranges of southern California

Nina S. Oakley, Jeremy T. Lancaster Michael L. Kaplan, F. Martin Ralph

Published as:

Oakley, N. S., Lancaster, J. T., Kaplan, M. L., & Ralph, F. M. (2017). Synoptic conditions associated with cool season post-fire debris flows in the Transverse Ranges of southern California. *Natural Hazards*, *88*(1), 327-354.

Glossary of Acronyms

PFDF: post-fire debris flow

I-D: intensity-duration

AR: atmospheric river

CL: closed low

ARCL: both AR and CL

OTH: other atmospheric feature

IWV: integrated water vapor

IVT: integrated water vapor transport

NCFR: narrow cold frontal rain band

NARR: North American Regional Reanalysis

LLJ: low-level jet

CAPE: convective available potential energy

VBG: Vandenberg, California

CW3E: Center for Western Weather and Water Extremes

Abstract

The Transverse Ranges of southern California often experience fire followed by flood. This sequence sometimes causes post-fire debris flows (PFDFs) that threaten life and property situated on the alluvial fans. The combination of steep topography, highly erodible rock and soil, and wildfire, coupled with intense rainfall, can initiate PFDFs even in cases of relatively small storm rainfall totals.

This study identifies common atmospheric conditions during which damaging PFDFs occur in the Transverse Ranges during the cool season, defined here as November-March. A compilation of 93 PFDF events during 1980-2014 triggered by 19 precipitation events is compared against previous studies of the events, reanalysis, precipitation, and radar data to estimate PFDF trigger times. Each event was analyzed to determine common atmospheric features and their range of values present at and preceding the trigger time. Results show atmospheric rivers are a dominant feature, observed in 13 of the 19 events. Other common features include low-level winds orthogonal to the Transverse Ranges and conditions favorable for orographic forcing, a strong upper level jet south of the region, and moist-neutral static stability. Several events included closed low-pressure systems or narrow cold frontal rain bands. These findings can help forecasters identify more precisely the synoptic scale atmospheric conditions required to produce PFDF-triggering rainfall and thus reduce uncertainty when issuing warnings.

1. Introduction

1.1. Post-Fire Debris Flows

The Transverse Ranges of southern California feature a combination of steep and complex terrain, combustible fuels, a prolonged dry season, and strong wind events such as Santa Anas. These factors combined produce the most intense fire climate in the United States (Figure 1.1; Wells 1981, 1987; Raphael 2003; Keeley et al. 2004). The Transverse Ranges are also prone to multi-year drought interspersed

with wet weather, a combination conducive to growth and then desiccation of the region's fire-prone chaparral vegetation.

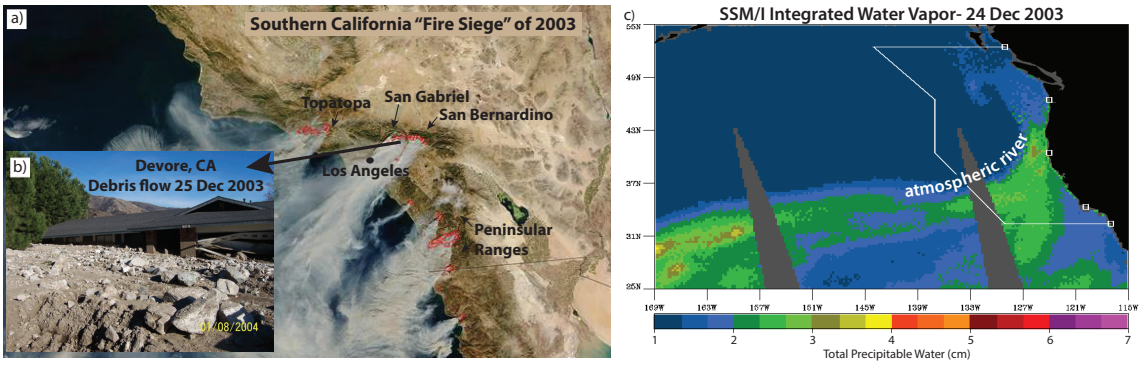

Figure 1.1: *a) Fires in the Transverse Ranges under Santa Ana wind conditions from NASA MODIS visible imagery during October 2003 (NASA Earth Observatory 2003). b) House buried by post-fire debris flow from the Old Fire burn area in December 2003 (Photo: J. Gartner, USGS). c) SSM/I imagery showing an atmospheric river impacting southern California on 24 Feb 2003, triggering the PFDF event shown in a) and b) as it moved south along the coast on the 25th*

Wildfire has profound effects on storm runoff, erosion, and sedimentation in the Transverse Ranges. For several years following a fire, runoff rates can more than double due to alteration or removal of the vegetation and litter cover, soil-sealing translocation of minerals and ash, fire-induced degradation of soil and rock, and the development of water repellant soil conditions (DeBano 1981, 2000; Neary et al. 1999; Parise and Cannon 2012). Post-fire debris flows (PFDFs), the most severe runoff response to precipitation on burned watersheds, tend to occur in steep watershed areas burned at moderate to high severity, with the largest events often

triggered by the first significant rainstorm (Cannon et al. 2008; Parise and Cannon 2012). PFDFs are a common threat to southern California communities (Eaton 1936; USGS 2005). Since the early 1900s urbanization on alluvial fans and floodplains within and adjacent to the Transverse Ranges has resulted in loss of life and property associated with PFDFs (e.g. Chawner 1935; Eaton 1936; Troxell and Peterson 1937; Shuirman and Slosson 1992; Cannon et al. 2010).

Previous work has cited "intense convection" as the main cause of rainfall intensities sufficient for PFDFs (Slosson et al. 1991; Cannon et al. 2008, 2010; Moody et al. 2013), but provides few details as to broader scale conditions present when this intense convection occurs. One recent study provides an in-depth meteorological case study of an individual PFDF event in the western Santa Monica Mountains (Sukup et al. 2016). Absent, however, is a comprehensive examination of atmospheric conditions across multiple PFDF events.

Our study presents an overview of the meso-beta (20-200 km) to synoptic (>2000 km) scale atmospheric conditions associated with PFDFs in the Transverse Ranges during 19 precipitation events between 1980-2014 (Table 1.1). This study extends earlier work by taking advantage of the recently developed understanding and documentation of atmospheric rivers, as summarized by Ralph et al. (2016), and of closed and cut-off lows, as documented by Oakley and Redmond (2014). This paper presents the first quantitative cross-disciplinary assessment of how prevalent these phenomena are to the occurrence of PFDFs in this region.

Meteorological case studies were generated for each PFDF event date, and common features observed among events serve as an "ingredient list" for conditions conducive to PFDFs in the Transverse Ranges. While many of these ingredients may already be familiar to weather forecasters, they can utilize the analysis of conditions across a broad range of events to put forecast events in context and examine variability across events. This work facilitates non-meteorologist understanding of weather forecasts presented by NWS related to PFDFs, builds on past collaborative multidisciplinary work (NOAA-USGS Debris Flow Task Force 2005; Jorgensen et al. 2011), and provides a foundation for new research directions that cross the boundaries between meteorology, geology, and hydrology.

Storm Date (LST)	Fire Name	PFDF trigger time (or range), LST	NARR time LST (UTC)	Rainfall rate (or range) mm/hr	Sediment yield (or range), m^3	# PFDF	Event type	Damage?
1980-01-09[1,2,3,4]	Daley	11:00	10:00 (18 UTC)	5-13 mm/hr	11,400	1	AR	Basin overtopped, 60 homes destroyed, 6-7 feet mud on Hampshire avenue over course of 4 events
1980-01-13[1,2,3,5]	Daley	20:00	19:00 (03 UTC 1/14)	5-13 mm/hr	45,100	1	AR	
1980-01-28[1,2,3,6]	Daley	22:00	22:00 (06 UTC)	3-13 mm/hr	33,300	1	OTH	
1980-02-16[1,2,3,7]	Daley	15:00	16:00 (00 UTC 2/17)	5-23 mm/hr	73,400	1	AR	
1980-02-16[8,9,10]	Çreek Road	10:00	10:00 (18 UTC)	8-23 mm/hr	13,400	1	AR	City recreation center on Day Road Inundated, Cars swept from street on Telegraph Road
1984-12-19[11,12]	San Dimas	16:15	16:00 (00 UTC 12/20)	12-13 mm/hr	Unknown	1	CL	Two simultaneous debris flows lasted 15 min (Uninhabited Area)
1995-01-10[8,9]	Steckel (Santa Paula)	04:00	04:00 (12 UTC)	17-32 mm/hr	45,900	1	ARCL	Presidential disaster declaration
1998-02-02[8,9,13]	Grand	06:00	04:00 (12 UTC)	9-15 mm/hr	2,200	1	AR	Presidential disaster declaration
1998-02-06[8,913]	Hopper/ Grand	10:00	10:00 (18 UTC)	14-19 mm/hr	19,000	2	AR	Presidential disaster declaration
2003-12-25[8,9]	Simi	12:00	13:00 (21 UTC)	6-14 mm/hr	4,500	1	AR	Unknown
2003-12-25 [14,15,16,17]	Grand Prix/Old	08:00-18:00	10:00 (18 UTC)	5-33 mm/hr	2,200-864,300	26	AR	16 deaths; 52 homes damaged or destroyed, $38 million in damages;

								Presidential disaster declaration
Storm Date (LST)	**Fire Name**	**PFDF trigger time (or range), LST**	**NARR time LST (UTC)**	**Rainfall rate (or range) mm/hr**	**Sediment yield (or range), m^3**	**# PFDF**	**Event type**	**Damage?**
2009-02-05[14,18]	Sayre	19:00	19:00 (03 UTC 2/6)	5-13 mm/hr	111,200-172,200	7	OTH	Several inches of mud, debris in road; 2 Cars trapped in debris flow
2009-02-13[14]	Sayre	15:00	13:00 (21 UTC)	2-6 mm/hr	1,900-47,000	3	ARCL	No data
2009-02-16[14,19]	Sayre	08:00	07:00 (15 UTC)	5-8 mm/hr	3,200	1	ARCL	Red flag mud alert issued
2009-11-12 [14,16,20]	Station	22:28	22:00 (06 UTC 11/13)	0-23 mm/hr 36 mm/hr*	300-10,800	6	OTH	Damaged houses, closed Highway 2
2009-12-12 [14,16,20]	Station	14:47-26:50	16:00 (00 UTC 12/13)	5-11 mm/hr 21mm/hr*	200-11,200	6	AR	70 cars trapped in mud/debris on Highway 2; debris flow closed streets, damaged homes in La Cañada Flintridge
2010-01-18 [14,16,20,21]	Station	09:48-12:08	10:00 (18 UTC)	6-24 mm/hr 32 mm/hr*	200-13,400	14	AR	489 Homes evacuated; Widespread flooding, debris flows along San Gabriel Mtn. Front; Presidential disaster declaration
2010-02-06 [14,16,20,21,22]	Station	03:17-07:22	04:00 (12 UTC)	6-26 mm/hr 72 mm/hr*	91,100	12	OTH	Widespread flooding, debris flows along San Gabriel Mtn.

								Front; 43 homes damaged, 12 of which had major structural damage; 25 vehicles damaged; Presidential disaster declaration
2010-02-27[14,20]	Station	07:15	07:00 (15 UTC)	6-9 mm/hr 32 mm/hr*	14,000	1	ARCL	Presidential disaster declaration
2014-10-31[23,24]	Springs	22:00	22:00 (06 UTC 11/1)	7-13 mm/hr	Unknown	3	OTH	Several homes with mud damage
2014-12-12[25,26]	Springs	02:10	01:00 (09 UTC)	15-24* mm/hr	Unknown	3	AR	16 homes damaged, 10 of which were destroyed

[1]Gartner et al. 2004
[2]Chin et al. 1991
[3]Slosson et al. 1991
[4]San Bernardino Sun 1980a (01-10)
[5]San Bernardino Sun 1980b (04-06)
[6]San Bernardino Sun 1980c (01-29)
[7]San Bernardino Sun 1980d (02-17)
[8]Gartner et al. 2008
[9]Santi and Morandi 2012
[10]Taylor 1982
[11]Riggan et al. 1985
[12]Schleiss et al. 2014
[13]County of Ventura 2015
[14]Gartner et al. 2014
[15]Staley et al. 2013
[16]Cannon et al. 2010
[17]URS 2005
[18]LA Times Blog 2009
[19]City of Sierra Madre 2009
[20]Kean et al. 2011
[21]CalOES 2010
[22]LA Times 2010
[23]CBS Los Angeles 2014
[24]ABC News 7 2014
[25]Sukup et al. 2016
[26]Daily Mail 2014
*15 min rate

Table 1.1: *Post-fire debris flow events analyzed in this study and their associated attributes. In event type column, AR indicates atmospheric river, CL indicates closed low, ARCL indicates both, and OTH indicates other type of event (not CL or AR). Rainfall rates indicate the maximum hourly rates available at stations in the vicinity of the burn area, both research gauges and permanent monitoring gauges as described*

in section 2.2. Where indicated with an asterisk (*), the hourly rates given are based on 15-minute observations.

1.2. Meteorological conditions associated with intense precipitation in southern California

Southern California and the Transverse Ranges experience some of the highest storm precipitation totals in the nation, on par with totals seen in hurricanes in the southeastern U.S. and thunderstorms in the Midwest (Dettinger et al. 2011; Ralph and Dettinger 2012). The highest probable 1-hour precipitation intensities in this region are on par with those seen in association with Midwest thunderstorms (NOAA HDSC 2017). At the synoptic (coarse) scale, mid-latitude cyclones are generally responsible for bringing cool season precipitation to California (Weaver 1962; Monteverdi 1995). These cyclones may vary in size, shape, intensity, and moisture transport; some may have associated atmospheric rivers or become closed lows, as described below. Additionally, many finer scale features and processes that go beyond the resolution of this synoptic-scale study are also at work to create convection "hotspots" that produce the short duration, high intensity precipitation conducive to PFDFs (Jorgensen et al. 2011; Moody et al. 2013). Some of the features considered in this study are atmospheric rivers, closed lows, orographic lift, and other types of lift.

Atmospheric rivers (ARs; Figure 1.1c; Figure 1.3d) are narrow corridors of high water vapor transport typically found in the lowest 2.5 km of the atmosphere

(Zhu and Newell 1998; Ralph et al. 2004, 2005). ARs are found ahead of the cold front in mid-latitude cyclones and source their moisture from the tropics and extratropics (Browning and Pardoe 1973; Ralph et al. 2004). They are typically <1000 km in width, >2000 km in length, and have integrated water vapor (IWV; specific humidity integrated over a vertical column) values exceeding 20 mm (Ralph et al. 2004; Neiman et al. 2008). Additionally, integrated water vapor transport (IVT; the product of specific humidity and wind integrated over a vertical column) exceeding 250 kg m^{-1} s^{-1} is a criteria of ARs that accounts for the importance of wind velocity in vapor transport, upslope vapor flux, and precipitation when the AR encounters terrain (Moore et al. 2013; Rutz et al. 2014). In southern California, ARs are most abundant in the cool season (November-April; Neiman et al. 2008; Dettinger et al. 2011) and account for roughly 40-50% of cool season precipitation (Dettinger et al. 2011; Ralph et al. 2013; Rutz et al. 2014). ARs are associated with most of the area's extreme precipitation events (Dettinger et al. 2011; Ralph and Dettinger 2012) and have been found to produce, on average, twice the precipitation of winter storms without ARs (Neiman et al. 2008). ARs feature low-level jets (LLJs), strong winds in the lowest 2 km of the atmosphere (Browning and Pardoe 1973; Ralph et al. 2005). LLJs impacting coastal California vary in strength, from >12.5 m s^{-1} in Ralph and Dettinger (2012) to >20 m s^{-1} in Ralph et al. (2005). The presence and strength of a LLJ can help dictate precipitation intensity in complex terrain, with stronger LLJs producing grater upslope flux and enhanced precipitation (Ralph et al. 2006).

Closed lows (CLs) are a sub-set of mid-latitude cyclones that are frequently observed over California in the cool season months. They have closed height contours and complete cyclonic (counterclockwise) flow around their centers at mid- to upper levels of the atmosphere. These properties help to impede a closed low's downstream motion such that CLs, often in concert with other features like ARs, can produce sustained precipitation (Oakley and Redmond 2014).

Tarleton and Kluck (1994) cite strong orographic forcing as one of the reasons a large concentration of major California precipitation events occur in the Transverse Ranges. Orographic precipitation occurs when moist air is forced to ascend a terrain barrier. As the moist air rises and cools, condensation, and ultimately precipitation occurs. Lin et al. (2001) define five common ingredients for intense orographic precipitation: 1) a conditionally or potentially unstable air mass- an air mass that, if forced to ascend, will continue to do so, 2) presence of a low level wind speed maximum containing moist air oriented orthogonal to the mountain barrier, 3) presence of a steep mountain, 4) a slow-moving weather system, and 5) high precipitation efficiency, a quantity related to the vertical flux of moisture, horizontal length of storm, and propagation speed of storm. During an AR impinging on the Transverse Ranges and its associated LLJ, these conditions are often met, resulting in heavy precipitation (Neiman et al. 2002; Neiman et al. 2004; Ralph et al. 2006).

Other types of forced ascent beyond orographic lift contribute to convective cells that trigger PFDFs in the Transverse Ranges as well. Along a cold front, air may

be forced to ascend as an incoming cold, dense air mass forces it upward. This can result in the formation of a narrow cold frontal rain band, a line of intense convective cells parallel to the cold front (Hobbs 1978; Hobbs and Persson 1982). Upper level (above 300 hPa) jet structure may also contribute to the development of convective cells. There are locations in the jet structure that produce divergence at upper levels, favoring lift (Carlson 1998). Isolated thunderstorms in this region, while uncommon in the cool season, are occasionally observed during the boundary months of the season. These storms occur on a spatial scale of tens of kilometers, thus producing precipitation over a much smaller area than that affected by a mid-latitude cyclone.

2. Methods

2.1 Compilation of PFDF catalog

A catalog of post-fire debris flow events in the Transverse Ranges and relevant details was compiled for the period 1980-2014. This range is based on the availability and qualities of PFDF events as well as availability of moderate resolution meteorological information from the North American Regional Reanalysis (NARR; Mesinger et al. 2006) used in generating case studies. The catalog was compiled using a variety of publications, U.S. Geological Survey reports, and newspaper articles as noted in Table 1.1. The requirements for a PFDF event to be included in the database are:

- Occurred within two years of a fire

- Identified as a PFDF in scientific literature
- Time of event triggering rainfall was either known, or could be determined
- Occurred in cool season (November-April)
- Event is generally of note and familiar to the PFDF community

Based on these criteria, an original compilation of several hundred PFDF events was refined, with the resulting catalog containing 93 individual PFDFs occurring as part of 21 "events" (multiple PFDFs in a burned area) on 19 distinct dates. The events occurred in 12 burn areas in the Transverse Ranges, shown in Figure 1.2.

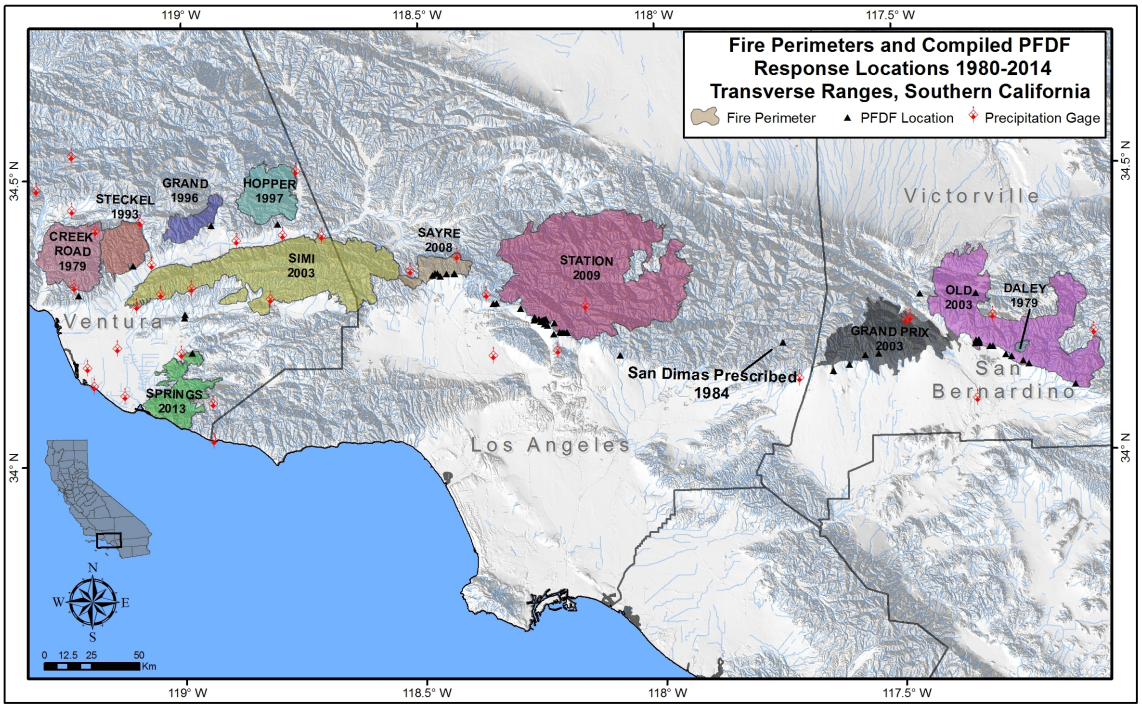

Figure 1.2: *Map of the study area showing selected fire perimeters (colored polygons; CALFIRE 2014), locations of individual debris flows (filled triangles), and location of*

precipitation gauges used to determine trigger time of debris flows. Year given for each burn area is the year fire occurred

2.2 Timing of PFDF events

To assess meteorological conditions associated with the occurrence of a PFDF, it was necessary to assign a trigger time to each event. This posed a challenge as time of occurrence is rarely provided in PFDF literature due to lack of observations. Indeed, Guzetti et al. (2008) found that globally, only 5.1% of the 2,626 published landslide and debris flow events had timing data accurate to +/- 12 h (Staley et al. 2013).

Precipitation intensity-duration (I-D) thresholds are developed through identification of runoff response in burned watersheds (Cannon et al. 2008; Staley et al. 2013) and are a common way of representing potential risk in a recently burned area. In this study, we have chosen to use I-D thresholds proposed by Staley et al. (2013). This approach improves upon the earlier threshold delineation approach of Cannon et al. (2008) by utilizing instrumented watersheds and analyzing rainfall prior to the debris flow event instead of approximating the PFDF trigger timing with peak rainfall intensity. This improved temporal correlation between PFDF event and threshold exceedance as well as assisted in developing thresholds that balance predictive success with false (debris flow does not occur when precipitation threshold is exceeded) and failed alarms (debris flow occurs when precipitation is below threshold). Recent work based on objective measurements of PFDFs in the

Transverse Ranges has suggested that I-D thresholds for periods <30 minutes are considered the best predictor of PFDF events (Kean et al. 2011; Staley et al. 2013). In this study we recognize the importance of sub-hourly I-D thresholds, and, where available, use these thresholds in our analysis. For the events where precipitation data was needed to help determine timing, we utilized hourly to sub-hourly precipitation data from the Remote Automated Weather Station (RAWS) network provided by the Western Regional Climate Center (WRCC; http://raws.dri.edu/), National Oceanographic and Atmospheric Administration (NOAA) Hourly Precipitation Data (HPD) network provided by the WRCC (http://wrcc.dri.edu/hpd/), as well as data from the Ventura County Watershed Protection District network (http://www.vcwatershed.net/hydrodata/); Figure 1.2 depicts station locations. The procedure used to estimate timing of events is as follows:

1. Documented trigger times established through instrumentation of a watershed were given priority as the trigger time of the event.
2. When a documented trigger time is available in the literature (regardless of instrumentation of the watershed), that time is used. If an event has several PFDFs over the course of a day, a time representative of the majority of PFDF occurrences is selected.
3. When precise timing is not available, the hour during which precipitation crosses the 1-hour minimum I-D threshold (12.4 mm; Staley et al., 2013) at the closest station(s) to the burn area is used as the trigger time. In

cases where stations were not particularly representative of the burn area or rainfall did not exceed the threshold, additional references were reviewed (4-6 below).

4. Information found in resources such as newspapers and blogs was used in conjunction with precipitation data to help estimate event timing.
5. For post-1995 events, National Reflectivity Mosaic imagery from National Centers for Environmental Information's Radar Data Map (NCEI 2016) was used to help determine when intense precipitation was present over a burn area.
6. In cases where precipitation did not exceed the 12.4 mm h^{-1} threshold in available precipitation data and no radar imagery was available, the intense precipitation was assumed to be very localized and the event time assigned corresponded to the greatest precipitation intensity on the PFDF date.

NARR data utilized span 1979-present and are available at 3-hour time steps beginning at 00 UTC each day. The NARR time step closest to the PFDF estimated trigger time is used for the meteorological case studies and hereafter referred to as the "NARR time". In the case of the 2009-02-13 and 1998-02-02 events, it was more desirable to use the closest *preceding* NARR time rather than the closest NARR time based on limited and variable precipitation observations and radar imagery, as this would more accurately capture the onset of the event.

2.3 Connecting PFDF events to meteorology

2.3.1 Comparison with established atmospheric river and closed low catalogs

For the list of PFDF dates and associated NARR times, a comparison was made with established AR and CL catalogs. The catalog of CLs, based off the methods in Oakley and Redmond (2014) covers the domain 20°-50° N, 110°-140° W at a 6 h time step. The catalog of ARs, based off methods of Rutz et al. (2014), determines whether AR conditions are present at individual grid points at a 6 h time step. Both catalogs are based off the 2.5° resolution NCEP/NCAR Reanalysis product (Kalnay et al. 2010). If the NARR time of a PFDF occurred within ±12 h of the presence of a CL in the catalog and NARR imagery revealed the feature to be pertinent to the precipitation event, the PFDF was associated with a CL. If the NARR time of a PFDF occurred within ± 12 h of AR conditions at 35° N, 122.5° W (closest grid point to study area), the PFDF was associated with an AR.

2.3.2 Development of meteorological case studies

Imagery of meteorological variables was generated for a 3-day period surrounding each PFDF event using the 32-km grid spacing, 3 h temporal resolution NARR data for a region spanning 20°-50° N, 105°-150° W. NARR data is generated by ingesting surface and upper air observations from the continental US into a meteorological simulation model to produce a spatially and temporally consistent meteorological record (Mesinger et al. 2006). The case studies were examined to

determine common meso-beta to synoptic features present during PFDF events by generating the following imagery:

1. **300 hPa vector wind, heights, isotachs:** This allows observation of the position of both the polar and subtropical jets, which can drive convection through patterns of convergence and divergence (Figure 1.3a).
2. **500 hPa height, IWV, and IVT**: 500 hPa heights reveal the ridge/trough pattern over the region. IWV and IVT help diagnose if an AR is present and moisture available for precipitation (Figure 1.3b).
3. **925 hPa height, vector wind, isotachs**: Winds slightly above the surface at 925 hPa (~750 m) provide insight into the potential for orographic forcing and this level is close to the core altitude of water vapor transport in ARs (Figure 1.3c).
4. **Vertical profiles of stability, moisture flux, and wind:** These variables are used to examine stability of the atmosphere and moisture flux. Profiles were taken at a grid point upstream (south) of each burn area and offshore in an attempt to reduce the effects of terrain-related issues in NARR and provide a full profile of the atmosphere (e.g., Figure 1.6).

Composites of these variables were also generated to identify atmospheric features that have a strong signal across events. Additional data used to support case studies includes radar imagery (NCEI 2016), wind profiler data (NOAA ESRL 2016) and Special Sensor Microwave Imager (SSM/I) satellite-derived IWV (CIMSS 2016).

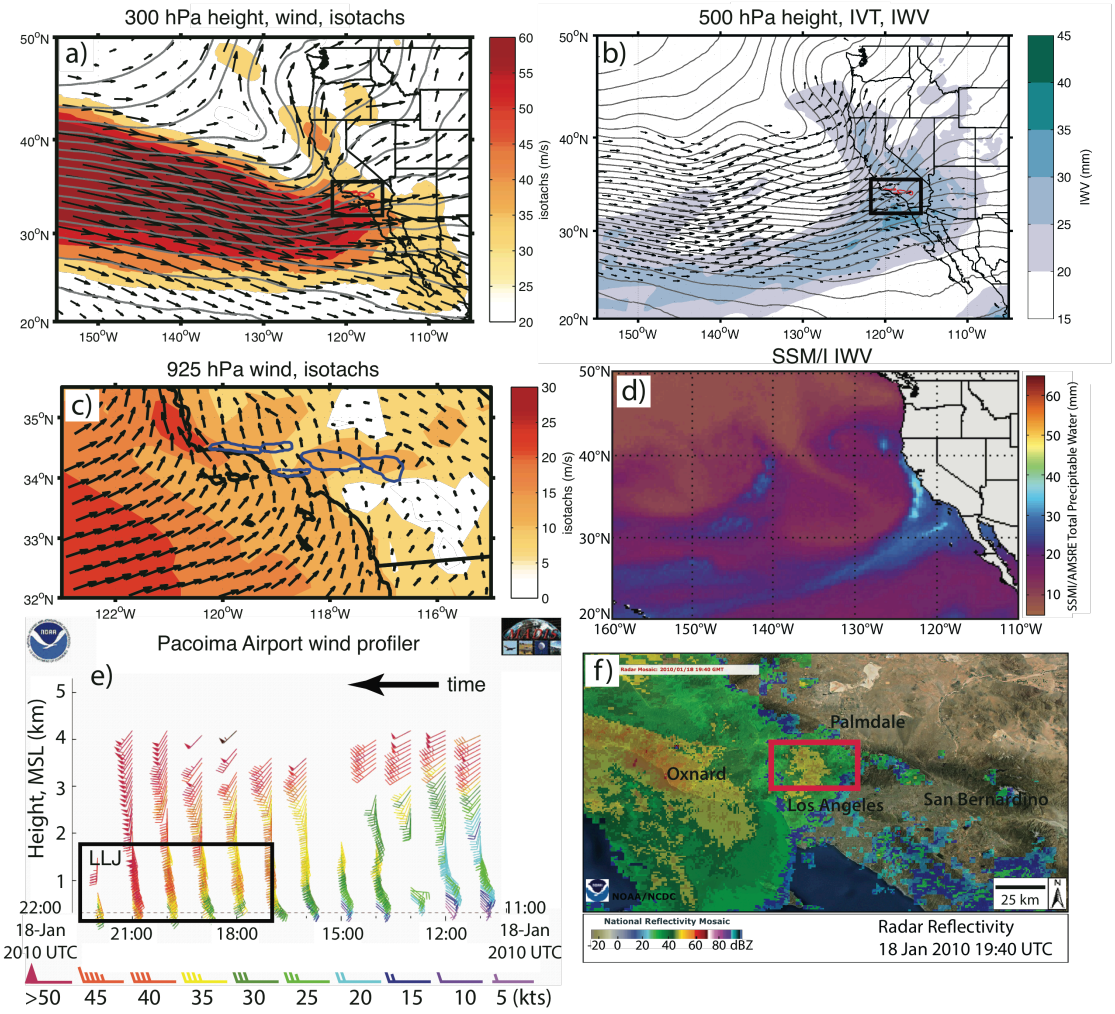

Figure 1.3 *Case study analysis for the 18 Jan 2010 post-fire debris flow in the Station Fire burn area, western San Gabriel Mountains. Subplots show the following: a) NARR 300 hPa geopotential height, wind vectors, isotachs (shaded) at 18:00 UTC. b) NARR 500 hPa geopotential height, IVT > 250 kg m^{-1} s^{-1} (vectors), and IWV > 20 mm (shaded) at 18:00 UTC. Note IWV maximum over study area. Black boxes in plots a and b indicate domain shown in plot c. c) 925 hPa wind vectors and isotachs (shaded) with Transverse Ranges outlined in blue at 18:00 UTC. d) SSM/I IWV at 17:00 UTC, showing AR land-falling on West Coast. e) Wind profiler data from Pacoima Airport 11:00 UTC-*

22:00 UTC with area of low-level jet boxed in black. Data provided by South Coast Air Quality Management District; base image from NOAA ESRL (2016). f) High radar reflectivity over the Station Fire burn area (rough outline shown by red box) at 19:40 UTC (NCEI 2016). Similar case studies were generated for a 3-day period surrounding each of the PFDF events studied.

2.3.3 Analysis of meteorological variables

For a variety of meteorological variables, NARR values were extracted for each event's NARR time, time-3 h, and time-6 h. Variables assessed include: winds at various levels, IWV, IVT, and convective available potential energy (CAPE, a measure of buoyant energy and an indicator of potential for severe weather). Value ranges were generated based on a set of 12 NARR grid points overlying each burn area, shifted for events in different parts of the region. The values of the 12 grid points for each of the 21 events (a total of 252 values) are then aggregated, providing a range of values across all analyzed PFDF events in the Transverse Ranges.

For scalar variables such as IWV, magnitude of IVT, and CAPE, boxplots showing the median, quartiles, and outliers among values were generated for the aggregated event data. To provide additional information based on direct observation, CAPE was also composited for events using rawinsonde data from Vandenberg Air Force Base (VBG), the closest rawinsonde launch location, approximately 200 km northwest of the study area. VBG rawinsonde data are available at 00 UTC and 12 UTC and were acquired from Plymouth State (2016)

upper air data archives. Data were obtained for the rawinsonde time closest to the PFDF event NARR time when possible. If rawinsonde observations were missing, then the next closest time available was used. If the NARR time for an event was 06 UTC or 18 UTC, exactly between VBG rawinsonde observations, the sounding with a higher CAPE value was used. For the vector variables wind speed and direction, wind roses were made from the aggregate event data at several different atmospheric levels.

To provide a climatological context for each event, climatologies were constructed from NARR for IVT, IWV, and CAPE. For each of the event dates, a period of +/- 5 days was considered, for a total period of 11 days. This was done such that each event is put in context of its particular time of year, as there may be considerable variability in the climatology of atmospheric variables within the cool season (e.g., Rutz et al. 2014). Each of the variables was then extracted from NARR for each 3h time step in this 11-day period (88 time steps) from each year of the NARR period of record. Values were extracted at each time step for an 8 x 5 grid cell area (256 km by 160 km) overlaying the study area, and the maximum value in the grid pulled at each time step. This generated a sample size of 3256 values. Percentiles were computed from these values for each of the variables. The maximum value at the time of each PFDF event was then evaluated against the climatology to determine its percentile ranking, and the rankings are provided in Appendix A.

3. Results and Discussion

3.1 Synoptic scale features

Atmospheric rivers and their associated features as well as the common ingredients for heavy orographic precipitation were found in a majority of PFDF events. AR conditions were present during 68% of case studies and CLs occurred in 26% of events. Five events featured neither an AR nor CL (Table 1.2; Appendix A).

Features in PFDF events
1. Atmospheric river (AR) or closed low (CL) presence (n=19 events)
AR only: 9 events CL only: 1 event AR and CL: 4 events None: 5 events Total events with AR: 13 events Total events with CL: 5 events
2. Upper level trough orientation (n=19 events)
Positive tilt: 4 events Negative tilt: 7 events Neutral: 8 events
3. Jet position in relation to Transverse Range study area (n=19 events)
Jet to south: 13 events Jet overhead/splitting: 5 events Jet to north: 1 event
4. Stability Profile (surface to 700 hPa; n=19 events)
Weakly unstable, $\frac{\partial \theta_{e*}}{\partial z} < 0$, slightly: 3 events Moist neutral, $\frac{\partial \theta_{e*}}{\partial z} \cong 0$: 9 events Unstable to moist neutral: 7 events
5. Features in radar imagery (n=14, only post-1995 available)
NCFR: 5 events Isolated cell: 1 event Other: 8 events

Table 1.2: *Summary of atmospheric features in 19 PFDF events. Attributions for individual PFDF events can be found in Appendix A.*

Consistent with the dominance of AR events, compositing of IWV shows the upper three quartiles of grid points at the time of event exceed the 20 mm AR

threshold (Figure 1.4). Averaged across events, IWV values were in the 92nd percentile with respect to climatology (Appendix A). For the IVT variable, the 250 kg m^{-1} s^{-1} AR threshold fell in the lower third of the lower middle quartile of the distribution at the time of event (Figure 1.4). All six non-AR events had a majority of their 12 grid points at the time of event below IWV and IVT thresholds for ARs. Averaged across events, IVT values were in the 95th percentile with respect to climatology (Appendix A). In some cases, IVT or IWV at event-3 h or event-6 h were higher than at event time (Figure 1.4). An AR is typically located in the warm sector of a storm, preceding the cold front. Since many of the events exhibit lift associated with the cold front, it is possible to see convection capable of initiating a PFDF occur following the maximum values of IVT or IWV in a storm. Averaged across events, 75% of the moisture flux (product of specific humidity and wind speed) was located below 600 hPa (~4 km; Figure 1.6b). This is higher in the atmosphere than in previous studies of ARs off the California coast, where 75% of moisture flux was observed below 2.25 km (Ralph et al. 2005).

Most events featured a neutral or negatively tilted trough (as seen in Figure 1.3a and 1.3b; Appendix A). In the case of a negatively tilted trough, instability and convection are favorable, as cold air advection occurs at upper levels above relatively warm air at low levels (MacDonald 1976). Instability can still occur within a neutral and positively tilted trough as well.

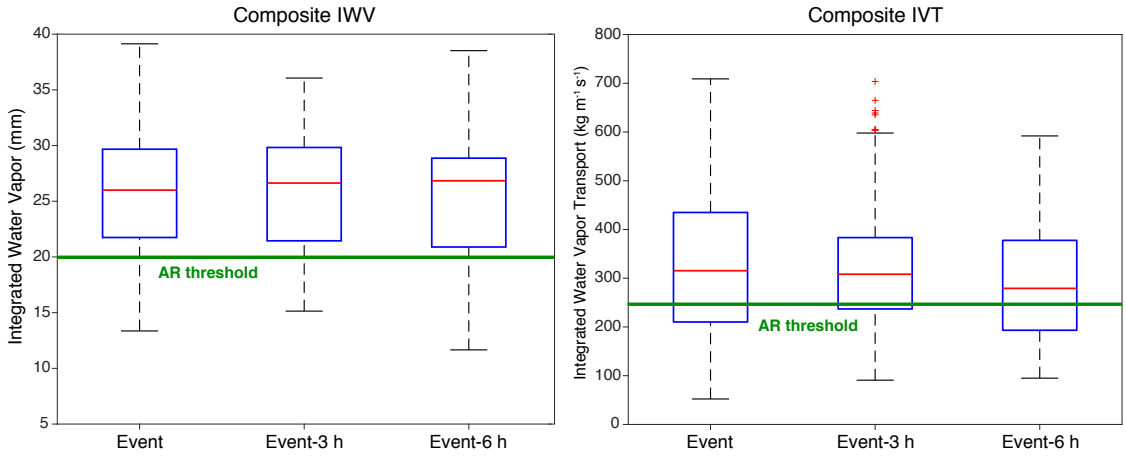

Figure 1.4: *Box and whisker plots for a) composite IWV and b) composite IVT from NARR data for 12 grid points pertaining to each of 21 PFDF events at NARR time of event, NARR time-3 h, and NARR time-6 h prior (n=252 points in each box and whisker diagram at each time). Blue boxes indicate the two middle quartiles, red line specifies the median, and whiskers indicate the upper and lower quartiles. Red +'s specify outlier data. Green horizontal lines indicated the threshold for atmospheric river conditions for each variable based on Ralph et al. (2004) for IWV; Rutz et al. (2014) for IVT.*

3.2 Jet position, structure, and winds

At the NARR event time, the dominant direction of the 300 hPa upper level flow over the composited study areas was southwest to west-southwest (Figure 1.5, top; Appendix A). All observations fell between 185°-285°, with 90% of observations falling between 215° and 275°. In a majority of observations (67%), the average speed of the 300 hPa flow over the area of interest was ≥ 40 m s^{-1}, indicative of a weak of a weak to moderate flow aloft. Several of the events

examined see 300 hPa wind speeds in excess of 50 m s^{-1}, indicating moderate to strong flow. The velocity of the upper level winds indicates the strength of the upper level divergence, which promotes upward vertical motions and potential for precipitation (Clark et al. 2009; O'Hara et al. 2009).

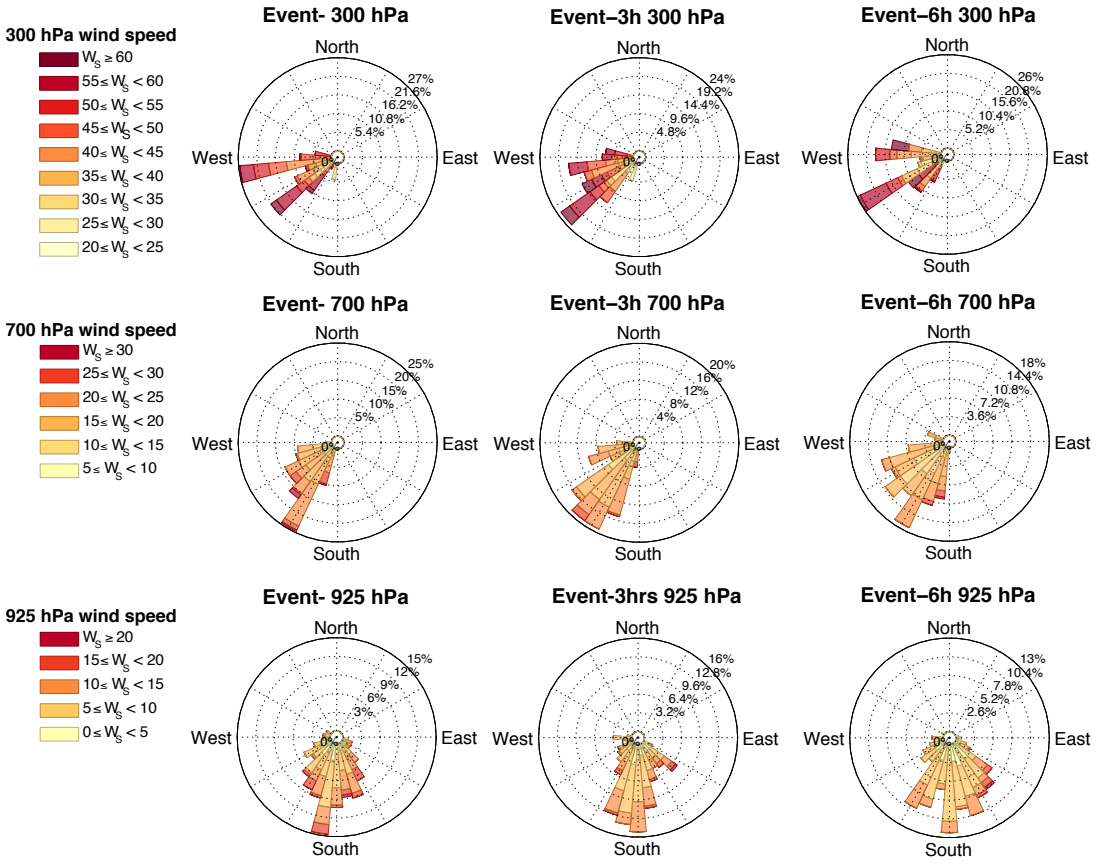

Figure 1.5: *Wind rose diagrams for composite 300 hPa wind (top row), 700 hPa wind (middle row) and 925 hPa wind (bottom row) from NARR data for 12 grid points pertaining to each of 21 PFDF events at NARR time of event, 3 hours prior, and 6 hours prior (n=252 points in each rose at each time). Total length of each bar indicates the frequency of grid points with wind in that particular direction. Length of colored areas within bar indicates the frequency of wind at a particular speed in that direction.*

The position of the upper level jet was to the south of the region of interest in a majority of events (68%; Table 1.2), typically placing the Transverse Ranges in the curved jet exit and/or the left exit of a jet streak, an area associated with strong upper level divergence and lift, as seen in Figure 1.3a. This is consistent with the "southerly displaced jet stream" cited by Tarleton and Kluck (1994) as a typical feature in extreme precipitation events in California. In several cases (26%), the upper level jet was directly over the study area, and finer scale splitting within the jet developed entrance or exit regions over the study area favorable for upper level divergence. In only one case, the upper level jet was located to the north of the region, though was positioned such that the right entrance of the jet was over the Transverse Ranges.

At mid- levels (700 hPa), winds were predominantly from the southwest at the time of the event, with 69% of observations falling between 205°-245° (Figure 1.5, middle row). The predominant speed was 15-20 m s^{-1} (38%); and 37% of observations were greater than 20 m s^{-1}. From NARR time-6 h through NARR time of event, wind speeds increased and direction became more uniformly from the southwest.

At low levels (925 hPa), wind direction was predominantly from 155°-215° (60% of observations; Figure 1.5 bottom row and Appendix A). The dominant speed was 5-10 m s^{-1} (49%), with 8% of observations exceeding 15 m s^{-1}. This is significant in that the low-level moderate intensity southerly winds are orthogonal

to the east-to-west oriented Transverse Ranges, providing one of the necessary conditions for heavy orographic precipitation (Lin et al. 2001).

Wind profiler data (NOAA ESRL 2016; as in Fig 3e) was used to diagnose the presence of LLJs for events when data were available. Profiler data was available for the ten post-2005 events, though available locations were inconsistent. Profiler data confirmed the presence of LLJs in the seven of these events; six of which were AR events. No LLJ was detected in three of the four non-AR events in this period (Appendix A).

3.3 Atmospheric stability

Stability profiles below ~3 km (700 hPa) as observed in vertical profiles could be broadly divided into weakly unstable, moist neutral, or unstable near surface becoming moist neutral with height (Table 1.2; Appendix A). A large majority of the events showed moist-neutral stability either in all levels below 3km or in the 1-2+ km layer (Figure 1.6a). Moist-neutral stability is recognized as little or no change in θ_{e^*} with height ($d\theta_{e^*}/dz = 0$). The significance of moist neutrality is that if the parcel is displaced upward, it will maintain its new position. Air parcels in a neutral setting can be forced to ascend relatively easily in the presence of a lifting mechanism such as a cold front or mountain barrier, resulting in convection. Moist neutral stability is a common feature of ARs (Ralph et al. 2005). Several events saw instability at low levels ($d\theta_{e^*}/dz < 0$; Figure 1.6a) transitioning to moist-neutral

near 1 km, distinct from the moist neutral layer observed from the surface to 2.8 km in a composite of AR events presented by Ralph et al. (2005).

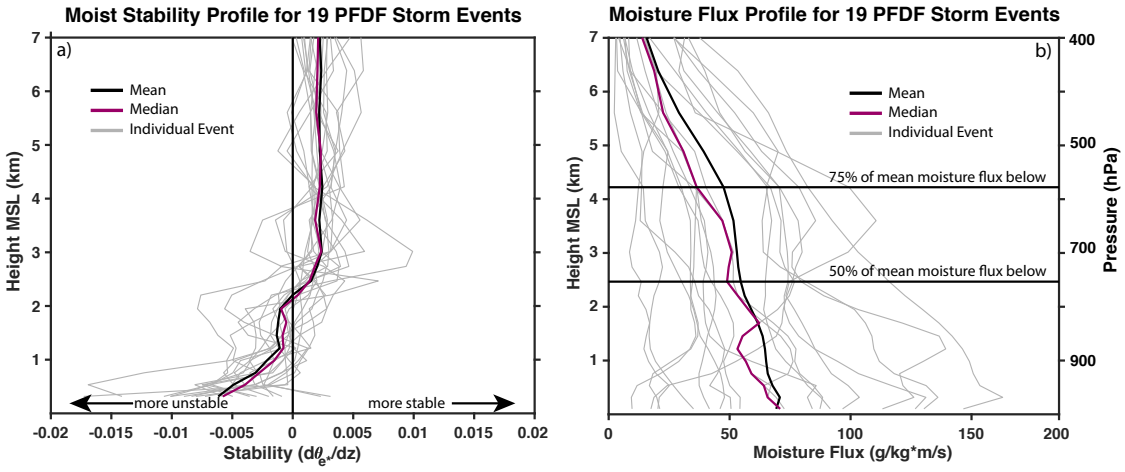

Figure 1.6: *a) Moist stability profile for 19 PFDF events and b) moisture flux profile for 19 PFDF events based on NARR data at NARR event time. In plot a), values close to 0 correspond to moist-neutral conditions.*

The scale for CAPE begins at 0, and higher values of CAPE indicate greater instability and severe weather. In the CAPE climatologies created for periods relative to the PFDF events studied here, a CAPE value of 100 J kg^{-1} was on average the 85th percentile for the maximum values in the study area (Appendix A). At the NARR event time, median NARR CAPE was 20 J kg^{-1} and ranged from 0 to 1330 J kg^{-1}, with the values exceeding 500 J kg^{-1} all coming from grid points associated with the two Springs Fire cases in the Santa Monica Mountains. At the time closest to the event, median CAPE from the VBG soundings was 40 J kg^{-1} and ranged from 0 to 463

J kg^{-1} (Figure 1.7; Appendix A). A general trend of increasing CAPE was observed in NARR in the 3 h and 6 h time steps leading up to the event (Figure 1.7).

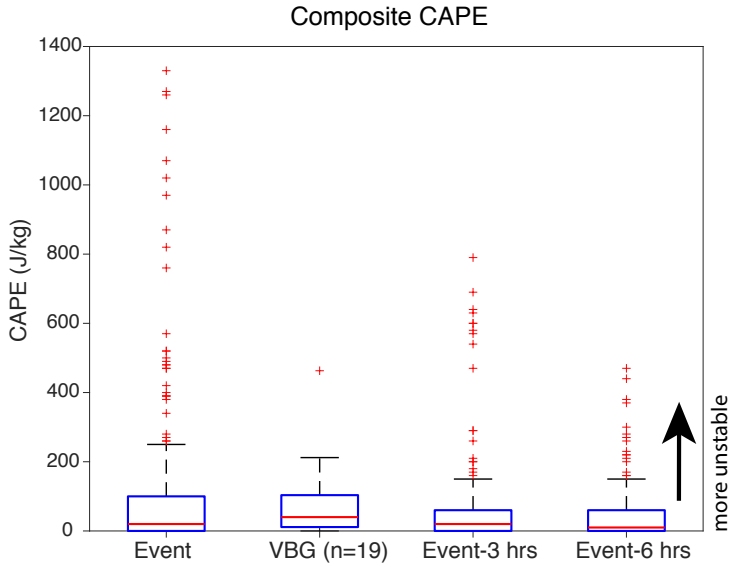

Figure 1.7: *Box and whisker plots for composite CAPE from NARR data for 12 grid points pertaining to each of 21 PFDF events at NARR time of event, NARR time-3 h, and NARR time-6 h prior (n=252 points in each box and whisker diagram at each time). Blue boxes indicate the two middle quartiles, red line specifies the median, and whiskers indicate the upper and lower quartiles. Red +'s specify outlier data. The second from left box-and-whisker in each plot represents the values acquired for rawinsonde soundings at Vandenberg AFB at closest time available to each event; as the sounding produces a single value, there is one value for each event date and n=19.*

3.4 Analysis of radar imagery

Radar imagery was available for 14 unique PFDF event dates through NCEI's Radar Data Map (https://gis.ncdc.noaa.gov/maps/ncei/radar). All events had radar

returns of at a minimum 50 dBZ (approximately >48 mm h^{-1}; as in Figure 1.3f)[1], indicative of heavy precipitation. Six of the 14 events had very strong returns over 60 dBZ (>200 mm h^{-1}), indicative of very intense precipitation. Narrow cold frontal rain bands (NCFRs) were identified in five of the 14 events (Table 1.2 and Appendix A; example in Figure 1.8). NCFRs show up in radar imagery as a narrow band of high radar reflectivity on the order of 200 km long with breaks and gaps along their length (Figure 1.8; Jorgenson 2003). The five NCFRs in this study all followed a similar west-to-east path across the southern California Bight with the northern half of the NCFR situated over land while the southern half was over water and the feature's long axis perpendicular to the coast. This preferential orientation likely occurs due to blocking and modification of the low-level front by coastal terrain (Neiman et al. 2004; Hughes et al. 2009).

[1] Rain rates based on Marshall and Palmer (1948). Note values given for rain rate are instantaneous corresponding to the imagery and do not represent the actual value observed over the course of an hour.

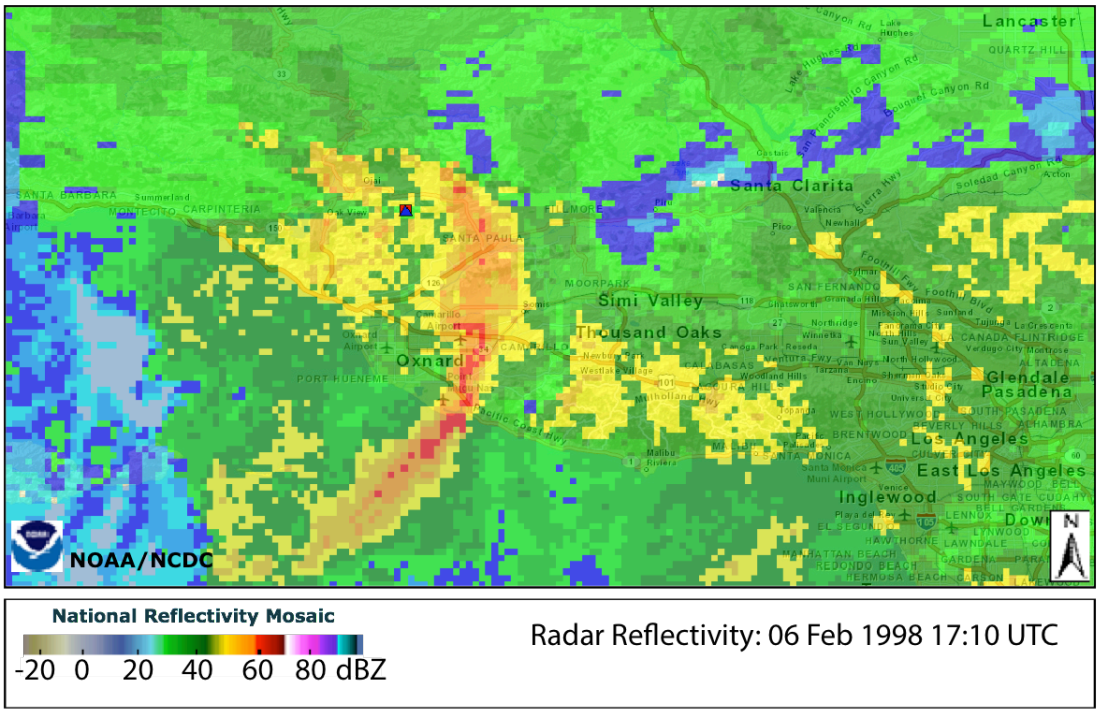

Figure 1.8: *Radar image of a narrow cold frontal rain band (NCFR) passing over the Transverse Range study area during the 06 Feb 1998 PFDF event in the Grand/ Hopper burn areas in the Topatopa Mountains.*

Radar imagery associated with one PFDF event on 12 Nov 2009 resulted from the development of a very isolated convective cell in the San Gabriel Mountains, reminiscent of a warm season thunderstorm event. The remaining eight of the 14 PFDF events for which radar data was available featured other types of convective activity such as orographic forcing and mesoscale rain bands (as in Figure 1.4f) that are not discussed in detail within this paper.

3.5 Tools and Applications

The prominence of ARs and their related features in the occurrence of PFDFs in the Transverse Ranges suggests that those concerned with PFDFs will benefit from incorporating the use of online AR forecast and diagnostic tools into their decision-making. One such tool is the US West Coast AR Landfall Tool available through the Center for Western Weather and Water Extremes (CW3E) at http://cw3e.ucsd.edu/?page_id=491. This tool provides a 16-day forecast where the user can see the probability, magnitude, location, and timing of AR conditions arriving along the West Coast as well as how AR conditions vary in a forecast model through time. Proper use of this tool among others can generate awareness of the potential for a PFDF and support planning and decision-making in both research and emergency response. Additionally, the IVT variable assessed in the aforementioned AR forecasting tool has been shown to be more successful in long-range forecasts than precipitation (Lavers et al. 2016). Thus, forecasts of IVT can be used to provide forecasts of likelihood for heavy rainfall with greater certainty further ahead than the traditional precipitation forecasts.

3.6 Limitations and Future Work

Limitations of this study lie in NARR's 32 km resolution and thus its inability to resolve fine-scale processes important to the development of convective cells such as blocking, barrier jet features, and low-level convergence along terrain barriers that are common in the region (Small 1999; Neiman et al. 2004; Hughes et

al. 2009). Additionally, Hughes et al. (2012) have noted challenges in how NARR represents low-level winds and winds at the land-sea boundary, which may impact results for winds at these levels. The coarseness of the NARR data may also impact the accuracy of estimates of stability. CAPE, for example, can vary greatly in the course of a storm event. Sukup et al. (2016) show a significant increase in CAPE following a frontal passage after the PFDF had already occurred during the 12 December 2014 PFDF event. Thus it is possible that with the spatial and temporal coarseness of both NARR and radiosonde data that stability variables assessed are not representative of the true event time and may be biased high or low based on times available.

While AR conditions make up a majority of cool season PFDF events in this study, there are, on occasion, isolated thunderstorm events such as the 12 November 2009 PFDF event included herein. Thus, we advise that all storm types should be considered in emergency preparedness; however, advantage should be taken of recent advancements in AR detection and prediction given the dominance of ARs among the PFDF cases explored in this study.

This work is, in essence, an analysis of cases of intense precipitation in the Transverse Ranges, subset by PFDF occurrence. A broader approach would be to look at all precipitation events over a particular threshold in the region. However, PFDF thresholds have been noted to vary in space (Staley et al. 2016) thus choosing one representative threshold may not suffice. Focusing on events known to produce impactful PFDFs ensures precipitation was indeed sufficient. Additionally, applying

meteorological analyses to verified impactful PFDF events allows us to make a direct connection with the experiences and concerns of our target audience in a way that a more abstract approach of exploring precipitation over a particular intensity may not.

The lack of observations of both post-fire debris flow activity and precipitation limits the assessment of null events. Without a high-resolution network of gauges and instruments that can record debris flow response and triggering rainfall within the burn area, it is difficult to determine whether precipitation of sufficient intensity and duration for PFDF activity did or did not fall on a burn area. In cases outside of research efforts that utilize instrumentation, PFDFs are often only noted if they impact human infrastructure. Thus, if a PFDF occurred in an inaccessible remote area of a watershed, it may not be documented. In the null case most relevant to this work (all favorable synoptic scale conditions present, but intense precipitation does not occur, field observations made, and no PFDFs present), analysis using mesoscale modeling would be needed to assess why intense cells did not develop, which is beyond the scope of this work. Thus, this work focuses on well-documented damaging debris flows that affected structures or infrastructure downstream of the burned watershed.

A major challenge that remains in this research topic is identifying the exact timing and location where intense convective cells might develop (isolated or within a larger storm system). Similar to the suggestions of Moody et al. (2013) and Shakesby et al. (2016), we propose future work should focus on high resolution (≤1

km) modeling of the region to identify favored areas for intense convection under a variety of flow regimes. For modeling efforts to be successful, precise timing of a greater number of PFDF events is necessary. There are many challenges to overcome in instrumenting basins, as described in Kean et al. (2011) and Staley et al. (2013), but, where present, we have found this timing data essential to assessment of the meteorological component of PFDF events.

4. Conclusions

A catalog of 93 individual post-fire debris flow (PFDF) events associated with 19 precipitation events was compiled for the Transverse Ranges using a variety of resources. Meteorological case studies were created for each event using hourly precipitation data from various weather stations, the North American Regional Reanalysis (NARR) dataset, radar imagery, wind profiler data, and rawinsonde observations.

The majority of the precipitation events producing PFDFs are moderate to strong in terms of moisture transport; 11/19 events have IVT >= 95th percentile for the location and time of year. A few of the events examined have weaker moisture transport (<90th percentile), though these events feature instability that is characteristic of only a few of the high IVT events. Thus, there is some variability in the synoptic scale characteristics of precipitation events that produce PFDFs. However, we do find a set of characteristics that are common across a majority of

PFDF events. These common atmospheric conditions associated with cool season PFDFs can be summarized as:

- Atmospheric rivers (ARs) were present in 13 of 19 PFDF events (9 had AR only, 4 had AR and a closed low)
- All 13 AR events featured IVT >= 90th percentile and 8 had IVT in the 99th percentile (strong events for the location and time of year)
- On average, 75% of moisture flux in PFDF events below 4 km
- Closed lows (CL) were present in 5 of 19 PFDF events (1 had CL only, 4 had AR and CL)
- Neither AR nor CL conditions were present in 5 events
- Moderate to strong flow aloft: Upper level (300 hPa) west-southwest flow typically > 40 m s^{-1}
- Upper level jet position in majority of events (13/19) is displaced to south such that the Transverse Ranges lie in divergent jet exit, an area favorable for upward vertical motions
- Presence of moderate speed (5-10+ ms^{-1}) southerly winds below 1 km
- Predominantly moist-neutral stability (AR feature), especially in the 1-2+ km layer; in some cases weakly unstable at low levels
- Median CAPE of 20-40 J kg^{-1} at time of event with a range from 0-1300 J kg^{-1} among events
- High radar returns (>50 dBz); in several cases narrow cold frontal rainbands

Together, these common conditions provide a general picture of the synoptic scale atmospheric phenomena present in storms that trigger PFDFs, and provide the framework for a conceptual cool season model, illustrated in Figure 1.9.

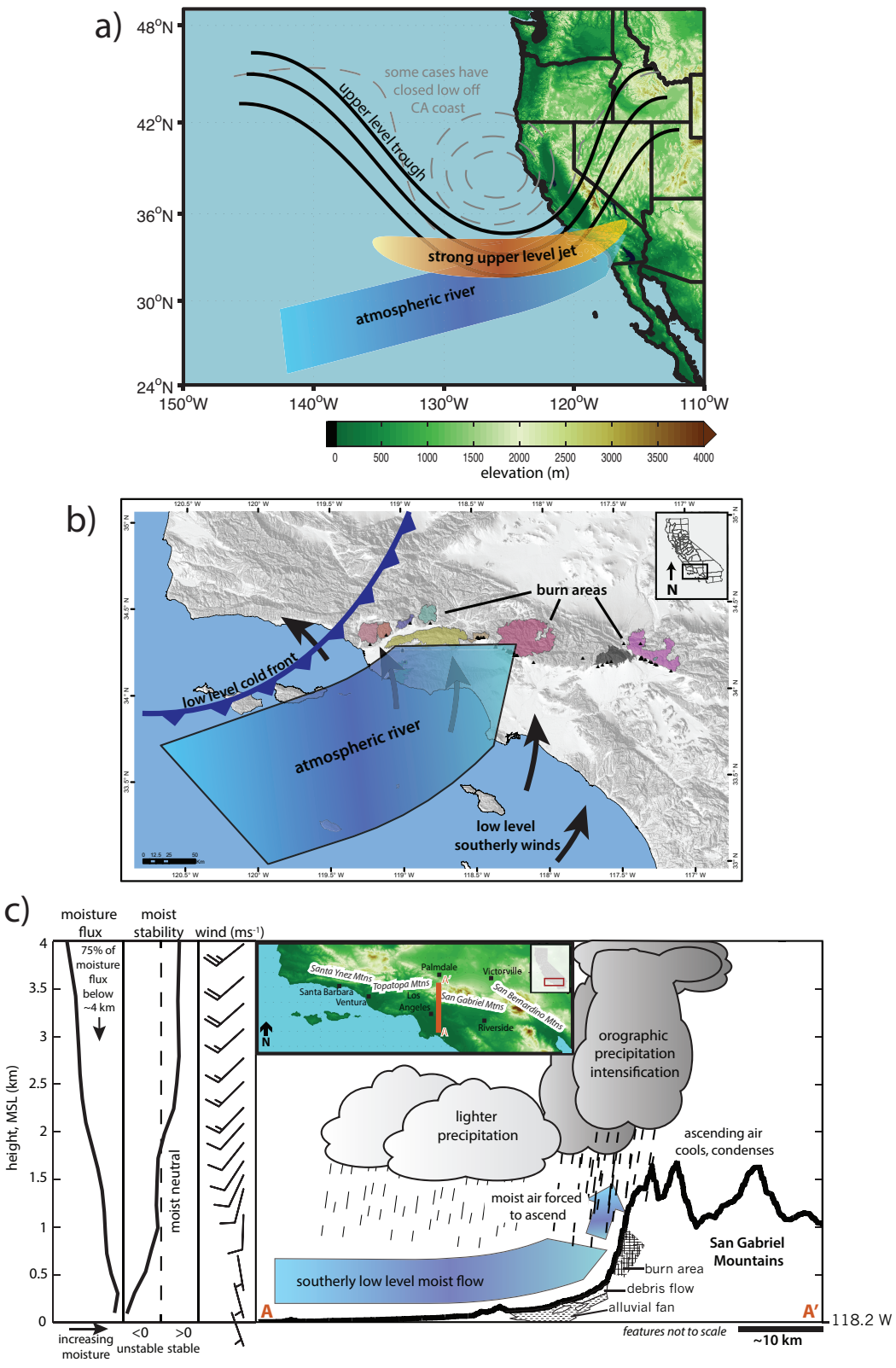
a)
48°N
42°N
36°N
30°N
24°N
150°W
140°W
130°W
120°W
110°W
some cases have closed low off CA coast
upper level trough
strong upper level jet
atmospheric river
0
500
1000
1500
2000
2500
3000
3500
4000
elevation (m)
b)
burn areas
N
low level cold front
atmospheric river
low level southerly winds
c)
moisture flux
moist stability
wind (ms-1)
75% of moisture flux below ~4 km
height, MSL (km)
4
3.5
3
2.5
2
1.5
1
0.5
0
moist neutral
increasing moisture
<0 unstable
>0 stable
Santa Ynez Mtns
Topatopa Mtns
Palmdale
Victorville
Santa Barbara
Ventura
Los Angeles
San Gabriel Mtns
San Bernardino Mtns
Riverside
N
A
orographic precipitation intensification
lighter precipitation
ascending air cools, condenses
moist air forced to ascend
San Gabriel Mountains
southerly low level moist flow
burn area
debris flow
alluvial fan
A'
118.2 W
features not to scale
~10 km

Figure 1.9: *Conceptual model of common features associated with PFDF in the Transverse Ranges at various scales. This represents the majority of events, which feature atmospheric rivers and their associated characteristics, but does not capture all variability seen among events. Panel a) depicts the synoptic scale features and typical positions. Panel b) provides a mesoscale perspective of the events in association with the burn areas and depicts a cold front moving into the region, which acts as a lifting mechanism for the NCFR events, and potentially others. Moisture flux is present primarily in low levels, and a generally moist-neutral stability profile indicates little resistance to orographic lift. Other lifting mechanisms may be at work as well; see section 1.2. Moisture flux and stability profiles as well as wind profile are composites of NARR data for all 19 post-fire debris flow events. Panel c) schematic designed after Ralph et al. (2005).*

The results presented here reinforce NWS forecaster experience pertaining to PFDF events (Cannon et al. 2010; Sukup et al. 2016) as well as illustrate and quantify these relationships. They also provide information on the variability of conditions observed among PFDF events that may be helpful in forecasting. The results of this study assists those evaluating runoff hazards in burned areas, as well as emergency managers, research geologists and hydrologists by going beyond the common descriptor of "intense convection" cited as the cause of PFDF events and identifying broad scale features that can be recognized in forecast models with more advanced notice than convective cells. Improved understanding by these groups can

help build awareness of the likelihood of PFDF events with more lead time and may improve interpretation and decision-making related to NWS forecasts, watches, and warnings.

Chapter 2

A 22-year climatology of cool season hourly precipitation thresholds conducive to shallow landslides in California

Nina S. Oakley, Jeremy T. Lancaster, Benjamin J. Hatchett, Jonathan Stock, F. Martin Ralph, Shawn Roj, and Stefani Lukashov

Abstract

California's winter storms produce intense rainfall capable of triggering shallow landslides, threatening lives and infrastructure. This study explores where hourly rainfall in the state meets or exceeds published values thought to trigger landslides, after crossing a seasonal antecedent precipitation threshold. We answer the questions: 1) Where in California are over threshold events most common? 2) How are events distributed within the cool season (October-May) and inter-annually? 3) Are these events related to atmospheric rivers? To do this, we compile and quality-control hourly precipitation data for a 22-year period for 147 Remote Automated Weather Stations (RAWS). Stations in the Transverse and Coast Ranges and portions of the northwestern Sierra Nevada have the greatest number of rainfall events exceeding thresholds. Atmospheric rivers coincide with 60-90% these events. Over threshold events tend to occur in the climatological wettest month of the year, and they commonly occur multiple times within a storm. This is the first statewide map depicting where to expect intense rainfalls that have historically triggered shallow landslides. It predicts that some areas of California are less susceptible to storm-driven landslides solely because high intensity rainfall is unlikely.

1. Introduction

Storm-triggered shallow landslides threaten life and property in California's steeplands. Where they mobilize into debris flows, they can result in loss of life, damage to infrastructure, homes, commercial buildings, and ecosystems (Jakob and Hungr 2005). Landslides and debris flows cause an estimated 25-50 deaths and $1-$3 billion in damages annually in the United States (NRC 2004). Impacts are anticipated to increase as

continued population and economic growth increases exposure to debris flow hazards (Santi et al. 2011).

Studies of historic events and monitoring of shallow landslides demonstrate that a range of rainfall rates can produce destabilizing increases in pore water pressure after the soil has absorbed a threshold amount of moisture from preceding rainfalls (e.g., Campbell 1975; Reid et al. 1997; Iverson 2000; Baum et al. 2010; Stock and Bellugi 2011). The soil moisture, or volumetric water content value at which water will flow out of a soil packet (column) at the rate at which it flows in is often called field capacity and represents a likely precondition to trigger widespread instability from intense rainfalls (Campbell 1975; Wilson and Wieczorek 1995; Baum et al. 2010). Rainfall that exceeds these values should be more likely to cause landslides (e.g., Godt et al. 2006). There are a number of historic estimates of antecedent rainfall totals and rainfall intensity-duration thresholds that will trigger shallow landslides (Campbell 1975; Caine 1980; Cannon and Ellen 1985; Wieczorek 1987; Wilson and Jayko 1997; Casadei et al. 2003; Guzetti et al. 2008; Stock and Bellugi 2011).

A few previous studies have evaluated characteristics of sub-daily precipitation in California. For example, hourly precipitation data are evaluated on a 2° x 2.5° in Lamjiri et al. (2017) and 15-minute data are grouped into clusters by climate zone in Palecki et al. (2005). Brooks and Stensrud (2000) analyze hourly station data across the U.S. to evaluate flash flooding hazards for rainfalls exceeding 25 mm h^{-1}, which is much higher than published landslide triggering threshold s for California. These worthwhile studies are all either at spatial scales that are too large, or thresholds that are too high or not relevant to historic landslide hazards.

Studies evaluating synoptic atmospheric conditions during mass movement events on the West Coast of the United States (Biasutti et al. 2016; Oakley et al. 2017; Young et al. 2017) find a relationship between mass movements and atmospheric rivers (ARs). ARs are narrow corridors of strong atmospheric water vapor transport that are typically associated with precipitation extremes and flooding in California (e.g. Ralph et al. 2006; Ralph and Dettinger 2012). These studies improve our understanding of the synoptic meteorology of storms that trigger landslides but do not provide guidance on where and how often to expect landslide-triggering rains.

Here, we create a quality-controlled statewide rainfall intensity data set for California from hourly gauges in the Remote Automated Weather Station (RAWS) network. These stations are often located in steeplands where landslides occur. We parse these data using published rainfall thresholds based on historic precipitation events that triggered shallow landslides. Rainfall events exceeding these thresholds are hereafter referred to as OTPE, "over threshold precipitation events". We address the following questions:

- What parts of California most frequently experience OTPE, and where are OTPE rarely observed?
- How frequently do OTPE occur after a seasonal rainfall total has been exceeded?
- How are OTPE distributed within the cool season?
- Are OTPE driven by atmospheric rivers?

California's soils are rarely susceptible to shallow landsliding during the dry season, when soil moisture is at its lowest. During the October-May period, when California receives most of its rain, soil moisture is replenished. This increase in initial soil moisture

precedes the occurrence of free water (or, positive pore water pressure) in the soil pores, widely thought to trigger instability during and shortly after storms (Wilson 1997a; Baum et al. 2010). Consequently, we analyze the wetting up period of October-May. We analyze the period 1995-2016 to maximize the number of RAWS stations with sufficient records while incorporating several extended wet and dry periods in California's historic record. After performing quality control on the data, we calculate the number of events exceeding selected thresholds at each station. We use seasonal precipitation sums as well as the Precipitation-elevation Regression on Independent Slopes Model (PRISM; Daly et al. 2008) to estimate the number of OTPE that occurred after a geomorphic province (CGS 2002) had exceeded a seasonal antecedent rainfall threshold, as those events would have the highest likelihood of triggering shallow slope failures. We use an AR catalog (Rutz et al. 2014) to assess whether OTPE are associated with ARs.

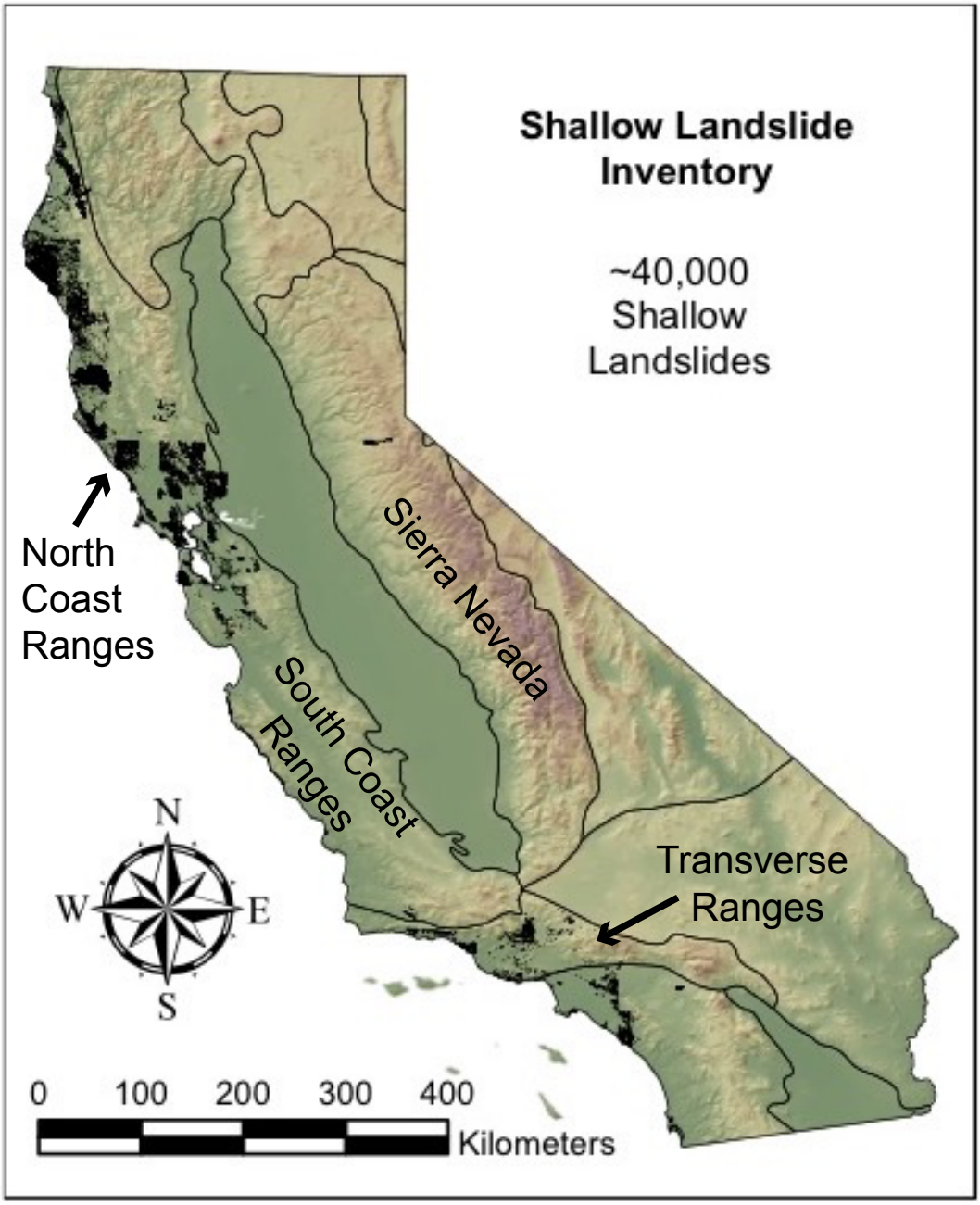

Figure 2.1. *Map of California landslide inventory from Wills et al. (2017) showing the general distribution of documented shallow landslides and the lack of documentation in many regions of the state. Because precipitation thresholds that trigger shallow landslides are developed from empirical data, this map serves as a general proxy for*

where threshold data may exist. Geomorphic provinces (CGS 2002) discussed herein are labeled.

2. Data and Methods

2.1. Rainfall threshold selection

There are good reasons to expect that there is no single value of rainfall intensity that will trigger storm-driven landsliding across California. A number of factors influence which rainfall intensities will create standing water in the soil column (e.g., Wilson 1997b; Larsen and Simon 1993; Baum and Godt 2010). These include properties that affect hydraulic conductivity through time (e.g., antecedent soil moisture), and space (e.g., vegetation, geology, topography). Once soils approach saturation, rainfall rates that exceed the rate at which the soil/bedrock interface can transmit water will likely produce standing water in the soil column, and hence instability (Campbell 1975; Reid 1997).

Most rainfall thresholds in California come from historic events in the Coast Ranges or Transverse Ranges, with the bulk of the studies near lifelines or population concentrations in Los Angeles and the San Francisco Bay Area. Much of California lacks historic records of storm-driven landsliding, and hence rainfall thresholds (Figure 2.1; Wills et al. 2017). The applicability of broad thresholds based on climate and other factors (e.g., Caine 1980; Guzzetti et al. 2008) is in doubt. Consequently, we use a range of existing intensity thresholds to cover this uncertainty. These thresholds collectively represent a range of intensity-duration possibilities from available studies.

1. 5 mm h^{-1} (T_5): approximate minimum hourly value proposed by Guzzetti et al. (2008) for triggering shallow landslides in Mediterranean climates.

2. 10 mm h^{-1} (T_{10}): Approximate hourly value stated by Wieczorek (1987) for triggering landslides in the Santa Cruz Mountains; adopted by Wilson (1997a) as a minimum "safety" threshold for Bay Area landslide activity, and also observed in Wilson (1997a) to be associated with widespread debris flow events in the Transverse Ranges in January-February 1993.
3. 15 mm h^{-1} (T_{15}): approximate value stated by Caine (1980) as a broad global threshold for shallow landslide and debris flow activity.
4. 20 mm h^{-1} (T_{20}): approximate value stated by Guzzetti et al. (2008) for triggering landslides in a "Mild Marine West Coast" climate; acts as an upper limit for hourly triggering thresholds that may be suitable for regions within California's generally Mediterranean climate.
5. 5 mm h^{-1} for 6h (T_{6h}): derived by Stock and Bellugi (2011) as a trigger for widespread shallow landslides in the Ventura area.
6. 7.5 mm h^{-1} for 3h (T_{3h}): not explicitly stated in literature reviewed, but falls between thresholds 1 and 2 in terms of both intensity and duration. This threshold is indirectly supported by Campbell (1975) who concludes 6.35 mm h^{-1} for a period long enough to establish a perched water table was relevant for debris flows in the Santa Monica mountains, and Wieczorek (1987) who found a duration of 3h was the most significant single index of the storms that caused debris flows in the San Francisco Bay Area.

2.2. Antecedent rainfall threshold selection

In considering intensity-duration thresholds for triggering shallow landslides, it is valuable to consider the role of antecedent rainfall (Bogaard and Greco 2018). We select 250 mm as a minimum estimate of antecedent rainfall needed to establish soil moisture conditions conducive to shallow landslide activity in California. This value is based on several published thresholds:

- Campbell (1975): 250 mm; Santa Monica Mountains, southern California
  Wieczorek (1987): 280 mm; La Honda, San Mateo County, northern California
- Cannon and Ellen (1988): 254-381 mm; San Francisco Bay Area, northern California

This static value and does not account for reductions in soil moisture and pore pressures that may vary with inter-storm dry periods, regional soil type, and hillslope hydrologic processes. However, its application provides a useful minimum estimate to evaluate threshold exceedance at a statewide scale.

2.3 Data selection and quality control (QC)

The RAWS weather station network (Brown et al. 2011) provides hourly meteorological data for mid-elevation locations in complex terrain, areas where landslides are likely to occur. These locations are typically not well covered by other observing networks that tend towards population centers or transportation corridors (Myrick and Horel 2008). RAWS are primarily used for fire weather monitoring and feature unheated and unshielded tipping bucket rain gauges. Due to these characteristics, RAWS may experience undercatch (e.g., Duchon and Essenburg 2001) and do not

accurately measure frozen precipitation (Daly et al. 2008). RAWS data were acquired from the Western Regional Climate Center (https://raws.dri.edu/) and a multi-step QC process was applied using the framework of Kondragunta and Shrestha (2006). A detailed explanation of data QC methods and limitations is provided in Appendix B. Following QC, stations with over 80% complete October-May data between 1995-2016 and below 1700 m elevation, the approximate mean snow elevation in the Sierra Nevada, were retained. This resulted in 147 stations throughout the state (Figure 2.2).

At each station, the number of OTPE associated with each of the six thresholds are counted and displayed on a map (Figure 2.2, 2.3). OTPE are considered to be part of the same "storm event" if they occurred within ±12 h of one another. The number of unique storm events at each station are counted and mapped, along with the ratio of storm events to total OTPE (Figures 2.8 and 2.9).

2.4 Exceedance of 250 mm season antecedent precipitation at stations

At each RAWS station, hourly precipitation values are summed for each October-May season in the station's record. For each season, the date on which a sum of 250 mm was achieved is recorded. Any OTPE occurring on or after this date are considered to happen after the 250 mm threshold was attained.

Only seasons with >70% of observations available are considered in this analysis. As the minimum 80% record completeness for a station record (Section 2.2) relates to the 1995-2016 period, some stations may have a substantial part of a particular season missing. Additionally, sub-0°C hours were removed in the QC process, reducing available valid data points at this stage of analysis, making a relatively low threshold of

70% completeness reasonable. Only stations with ≥15 seasons (132 of 147 stations) of such data are displayed on the resulting maps (Figures 2.5 and 2.6). Due to missing data challenges, this analysis represents a best estimate of achieving the 250 mm threshold in each season at each station.

2.5. Relation to atmospheric rivers

Relation of each OTPE to AR conditions is examined by comparing the OTPE date and time to an AR catalog developed by Rutz et al. (2014). This catalog is based on a six-hourly 2.5° reanalysis product (Kalnay et al. 1996) for 1995-2015. If at least one of the two gridpoints closest to a station at the time closest to an OTPE observes AR conditions, the OTPE in question is considered to result from an AR event. Using two closest gridpoints provides a minimum estimate of OTPE relationship to AR conditions; using four closest gridpoints produces OTPE-AR relationships 0-5% higher across each province.

2.6. Geomorphic province-wide precipitation data (Transverse Ranges province)

As an example of how seasonal precipitation and OTPE vary over the period of record in a province, we examine OTPE, monthly precipitation, date 250 mm is reached, and widespread landslide events for the Transverse Range province (Figure 2.12). We select this province as an example because it spans a small latitudinal gradient, has a high number of stations (16) for its areal extent compared to other provinces, and thresholds are well defined (Section 2.1).

Daily gridded 4-km PRISM precipitation estimates (Daly et al. 2008) are averaged across all grid cells in the Transverse Range province for each date January 1995-December 2016, and summed into monthly totals. Province-averaged 30-year (October 1981- May 2011) averages are also calculated for each month of the cool season, and percent of normal values determined for each month in the study period. From the start (October 1) of each cool season, a cumulative sum of daily average precipitation is calculated and the date of exceedance of the 250 mm threshold is noted as pink bars in Figure 2.12.

Dates of several regional shallow landslide responses are shown together with OTPE and antecedent rainfall to illustrate the relationship among these variables. Regional landslide events shown (as red diamonds in Figure 2.12) in the Transverse Ranges are as follows:

- 10 January 1995: “numerous events” (Bedrossian 1996; Irvine 1996; Wills et al. 2017)
- 3 February 1998: “>20,000 events” (Hansch et al. 2001; Morton et al 2003; Wills et al. 2017)
- 5 March 2001: “382 events” (Stock and Bellugi 2011; Wills et al. 2017)
- 9-10 January 2005: “>2000 events” (Stock and Bellugi 2011; Wills et al. 2017)

2.7 Coastal wind observations

To examine the relationship between coastal OTPE and flow direction, surface wind speed and direction derived from Advanced Scatterometer (ASCAT; Ricciardulli and Wentz 2016) are composited for four stations at representative locations in coastal

terrain that experienced the greatest numbers of OTPE during the study period. Only ASCAT passes within three hours of the OTPE observation are used and ASCAT is available for the period 2007-2015. ASCAT has 12.5 km horizontal resolution and was chosen over station wind observations as it more accurately represents the larger scale flow and potential for orographic enhancement in the area, where individual station wind observations may be biased by local terrain.

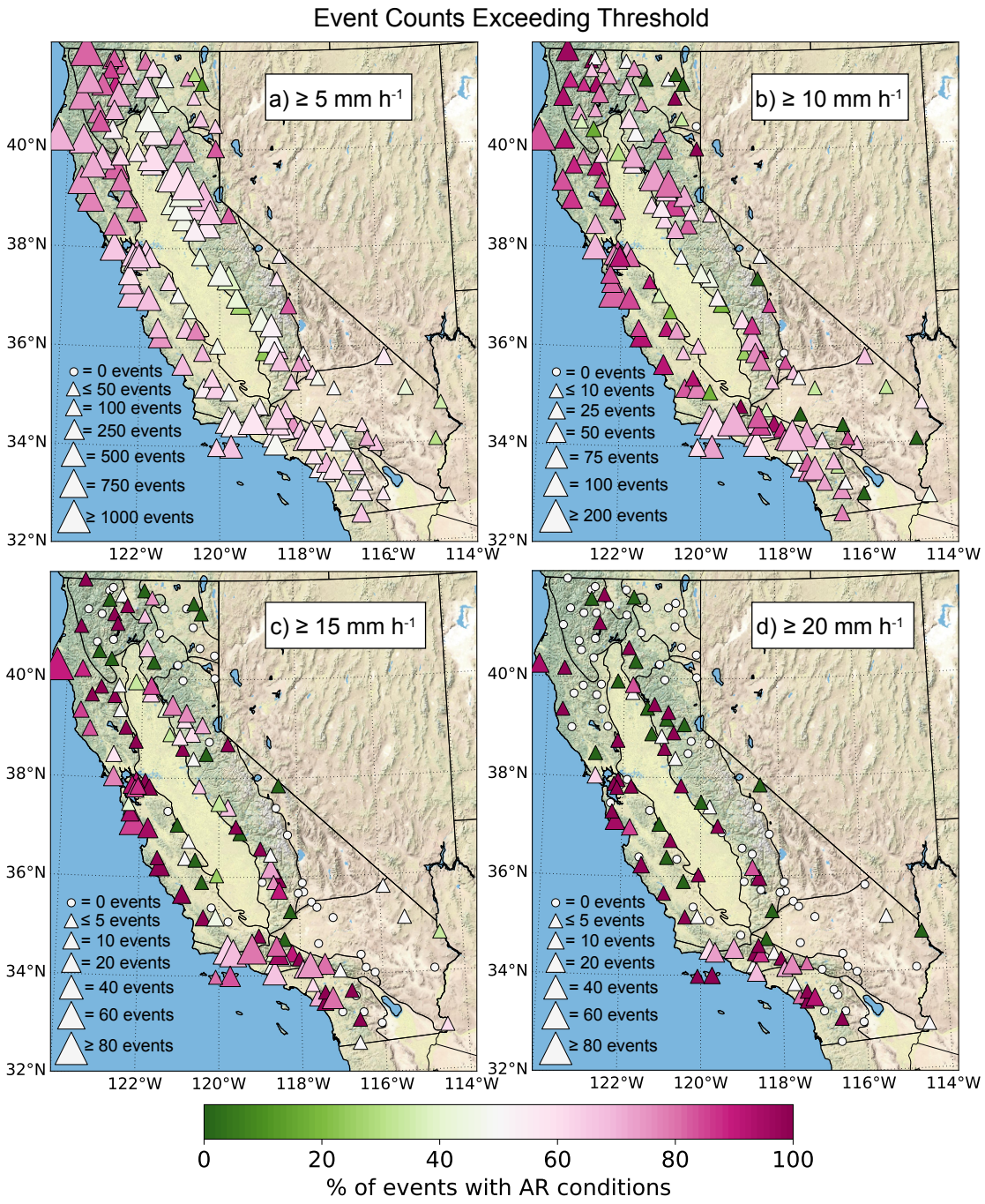

Figure 2.2. *Marker size indicates the number of over threshold precipitation events (OTPE) for months of Oct-May spanning the period 1995-2015. Percent of events associated with atmospheric rivers (ARs) are represented by marker color. For: a)* T_5

threshold, b) T_{10} threshold, c) T_{15} threshold and d) T_{20} threshold. AR catalog ends in 2015, thus 2016 could not be incorporated.

All OTPE	**Sierra Nevada**	**North Coast Ranges**	**South Coast Ranges**	**Transverse Ranges**
# stations	30	13	25	16
elevation	Range: 210-1677 m Mean: 1039 m Med: 1133 m	Range: 175-1310 m Mean: 501 m Med: 378 m	Range: 107-1524 m Mean: 553 m Med: 488 m	Range: 76-1661 m Mean: 753 m Med: 565 m
5 mm h^{-1} **T_5**	Range: 35-1519 Mean: 487.3 Median: 425	Range: 225-2883 Mean: 741.2 Median: 654	Range: 49-1348 Mean: 358.2 Median: 307	Range: 122-823 Mean: 384.6 Median: 326
10 mm h^{-1} **T_{10}**	Range: 0-185 Mean: 43.2 Median: 33	Range: 10-615 Mean: 87.6 Median: 41	Range: 6-310 Mean: 55.6 Median: 41	Range: 8-198 Mean: 78.9 Median: 51
15 mm h^{-1} **T_{15}**	Range: 0-22 Mean: 5.9 Median: 4	Range: 1-130 Mean: 15.5 Median: 5	Range: 0-77 Mean: 13 Median: 6	Range: 2-71 Mean: 22.5 Median: 16
20 mm h^{-1} **T_{20}**	Range: 0-6 Mean: 1.1 Median: 1	Range: 0-21 Mean: 2.6 Median: 0	Range: 0-24 Mean: 3.2 Median: 1	Range: 0-26 Mean: 7.4 Median: 4
7.5 mm h^{-1} 3h **T_{3h}**	Range: 0-109 Mean: 23.1 Median: 8	Range: 0-316 Mean: 38.2 Median: 12	Range: 0-188 Mean: 25.7 Median: 8	Range: 4-107 Mean: 35.5 Median: 19
5 mm h^{-1} 6h **T_{6h}**	Range: 0-164 Mean: 32.3 Median: 16	Range: 2-385 Mean: 49.5 Median: 22	Range: 0-179 Mean: 22.4 Median: 7	Range: 1-97 Mean: 29.1 Median: 14

Table 2.1. *For four selected geomorphic provinces: Number of stations per province (row 1); range, mean and median elevation of stations in each province (row 2); and range, mean and median count of OTPE among stations in each province (rows 3-8). Information in Table 2.1 corresponds with Figures 2.1 and 2.2.*

3. Results

For brevity, only the four provinces of greatest interest due to known high landslide occurrence or high numbers of OTPE are described within the manuscript: North Coast Ranges, South Coast Ranges, Transverse Ranges, and Sierra Nevada (Figure 2.1).

3.1. Spatial distribution of OTPE

Events exceeding the T_5 threshold were abundant throughout much of the state, excepting the desert areas lying east of the Sierra Nevada, Transverse, and Peninsular Ranges. Some stations experienced over 1000 such events over the period studied (Table 2.1). For comparable scaling with other thresholds, markers indicating a maximum of 300 events are shown.

At the T_{10} threshold (Figure 2.2b), the number of OTPE is lower than the T_5 threshold; the province median drops from several hundred events in T_5 to 30-50 events for T_{10} (Table 2.1). The low instance of T_{10} events is consistent with analysis by Lamjiri et al. (2017) who show this threshold to be at the extreme tail of hourly precipitation distributions along the West Coast. At T_{10}, regions experiencing high OTPE begin to stand out: the Transverse Ranges, Cape Mendocino, the San Francisco Bay Area, and the northern Sierra Nevada.

The number of OTPE further drops across the state at the T_{15} threshold (Figure 2.2c); the median event count falls substantially at this threshold to <10 in the Sierra Nevada, North and South Coast Ranges. The Transverse Ranges have a higher median of 16 OTPE, more than triple the other provinces. This may be related to more stations

situated at higher elevation in this province; mean and median elevation is higher than in the North and South Coast Ranges. The Sierra Nevada stations tend to be higher than Transverse Range stations (Table 2.1), but may have circulation characteristics less conducive to high intensity events. Regions with high OTPE count at T_{15} are similar to those observed for T_{10}. Achieving the T_{20} threshold (Figure 2.2d) is rare across the state; many stations have no OTPE at this threshold. The highest count of 26 T_{20} OTPE was observed in the Transverse Ranges (Table 2.1). Median province values range from 0 to 4 (Table 2.1). Regions experiencing T_{20} OTPE are similar to those observed for T_{10} and T_{15}.

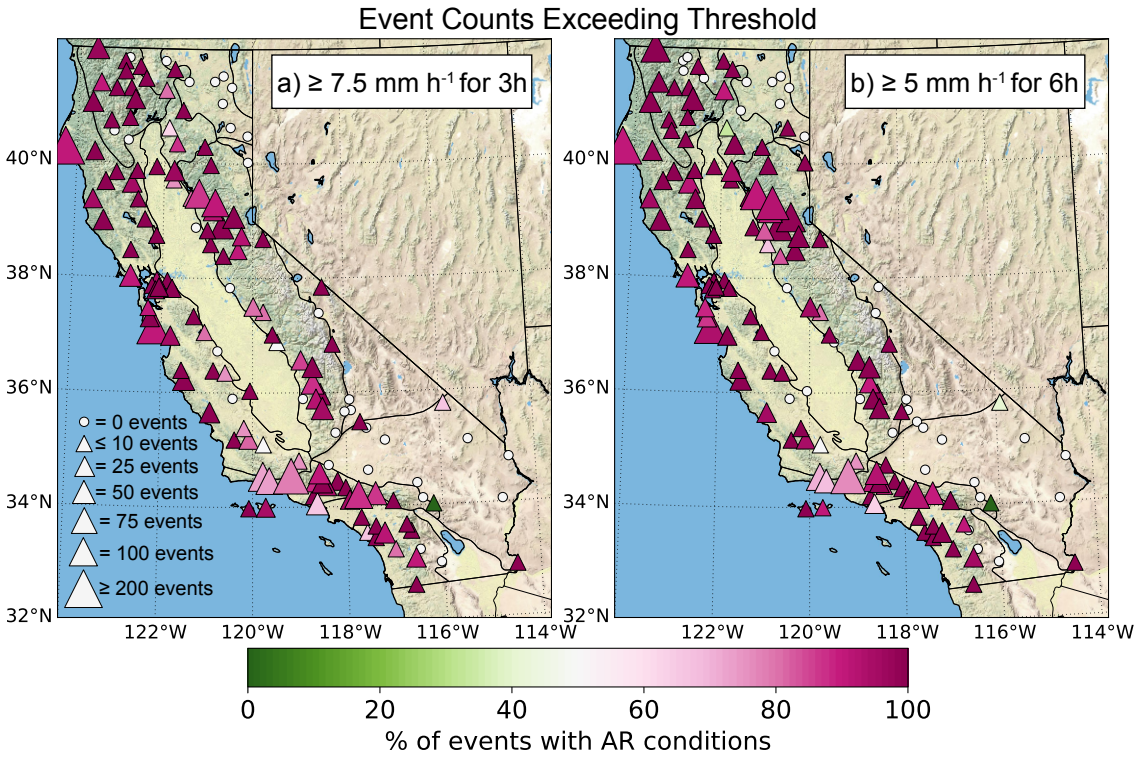

Figure 2.3. *As in Figure 2.2, for: a) T_{3h} threshold, b) T_{6h} threshold.*

For the multi-hour thresholds, similar spatial patterns emerge as observed in the hourly rates. For both T_{3h} and T_{6h}, the areas of greatest number of OTPE are found in the North Coast Ranges, San Francisco Bay Area, the Transverse Ranges, and the northern Sierra Nevada (Figure 2.3). The range and median number of T_{3h} OTPE is higher than that of T_{6h} OTPE for the South Coast and Transverse Range provinces, while the range and median number of T_{6h} OTPE is greater than T_{3h} for the Sierra Nevada and North Coast Ranges (Table 2.1). Multi-hour frequencies are overlapping such that a seven hour period where each hour exceeds 5 mm h^{-1} would count as two T_{6h} OTPE.

The provinces experiencing the highest frequencies of OTPE are consistent with Brabb et al. (1999) and Wills et al. (2017) who indicate the North Coast Ranges are the most landslide-prone province, with the South Coast and Transverse Ranges also having high landslide incidence and susceptibility. The Sierra Nevada have infrequent landslide occurrence (Wieczorek 2002; Wills et al. 2017) but high counts of OTPE. This discrepancy may stem from a lack of shallow landslide observations in the sparsely populated Sierra, or a geology that requires extremely high precipitation rates or is not conducive to landslide activity (Wieczorek 2002).

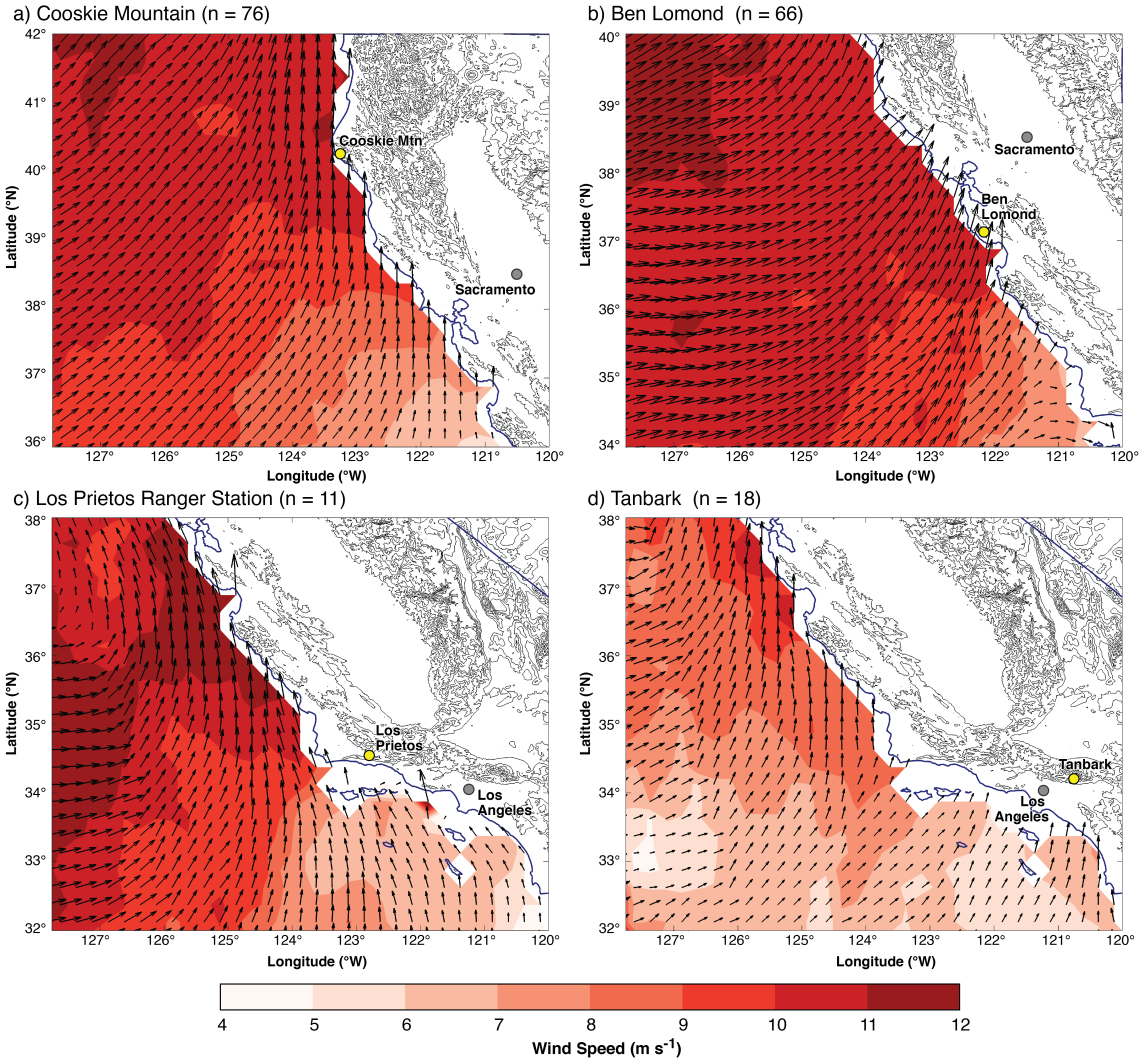

Figure 2.4. *Composite ASCAT-derived surface wind speeds (filled contours, units in ms^{-1}) and directions (shown as vectors) for T_{10} (10 mm h^{-1}) precipitation events observed from 2007-2015 for RAWS stations: a) Cooskie Mountain, b) Ben Lomond, c) Los Prietos Ranger Station, and d) Tanbark. The number of ASCAT observations included each composite are noted on each map.*

3.2 Relationship with atmospheric rivers and other atmospheric features

At the T_5 threshold, the strongest relationship with ARs is in the northwestern part of the state. Further south, the relationship is more variable, with much of the Transverse Range region observing 50-70% of OTPE associated with ARs (Figure 2.2a). A similar pattern is observed in the T_{10} threshold (Figure 2.2b). Though overall AR prevalence is higher (and number of OTPE is lower) across the state at T_{10}, a higher fraction of OTPE are associated with ARs in the North and South Coast Ranges and northern Sierra Nevada than the Transverse Ranges. This pattern is consistent with previous work that has examined AR contribution to annual precipitation, where the fraction of cool season precipitation associated with ARs is much higher in the northern two-thirds of California (Rutz et al. 2014).

As the number of OTPE dwindle in the T_{15} and T_{20} thresholds (Figure 2.2 c, d), the relationship with ARs becomes more variable in space, however AR conditions still dominate in the coastal areas and some Sierra Nevada locations. These high intensity precipitation events are associated with vigorous convection, which can occur both within an atmospheric river system and during other types of events, such as cutoff low-pressure systems, that feature instability (Abatzoglou 2016). Other features such as convergence and high intensity precipitation along a cold front (e.g., Neiman et al. 2004) can also produce somewhat isolated high intensity precipitation in the absence (or presence) of an AR and can help explain variations in counts of OTPE across provinces and non-AR events.

For the multi-hour thresholds, typically >80% of OTPE are associated with ARs across the state. A few locations in the Transverse Ranges and the South Coast Ranges

for T_{3h} are in the 60-80% range. This is consistent with findings that ARs produce long duration precipitation and high storm total rainfall along the West Coast (e.g., Ralph et al. 2006; Ralph and Dettinger 2012; Lamjiri et al. 2017).

The high percentage of OTPE at all intensities and durations associated with ARs helps to explain the spatial distribution of OTPE throughout California. One key feature of an AR is a low-level southerly jet (LLJ; Ralph et al. 2005, 2006), which typically spans a horizontal width of several hundred kilometers. The strength of the LLJ is positively correlated with hourly rainfall rates in coastal terrain (Neiman et al. 2002). Along south facing coastlines, the LLJ is often orthogonal to the terrain, favoring the greatest upslope wind speeds and thus high precipitation rates. This hypothesis of stations with a southerly exposure preferentially observing OTPE is supported by composite ASCAT surface winds during T_{10} events (Figure 2.4). Composite winds are southerly with respect to each station and its surrounding area.

The northern Sierra OTPE maximum can be explained by a known coastal terrain gap at the San Francisco Bay. Moist, low-level air associated with ARs can pass through this gap and across the Central Valley, where it is then lifted orographically by the Sierra Nevada (Rutz et al. 2015; White et al. 2015). The stations representing the central Sierra are generally lower in elevation than stations in the northern and southern regions and also blocked by the Coast Ranges, which may explain low OTPE counts in that area. The elevation of the Coast Ranges upstream of the southern Sierra is characteristically lower, which potentially allows greater moisture transport to this area in a process similar to the San Francisco Bay gap and results in slightly higher OTPE values in the southern Sierra than the central Sierra.

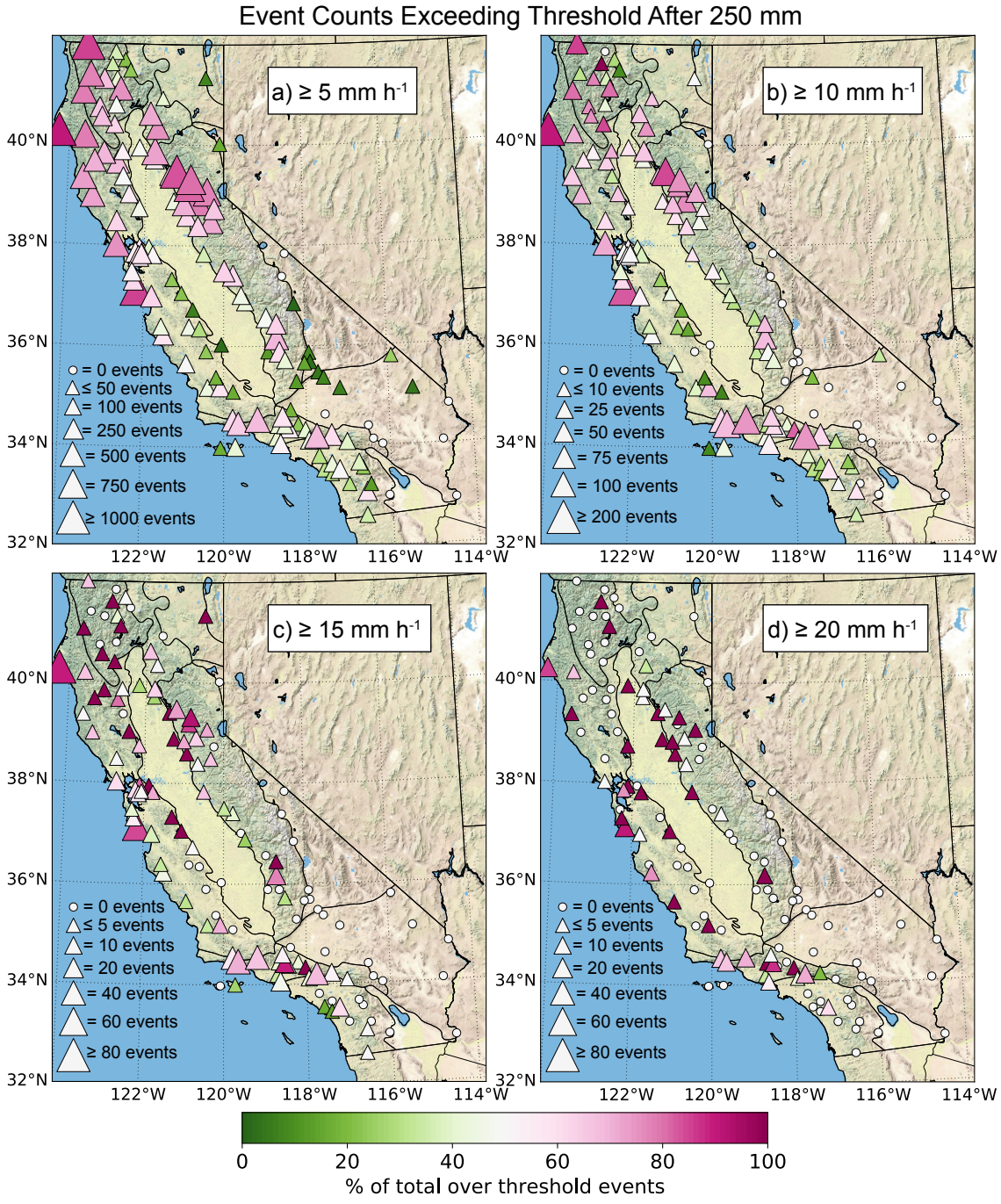

Figure 2.5. *Marker sizes indicate the number of OTPE occurring after the 250 mm antecedent precipitation threshold is met summed over each Oct-May season, 1995-*

2016 for a) T_5 threshold, b) T_{10} threshold, c) T_{15} threshold and d) T_{20} threshold. Marker colors indicate the fraction of total OTPE events at a station occurring after the 250 mm threshold has been met. Only Oct-May seasons with ≥70% of data available are incorporated, and only stations with ≥15 seasons of such data are displayed on map.

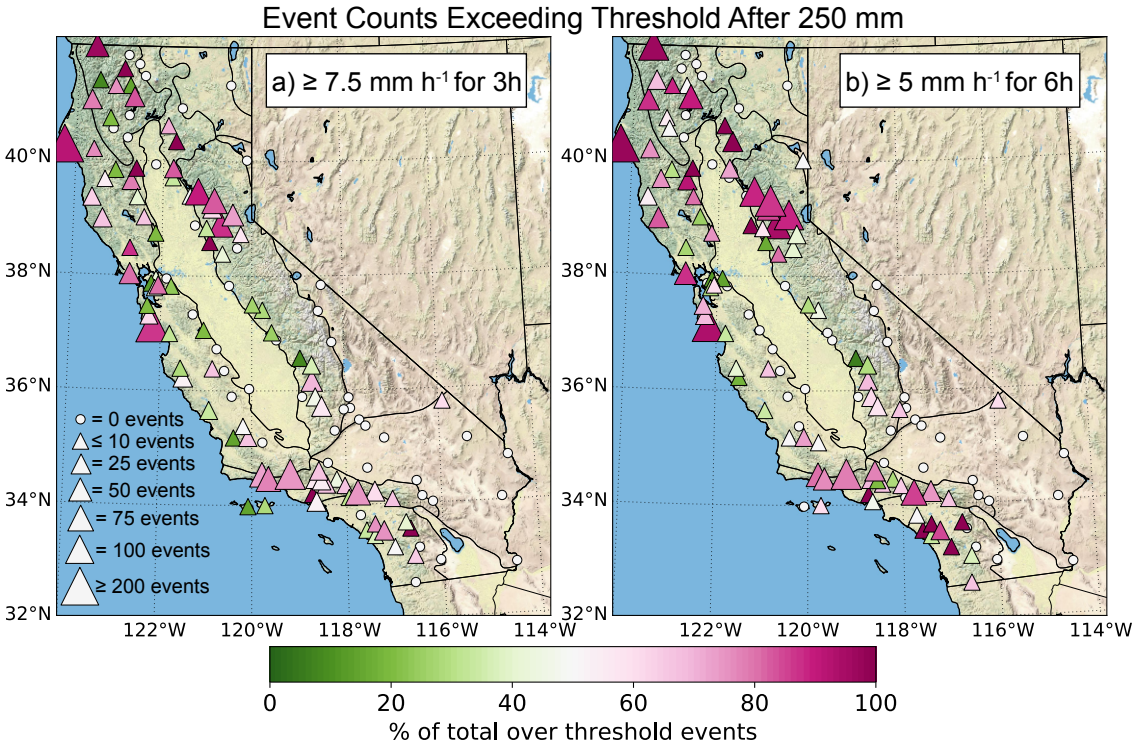

Figure 2.6. *As in Figure 2.5, for: a) T_{3h} threshold and b) T_{6h} threshold.*

After 250 mm OTPE	Sierra Nevada	North Coast Ranges	South Coast Ranges	Transverse Ranges
# stations	26 (of 30)	13 (of 13)	25 (of 25)	15 (of 16)
5 mm h^{-1} $T_{5\text{-}250}$	Range: 1-1156 Mean: 332.2 Median: 255	Range: 123-2544 Mean: 531.4 Median: 384	Range: 2-1147 Mean: 191.2 Median: 145	Range: 24-501 Mean: 192.9 Median: 150
10 mm h^{-1} $T_{10\text{-}250}$	Range: 0-141 Mean: 28.4 Median: 18	Range: 4-551 Mean: 67.4 Median: 21	Range: 0-255 Mean: 30.1 Median: 15	Range: 2-135 Mean: 44.4 Median: 31
15 mm h^{-1} $T_{15\text{-}250}$	Range: 0-17 Mean: 3.6 Median: 2	Range: 0-116 Mean: 12.5 Median: 4	Range: 0-61 Mean: 7.2 Median: 2	Range: 0-42 Mean: 12.1 Median: 4
20 mm h^{-1} $T_{20\text{-}250}$	Range: 0-6 Mean: 0.7 Median: 0	Range: 0-18 Mean: 1.9 Median: 0	Range: 0-19 Mean: 2 Median: 0	Range: 0-15 Mean: 4.1 Median: 1
7.5 mm h^{-1} 3h $T_{3h\text{-}250}$	Range: 0-83 Mean: 15 Median: 6	Range: 0-289 Mean: 31.1 Median: 7	Range: 0-161 Mean: 15.4 Median: 2	Range: 1-71 Mean: 21.6 Median: 12
5 mm h^{-1} 6h $T_{6h\text{-}250}$	Range: 0-127 Mean: 24.2 Median: 6	Range: 0-371 Mean: 41.1 Median: 12	Range: 0-153 Mean: 14.2 Median: 2	Range: 0-75 Mean: 19.3 Median: 9
5 mm h^{-1} 6h with one 10 mm h^{-1} $T_{6h10\text{-}250}$	Range: 0-86 Mean: 13.8 Median: 3	Range: 0-302 Mean: 30.1 Median: 3	Range: 0-121 Mean: 11.3 Median: 1	Range: 0-68 Mean: 16.6 Median: 7

Table 2.2. *For four selected geomorphic provinces: Number of stations per province (row 1); range, mean and median count of OTPE among stations in each province after the 250 mm antecedent precipitation threshold has been met (rows 2-7); range, mean and median count of OTPE for exceedance of 250 mm antecedent precipitation threshold, T_{6h} threshold, and T_{10} threshold ($T_{6h10\text{-}250}$) among stations in each province (row 8). Information corresponds to Figures 2.4, 2.5, and 2.6b.*

3.3 OTPE after 250 mm antecedent seasonal precipitation threshold met

As to be expected, the count of OTPE occurring after the 250 mm antecedent season threshold was met decreased across all thresholds examined (Figures 2.5 and 2.6, Table 2.2) as compared to all OTPE (Figures 2.2 and 2.3, Table 2.1). For the single hour thresholds $T_{5\text{-}250}$, $T_{10\text{-}250}$, and $T_{15\text{-}250}$, the median count of OTPE was nearly half of that observed for T_5, T_{10}, and T_{15}. For the multi-hour thresholds $T_{3h\text{-}250}$ and $T_{6h\text{-}250}$, there is a bit more variability in decrease from count of all OTPE, with reductions in median ranging from 25-70% fewer events after 250 mm. These numbers are impacted by exclusion of some seasons and stations from the analysis due to lack of complete data (Section 2.4), but still provide an estimate for the change in number of OTPE across the state after the 250 mm season threshold has been met.

The same regions dominate in having the greatest number of OTPE after 250 mm as in analysis of all OTPE: portions of the Coast Ranges, the northern Sierra Nevada, and the Transverse Ranges. Across all thresholds, northern California tends to have a greater fraction of total OTPE occurring after 250 mm than in southern California, shown in darker magenta in Figures 2.5 and 2.6. Much of the northern part of the state observes higher mean annual precipitation totals than the southern portion. Additionally, the wettest month of the year is February for the Transverse and South Coast Ranges, whereas December and January are the wettest months for the Sierra Nevada and North Coast Ranges (Figure 2.10). This means the 250 mm threshold is typically reached much earlier in the year in the northern part of the state, allowing for more opportunities later in the season to have OTPE occur after the 250 mm threshold has been met. Using the 250 mm threshold across the state

creates a bias towards more after-250 mm OTPE in areas with higher mean annual precipitation, but as we do not know antecedent precipitation thresholds across most of the state, we apply this as a minimum estimate.

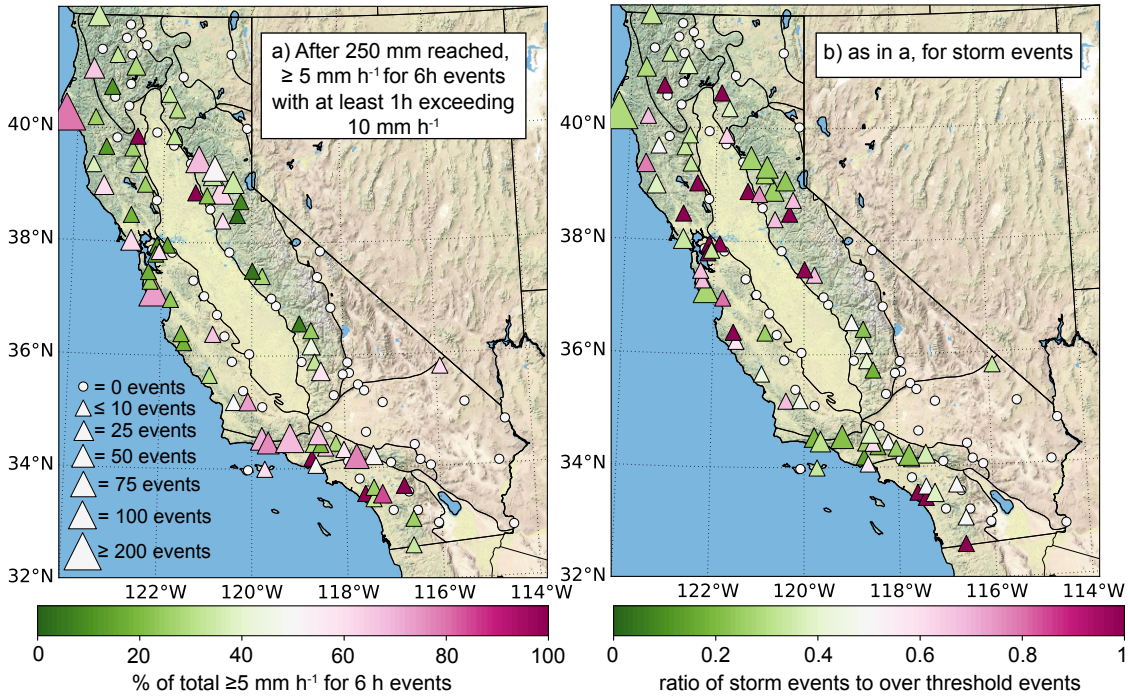

Figure 2.7: *In panel a), marker sizes indicate the number of events over the 1995-2016 period where the 250 mm antecedent precipitation threshold has been met, a ≥5 mm h^{-1} for 6h OTPE has occurred, and at least one of those six hours had a precipitation rate ≥10 mm h^{-1} (the $T_{6h10\text{-}250}$ threshold). Marker colors indicate the fraction of total ≥5 mm h^{-1} for 6h events at a station that meet these criteria. In panel b), marker sizes indicate the number of storm events producing $T_{6h10\text{-}250}$ events, and marker color indicates the ratio of storm events to $T_{6h10\text{-}250}$ events. Smaller (darker green) values indicate more $T_{6h10\text{-}250}$ events per storm, and larger values (darker magenta) indicate fewer $T_{6h10\text{-}250}$ events per storm.*

Some of California's most devastating landslides have occurred when soils were already moist (>250 mm antecedent rainfall), hourly rainfalls were intense (T_{10} event) and rainfall duration was sufficiently long to generate widespread pore pressures (T_{6h} event). The cases of this triple consequence (Figure 2.7 a) are significantly fewer than for the $T_{6h\text{-}250}$ threshold, especially in the northern part of the state. For example, Cooskie Mountain on Cape Mendocino in the North Coast Ranges observed 371 $T_{6h\text{-}250}$ events and only 302 $T_{6h10\text{-}250}$ events. In contrast, incidences in the Transverse Ranges did not decrease as much as other regions with the addition of the T_{10} requirement. Tanbark, in the central Transverse Ranges, observed 75 $T_{6h\text{-}250}$ events and 68 $T_{6h10\text{-}250}$ events (Table 2.2).

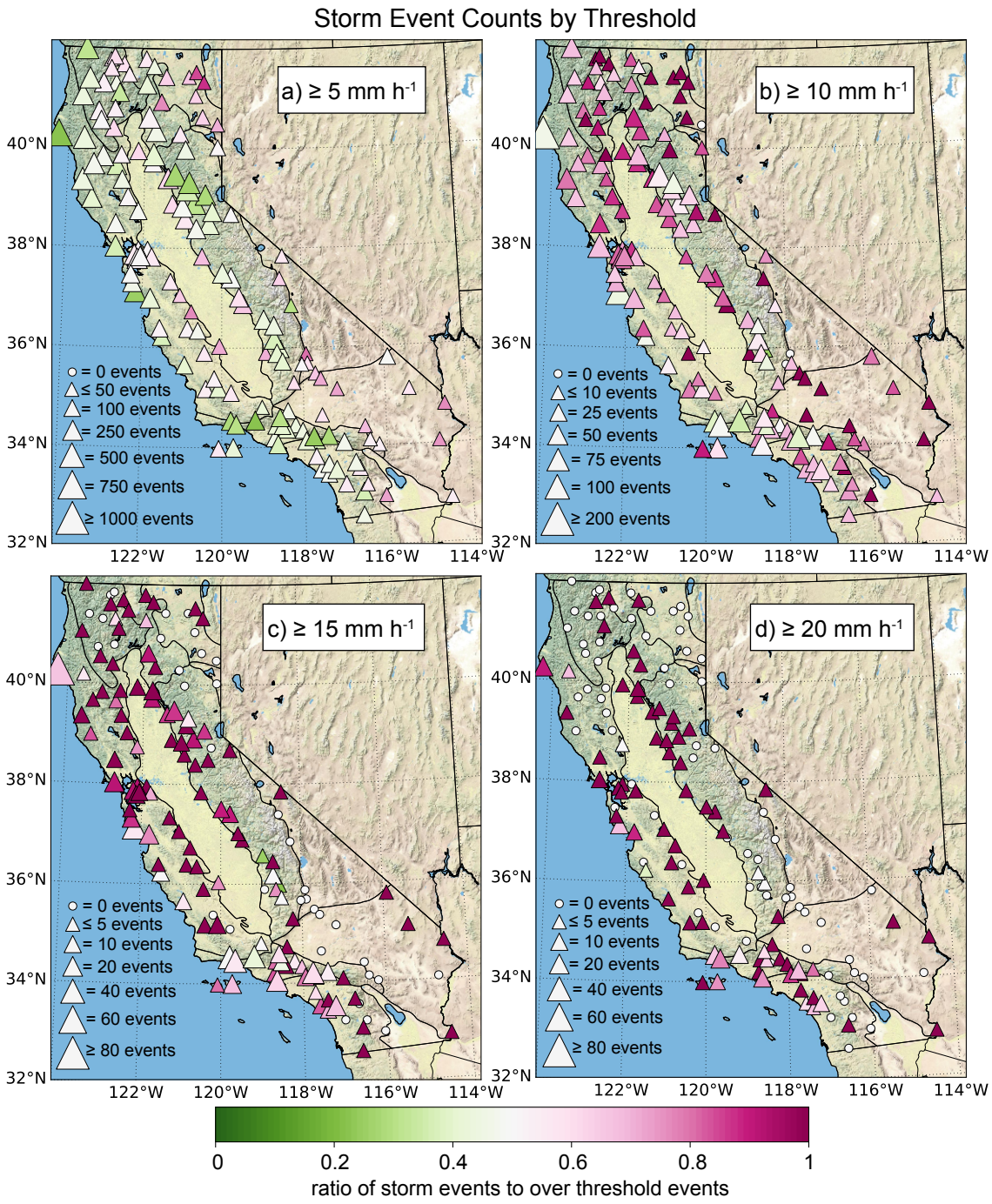

Figure 2.8. *Marker sizes indicate the number of storm events producing OTPE, and marker color indicates the ratio of storm events to OTPE at each threshold. Smaller (darker green) values indicate more OTPE events per storm, and larger values (darker*

magenta) indicate fewer OTPE per storm. For: a) T_5 threshold, b) T_{10} threshold, c) T_{15} threshold and d) T_{20} threshold.

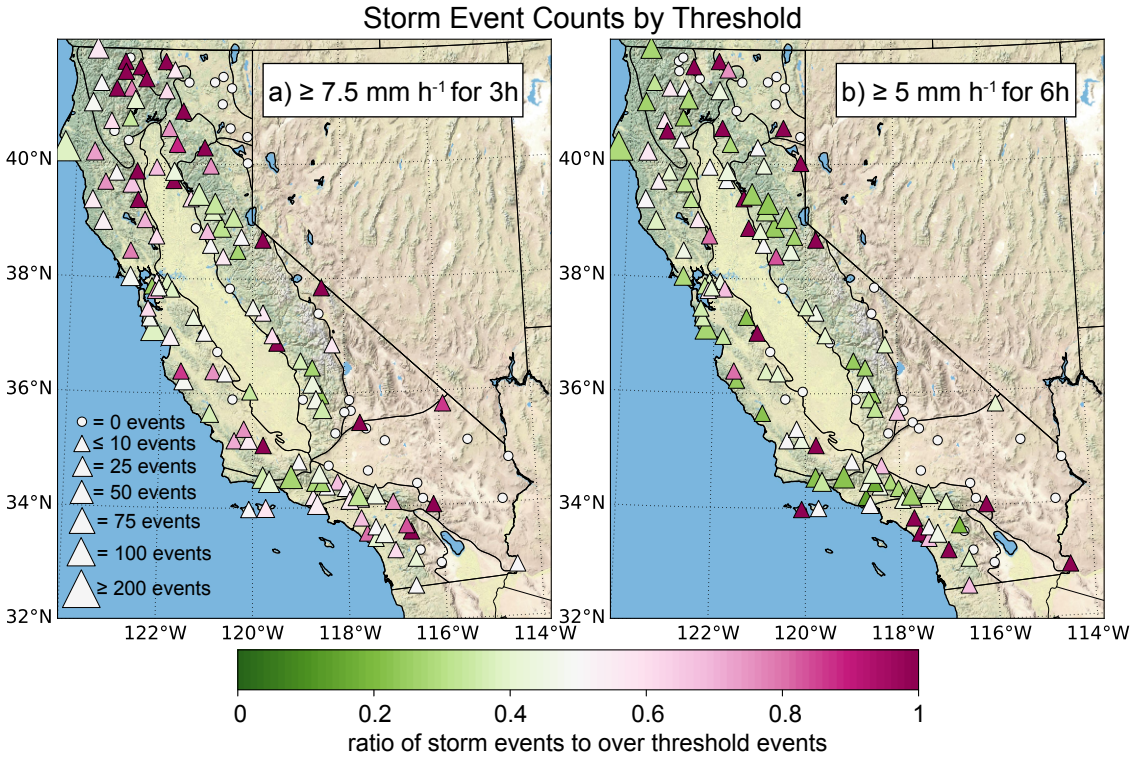

Figure 2.9. *As in Figure 2.8, for: a) T_{3h} threshold, b) T_{6h} threshold.*

3.4 Temporal distribution of OTPE

OTPE are considered to be part of the same storm event if they occur within 12 hours of each other. At the T_5 threshold, there is a generally a low ratio of storm events to OTPE across the state, indicating it is common for several OTPE to occur during a storm event (Figure 2.8a). At the more extreme T_{10} threshold, the ratio increases, indicating fewer OTPE per storm (Figure 2.8b). At the T_{15} and T_{20} thresholds, for most areas of the state, there is a close to 1:1 ratio between storms and OTPE (Figure 2.8 c, d). The

exception at these thresholds occurs in the Transverse Ranges, where there are cases of multiple OTPE per storm, shown by the <1.0 ratio. A few other stations in the state observe multiple OTPE per storm at these thresholds as well.

For the multi-hour thresholds T_{3h} and T_{6h} it is common to see a low ratio of storm events to OTPE, especially in the areas of frequent OTPE (Figure 2.9; Cape Mendocino and parts of the North Coast Ranges, northern Sierra Nevada, San Francisco Bay Area, and the Transverse Ranges). Across the state, the T_{6h} threshold displays slightly more OTPE per storm than the T_{3h} threshold. For the multi-threshold OTPE, $T_{6h10\text{-}250}$, it is common for multiple events to occur within a storm (Figure 2.7 b). This suggests that these OTPE are not necessarily frequent over time, but are likely to occur multiple times in a significant storm.

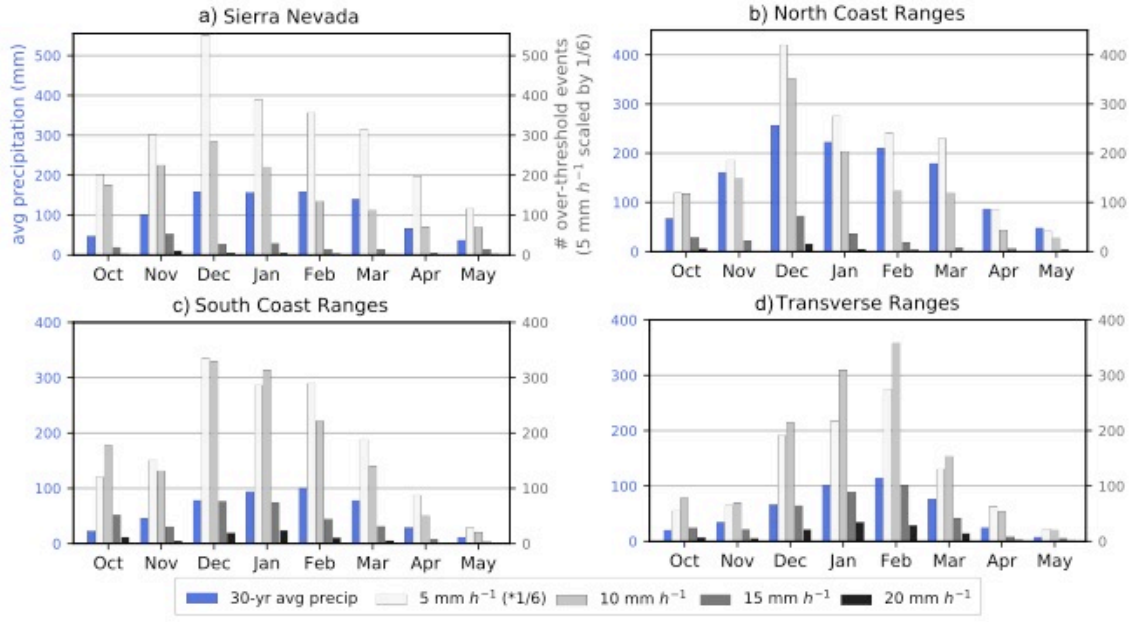

Figure 2.10. *Histograms of 30-year average precipitation derived from PRISM averaged over each province (blue bars), and monthly count of T_5 (white bars), T_{10} (light grey bars), T_{15} (dark grey bars), and T_{20} (black bars) OTPE by province. Due to*

the large number of T_5 events, they are scaled by a factor of 1/6 such that they can be displayed alongside the other hourly thresholds. Plots are show for the a) Sierra Nevada, b) North Coast Ranges, c) South Coast Ranges, and d) Transverse Ranges provinces.

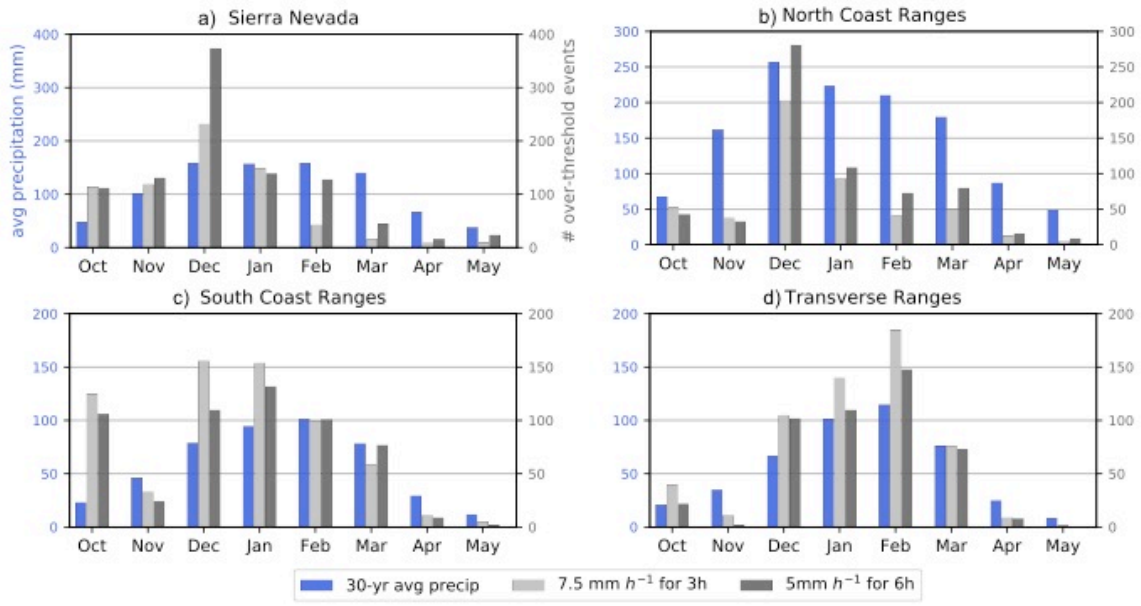

Figure 2.11. *Histograms of 30-year average precipitation derived from PRISM averaged over each province (blue bars), and monthly count of T_{3h} (light grey bars) and T_{6h} (dark grey bars) OTPE by province. Plots are show for the a) Sierra Nevada, b) North Coast Ranges, c) South Coast Ranges, and d) Transverse Ranges provinces.*

Across all four provinces and all six thresholds, OTPE were most frequent in the months of December, January, and February (Figures 2.10 and 2.11). Broadly across California, the wettest month of the year is typically December in the northern part of the state, January in the central portion, and February in the south, with transitional areas in between (WRCC 2017; Figure 2.10). The month of highest incidence of OTPE at stations

within each province generally coincides with this pattern. There is an exception in the Sierra Nevada and South Coast Ranges. These provinces span a large latitudinal range across transitional areas, producing a discrepancy between the climatological wettest month and peak month for OTPE, though the relationship generally holds at the station level.

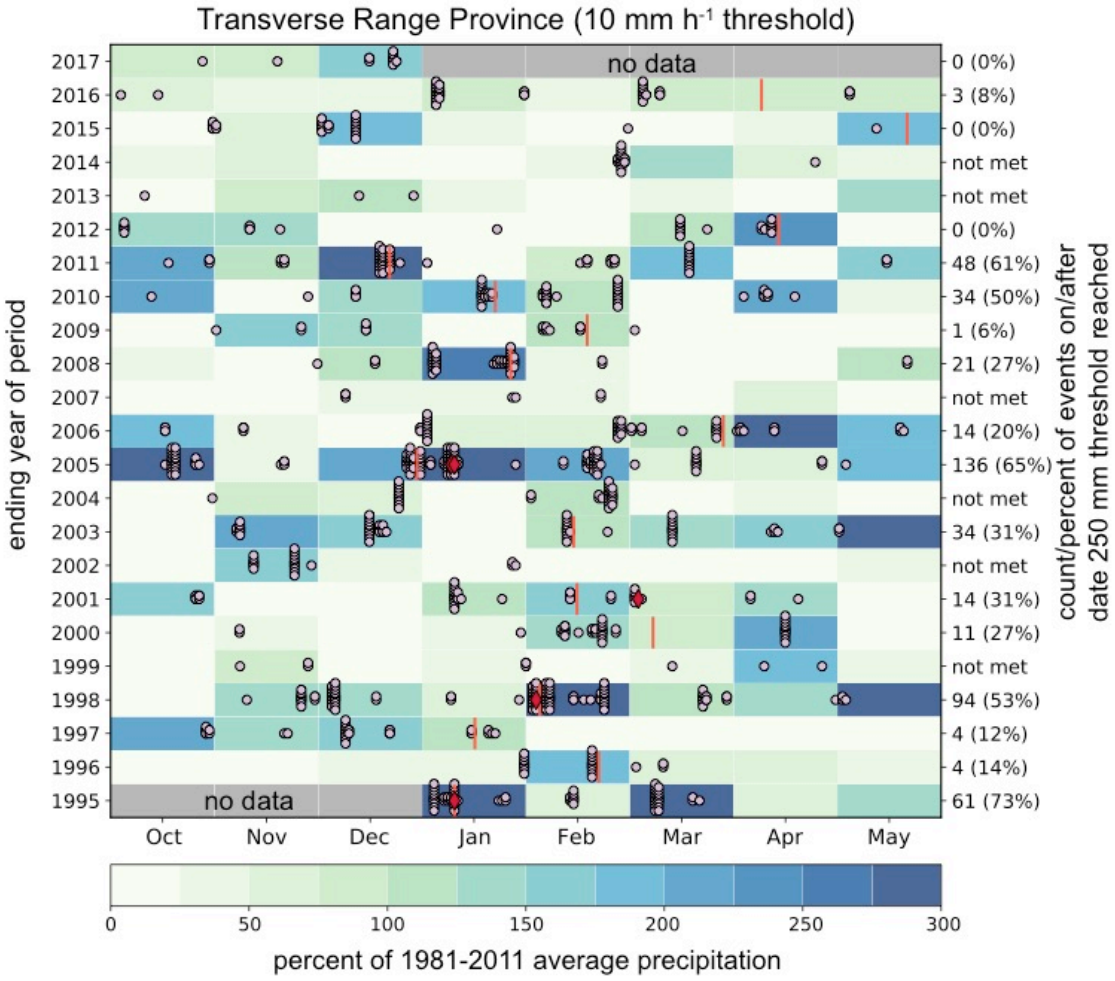

Figure 2.12. *Monthly percent of normal precipitation (colored squares), date on which 250 mm antecedent precipitation threshold is achieved (pink bars), date and number of T_{10} OTPE (light pink circles; a maximum of 10 OTPE for a date shown), and*

regional shallow landslide events (red diamonds) for the Transverse Ranges geomorphic province. Text on right side of each panel provides the number of OTPE occurring after the 250 mm threshold is achieved in each season and that number as a percent of season total OTPE. References for shallow landslide events are provided in Section 2.6. No OTPE are included for October-December 1994 and neither OTPE nor percent of normal precipitation data are included for January-May 2017; OTPE analysis spans only calendar years 1995-2016.

Figure 2.12 provides an example of the variability of OTPE through time, demonstrated using the Transverse Range province and the T_{10} threshold. The number of total OTPE and OTPE occurring after the 250 mm antecedent precipitation threshold is highly variable from year to year. Six years in the Transverse Ranges did not reach 250 mm threshold based on PRISM data. OTPE tend to occur in clusters during storm events, with multiple OTPE across the province happening on a single day or sequence of days. Regional shallow landslide events (red diamonds in Figure 2.12) occur coincident with, or following, exceedance of after the 250 mm threshold and multiple OTPE in the province.

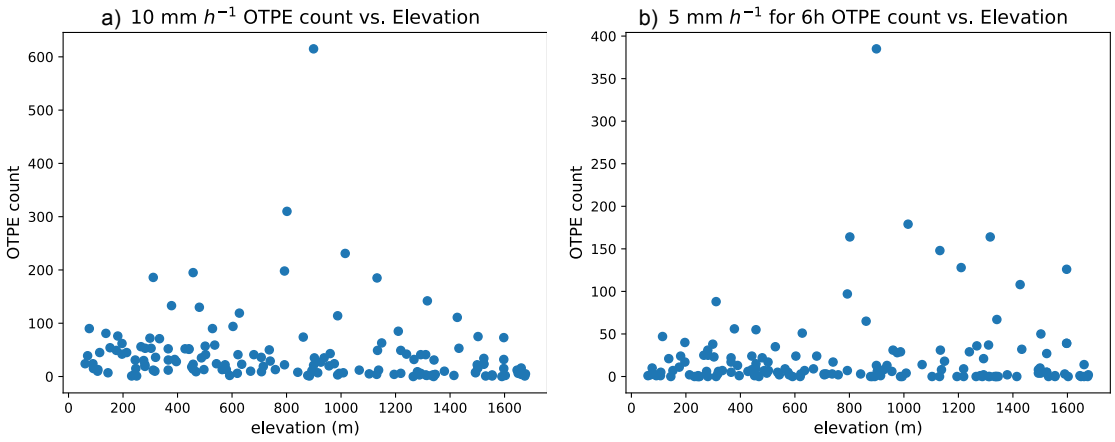

Figure 2.13. *Number of over threshold precipitation events compared with elevation for a) 10 mm h^{-1} (T_{10}, r^2 = 0.01) and b) 5 mm h^{-1} for 6h (T_{6h}, r^2 = 0.01) for 147 RAWS stations used in this study.*

3.5 OTPE relationship to elevation

We use a scatterplot (Figure 2.13) to examine potential relationships between OTPE count and elevation. For brevity, only results of this analysis for only T_{10} and T_{6h} are provided. In an idealized case at a local scale, we would anticipate precipitation intensity to increase with elevation (e.g., Lin et al. 2001; Neiman et al. 2002). In the California-wide approach taken here, no relationship between OTPE and elevation exists ($r^2 < 0.05$ for all thresholds). Table 2.1 also illustrates the tenuous relationship between elevation and OTPE; provinces with higher elevation stations do not necessarily observe a greater number of OTPE at each threshold.

There are several possible explanations for why we do not see a clear elevation-OTPE relationship. First, station siting with respect to upstream large-scale terrain features play a major role in precipitation distribution. Moisture flux convergence driven

by regional topography or gaps in upstream terrain can enhance the likelihood of heavy precipitation (White et al. 2015) while higher elevation upstream can reduce this likelihood by creating a rain shadow effect (Ralph et al. 2003). We do not account for station aspect in this analysis as aspect can be considered at many different spatial scales; to evaluate the best representation of aspect with respect to precipitation for each station is beyond the scope of this study. Second, mesoscale circulations related to terrain such as the Sierra Barrier Jet (Lundquist et al. 2010) or other blocking regimes (e.g., Hughes et al. 2009) can affect orographic precipitation gradients. Third, there are climatological variations in precipitation across the state that affect the number of opportunities for OTPE to occur, and those variations are not considered in this bulk analysis. Regional evaluations would yield a much smaller station sample size and still do not provide the elevation transect information needed to adequately address this issue.

4. Discussion

Exceedance of antecedent moisture and precipitation intensity-duration thresholds has long been the standard for forecasting which rainfall intensities will trigger shallow landslides (e.g., Caine 1980; Guzzetti et al. 2008). Previous work has evaluated variability of sub-daily precipitation intensities in California (Brooks and Stensrud 2000; Palecki et al. 2005; Lamjiri et al. 2017) and tools such as NOAA Atlas 14 (https://hdsc.nws.noaa.gov/hdsc/pfds/pfds_map_cont.html) provide precipitation intensities at various recurrence intervals at a point. This study fills an important information gap by presenting a climatological analysis of the spatial and

temporal distribution of precipitation exceeding intensities pertinent to historic landsliding.

Our results support the refinement and development of landslide-triggering thresholds by demonstrating where and how frequently precipitation over various intensities occurs. For example, the northern Sierra Nevada have some of the highest counts of OTPE in the state for most thresholds; however, observed landslide incidence is low in the region (Figure 2.1). This information can help geologists weigh the impacts of observation bias, geology, and precipitation intensity in representing landslide activity in this region. For some stations in the Transverse Ranges, the number of storm events where multiple triggering thresholds are met (e.g., Figure 2.7b) is greater than the number of known widespread landslide events in this region. This provides confirmation that factors beyond exceedance of precipitation thresholds play a role in landslide susceptibility. For example, mid-winter dry periods may reduce soil moisture such that a simple seasonal antecedent rainfall total is not applicable. Alternatively, shallow landslides in excessively well-drained soils may have little dependence on antecedent rainfall. The existence of storms where multiple triggering thresholds are met multiple times highlights the need for accurate forecasting of these storms and hourly to sub-hourly precipitation intensity and duration, a capability that is currently emerging in atmospheric science.

Permanent soil moisture sensors are limited in California, yet are a necessary tool for forecasting landslide activity (e.g. Baum and Godt 2010). Our results

elucidate where triggering rainfall is most likely to occur and, as a supplement to geological information, can inform where siting of new soil moisture sensors may provide the greatest benefit in landslide monitoring and warning systems. The precipitation intensity information generated in this study facilitates the development of a null shallow landslide map by indicating where high intensity precipitation during the cool season is unlikely in California. Incorporating climatological precipitation intensity data into landslide hazard mapping algorithms can be used to move from susceptibility maps to potential maps, as suggested in Wills et al. (2011).

The relationship of ARs to OTPE has implications for forecasting and situational awareness of potential landslide events. Integrated water vapor transport (IVT), one measure of AR conditions, has been shown to have better predictability than precipitation forecasts for a longer lead-time (Lavers et al. 2016). A variety of tools exist at the Center for Western Weather and Water Extremes (http://cw3e.ucsd.edu/) for monitoring the forecasted and observed intensity and duration of AR conditions in California. People involved in research or monitoring of landslide hazards can utilize these tools to support their work.

Several limitations exist in this research. The period analyzed is relatively short, spanning only slightly more than two decades, thus is limited in how much climatological variability is represented. The RAWS precipitation data have limitations due to their instrumentation and other factors described in Appendix B. The locations of RAWS used in this study do not represent all elevations and aspects,

and there are an unequal number of stations per province. We utilize only one precipitation gauge network in this study; during the research period, it was the most spatially relevant data that was both accessible and usable. This limited the challenges of evaluating inhomogeneity between station networks. Future work could expand this study to include multiple networks and sufficient data for interpolation between points in complex terrain.

There are a limited number of thresholds available in the literature that describe landslide triggering in California, and most are developed for the Transverse Ranges or San Francisco Bay Area (Guzzetti et al. 2007; http://rainfallthresholds.irpi.cnr.it/). The geologic and hillslope processes in these areas are a small sample of a geologically diverse state. While all potential intensity-duration thresholds are not assessed in this work, we cover a range that is inclusive of minimum and maximum values in published literature. We do not suggest the thresholds provided should be applied across the state, but rather provide these results as a guide to where OTPE at various thresholds occur such that the reader can relate them to known landslide activity or potential and other topics of interest dependent on high intensity precipitation.

5. Conclusions

We assessed the spatial and temporal variability of precipitation events exceeding published estimates of rainfall intensities that triggered historic shallow landslides. To do this, we utilized quality-controlled data (Appendix B) from Remote Automated Weather

Stations (RAWS) during the October-May season when landslides are likely to occur. We found that stations with exposure to southerly atmospheric flow in the Coast Ranges and Transverse Ranges experience high numbers of OTPE. The northwestern Sierra Nevada also observe frequent OTPE, related to the San Francisco Bay Area terrain gap (White et al. 2015). In the regions experiencing the highest OTPE, approximately 60-90% of OTPE are associated with atmospheric rivers. Number of OTPE varies greatly both within a season and inter-annually, though the greatest frequency of OTPE tends to coincide with the climatological wettest month of the year at all thresholds. It is common for many OTPE events to occur within an individual storm event, especially at lower intensities (T_5, T_{10}) or multi-hour thresholds. Areas of frequent OTPE generally match areas known to have the greatest landslide incidence or hazard (Figure 2.1; Brabb et al. 1999; Wills et al. 2017).

Shallow landslides that mobilize as debris flows threaten the lives and welfare of Californians and others living within and near steep around the world. Climate model projections suggest an increase in the frequency and duration of dry periods in California. These periods may be punctuated by more extreme precipitation events (Polade et al. 2015; Cook et al. 2015; Dettinger 2016), which can reduce the likelihood of reaching season antecedent precipitation thresholds. However, short duration precipitation extremes have already been observed to intensify over the observed record (e.g., Russo et al. 2013) and will likely intensify in a changing climate (Modrick and Georgakakos 2015; Prein et al. 2017), raising concern from the landslide triggering standpoint. Our work provides information on the current spatial and temporal patterns of precipitation at a

variety of intensities. This can serve as a baseline for considering future change and where intensification of extremes may pose the most significant threats.

Chapter 3

Origins and Variability of Extreme Precipitation in the Santa Ynez River Basin of Southern California

Nina S. Oakley, Forest Cannon, Eric Boldt , John Dumas, F. Martin Ralph

Abstract

Study Region: Santa Ynez River Basin, Santa Barbara County, California

Study Focus: Lake Cachuma, a reservoir on the Santa Ynez River, provides water for over 280,000 residents and agricultural lands of Santa Barbara County, California. This area experiences high inter-annual precipitation variability, which we hypothesize is driven by the presence or absence of a few large precipitation events each year. We use daily precipitation observations from 1965-2017 to identify extreme precipitation events, defined as those exceeding the 90th percentile. We examine the role of these events, their associated synoptic patterns, and the El Niño Southern Oscillation (ENSO) in driving inter-annual precipitation variability in this basin.

New Hydrological Insights for the Region: On average, a wet year features three or more extreme events, a normal year 1-2 events, and a dry year 0-1 events. We identify four distinct synoptic-scale weather patterns associated with extreme events and find that 74% of events are associated with atmospheric rivers. El Niño years tend to have a greater number of extreme events, though this relationship is not dependable. The reliance on just a few extreme precipitation events and diversity among these events highlights the challenges of seasonal prediction and resource management in this area. This novel approach to defining variability on a watershed scale can support ecological, geological, and hydrological studies as well as regional water resource management.

Highlights:

- The Santa Ynez River Basin exhibits high inter-annual precipitation variability
- The difference between a wet/dry year hinges on a few extreme precipitation events
- Observing ≥4 extreme events ensures wet year; 0-1 events dry to normal year
- El Niño years tend to have more extreme events, though considerable variability
- Extreme precipitation events are associated with multiple synoptic patterns

1.0 Introduction

Lake Cachuma, a reservoir on the Santa Ynez River in Santa Barbara County, California, gained local and national attention in early 2017 (e.g., Serna 2017). Following a multi-year drought, in early January 2017 Cachuma storage stood at 8% of capacity and 12% of historical average (California Department of Water Resources 2017), nearly shutting off agricultural deliveries and prompting water agencies to utilize other resources in their portfolios (e.g., purchasing water from other agencies). Two atmospheric river storms, featuring narrow corridors of high water vapor transport from the tropics (AMS 2017a), in late January and mid-February 2017 provided some relief for the area. These events raised the lake level to nearly 50% of capacity by late February. Without these two large storms, those

who depend on Cachuma for water resources would have been facing dire circumstances.

As observed in 2017, it is noted by individuals with water resource and hydrologic interests in the area that the difference between a wet, dry, or "average" year is often just a few storms (e.g. Burns 2017). However, the magnitude of this dependence has not been quantified at a local scale. We analyze station data from within the Santa Ynez River Basin to document precipitation variability due to large storms and investigate the associated synoptic meteorological conditions.

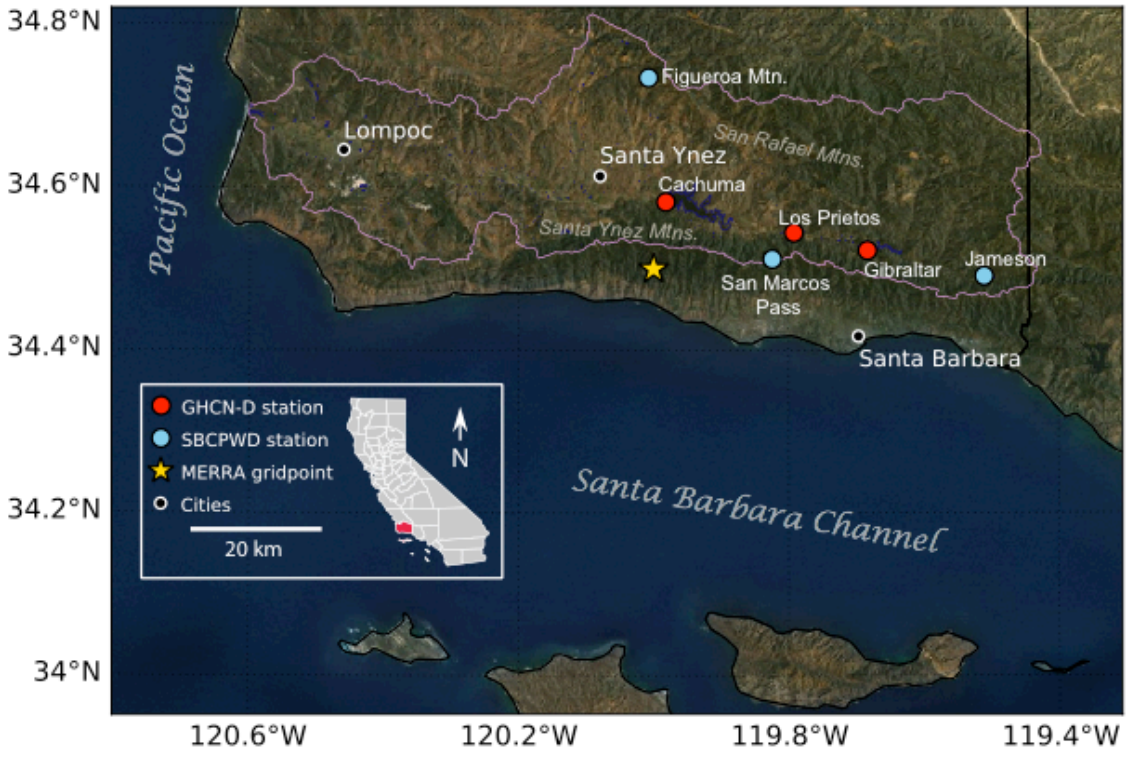

Figure 3.1. *Map of study area with relevant data points noted. The Santa Ynez River Basin is outlined in pink, and the six weather stations in the Basin are shown with blue and red markers.*

The Santa Ynez River drains a 2,322 km^2 area nestled in the Transverse Ranges of southern California (Figure 3.1). The basin is bounded to the south by the Santa Ynez Mountains (~300-1400 m) and to the north by the San Rafael Mountains (~600-2000 m). From east to west, the basin increases in elevation from sea level at its terminus near Lompoc, CA, to over 1200 m at its headwaters. Cachuma is the largest of three reservoirs on the river and was built in 1953 to meet growing water demands of the surrounding communities (Latousek 1995; Loáiciga 2001). Cachuma currently provides up to 85% of the water supply depending on district for over 280,000 Santa Barbara County residents and is used to irrigate over 15,000 acres of agricultural land (e.g., Goleta Water District 2017; Carpinteria Valley Water District 2017; Montecito Water District 2017).

Santa Barbara County is a semi-arid region characterized by high precipitation variability (Figure 3.2) and has a long history of impactful multi-year droughts (Upson and Thomas 1951; Latousek 1995; Loáiciga 2001). Several studies have addressed precipitation variability in California. The southern portion of the state observes larger differences between wet and dry years than anywhere else in the United States (Dettinger 2011), and some of the most extreme three-day precipitation events in the country occur in the Transverse Ranges (Ralph and Dettinger 2012). Additionally, the seven wettest days of each year account for more than 80% of the variations in total precipitation in southern California (Dettinger 2016). With regards to variability and the El Niño Southern Oscillation (ENSO),

>90th percentile precipitation days at San Diego are more likely during El Niño than La Niña. Over the period 1931-1995, 12 of 21 El Niño winters produced above normal (>5 days) of >90th percentile precipitation while only three of nine La Niña winters did the same (Cayan et al. 1999).

This research investigates the findings of previous studies relative to the Santa Ynez River Basin, using a unique approach of parsing daily precipitation observations into extreme precipitation events rather than using wet days. This definition is more representative of colloquially defined "storms", which relate more directly to local hazard and water management preparations and also agree well with a hydrologic approach of looking at the impact of wet periods rather than individual days (e.g., SBCPWD 2017). With the storm events generated, we answer these questions for the Santa Ynez River Basin:

1) What is a meaningful way to define normal, above normal, and below normal wet season precipitation totals?
2) What frequency and magnitude of precipitation events best represents inter-annual precipitation variability?
3) What synoptic patterns are favorable for large storm events, and what is the role of atmospheric rivers?
4) Does ENSO modify the frequency of extreme precipitation events in a way that offers predictive capabilities?

The results of this analysis provide quantitative knowledge that can be used by local agencies to communicate regional precipitation variability and impacts to

their stakeholders. These materials provide a broad understanding of regional drought mechanisms and risk, give insight to the challenges of seasonal prediction, and augment water managers' abilities to understand and plan for impactful events. Additionally, the novel investigation of regional precipitation variability may inspire new insights in ecological, geological, and hydrologic studies in Santa Barbara County, and serve as a baseline for evaluating change in the future.

2.0 Methods

We focus on precipitation during the wet season, which we define as October through May. Nearly all (>95%) of the area's precipitation occurs during this period (WRCC 2017).

2.1 Precipitation data

Period-of-record daily precipitation data were acquired from long-record (>50 years) stations in Santa Barbara County Public Works Department's (SBCPWD) Automated Local Evaluation in Real Time (ALERT) network of automated tipping bucket gauges (accessed online at http://www.countyofsb.org/pwd/dailyrainfall.sbc). These data have been quality controlled by SBCPWD and observation time is stated as 0800 Local Standard Time (LST) throughout the period of record. For precipitation days or periods where a particular gauge is not reporting, SBCPWD fills the station's record with data from another station of the network of similar elevation and situation within the terrain;

these stations are not displayed in Figure 3.1. SBCPWD data only reports dates on which precipitation occurred, thus it cannot be determined if missing dates are present. We make the assumption that the record is complete.

We also acquired period-of-record daily precipitation data for long record (>50 years) stations in the Global Historical Climatology Network-Daily (GHCN-D; Menne et al. 2012) through SC-ACIS (http://scacis.rcc-acis.org/; Figure 3.1). These data have been quality controlled by the National Centers for Environmental Information. Observation time ranges across the period of record for each station, but is generally 800 or 900 LST. While the records for the GHCN-D stations are fairly complete, some missing dates or periods were present. To build more complete precipitation events and season totals and in keeping with the approach used by SBCPWD, we fill missing data with a nearby station of similar elevation. Filled data represented the following fraction of non-zero precipitation days: 0.7% at Cachuma, 11% at Gibraltar, 21% at Los Prietos, and 3.75% at Santa Barbara. After the filling process, only wet seasons with >80% (>194 of 243 days) of complete observations at the GHCN-D stations are utilized in subsequent analysis.

2.2 Identifying precipitation events

Precipitation events are defined as one or more consecutive days with daily totals ≥2.54 mm (0.1 in). When applicable, events are additionally inclusive of days immediately preceding or following the event that have daily totals <2.54 mm.

Marine stratus occurs frequently in Santa Barbara County (Dorman and Winant 2000) and "fog drip" can result in measurable precipitation. As we are interested in dynamically driven events, we set the minimum event threshold and within-event threshold at 2.54 mm to avoid investigating periods of very light precipitation and to avoid bridging independent precipitation events.

The hydrologic definition of "precipitation event" used here references the space- and time-distribution of rainfall over a given region (AMS 2017b). This definition agrees with the colloquially defined concept of a "storm" in the region and informs non-meteorological interests such as geology, hydrology and ecology.

The only notable caveat to this methodology occurred during an active storm period in late January 1969. During the event, lower elevation stations observed a 1-day break in rainfall while higher elevation stations at Jameson and San Marcos did not. This merged what appear to be two independent storms at those higher elevation stations, resulting in a very long (9-day) event with an outlying precipitation total.

2.3 Developing a Basin Index

To describe characteristics of the Santa Ynez Basin collectively rather than by individual station, a "Basin Index" was created from six stations in the Basin: Cachuma, Gibraltar, Los Prietos, Jameson, San Marcos Pass, and Figueroa (Figure 3.1). The Index is calculated as a mean across the six stations at a seasonal timescale for each variable explored in this analysis (season precipitation total, season

extreme event total, contribution of extreme and non-extreme precipitation events). This approach is similar to that used in several multi-station indices in California (e.g., Northern Sierra 8-Station Index; http://cdec.water.ca.gov/snow_rain.html) used by the California Department of Water Resources to support management decisions.

Due to differences in observation time and precipitation event timing across the stations, it was not feasible to create the Index at the daily time scale. The resulting Basin Index record spans 1965-2017. The year 2006 is missing, as Cachuma and Los Prietos did not report sufficient data. Figure 3.2 shows the October-May precipitation total distribution for the Basin Index relative to its component stations.

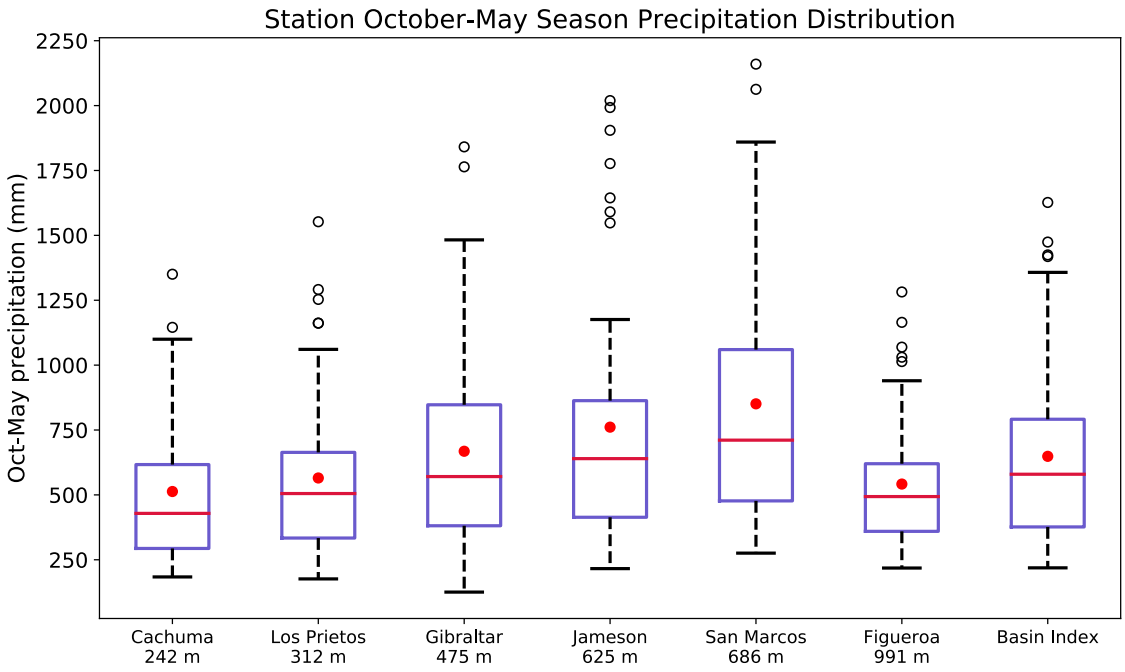

Figure 3.2. *Boxplots showing the precipitation distribution for the wet season (October-May) 1965-2017 for the six stations in the Santa Ynez Basin. The red dot in each box represents the station mean, while the horizontal red line reports the median among wet season precipitation totals.*

2.4 Extreme precipitation event definition

To determine what magnitude of precipitation event has the best relationship with wet season total precipitation, we calculated a variety of percentile values at each station from all precipitation events identified in Section 2.2. We focused on values above the 80th percentile, as previous work on extreme precipitation and variability used >90th percentile precipitation days (Cayan et. al 1999) and >95th percentile precipitation days (Dettinger 2016). We calculated the Pearson correlation coefficient between the precipitation contribution from events exceeding each percentile and total wet season precipitation for the Basin Index. Precipitation events exceeding the 90th percentile exhibited the strongest relationship with wet season total precipitation (r^2=0.89; Figure 3.3b), thus we select this threshold for subsequent analyses of variability. Precipitation events meeting or exceeding the 90th percentile are hereafter referred to as "extreme events". In contrast, precipitation from non-90th percentile events has a much weaker relationship with total wet season precipitation (r^2=0.38; Figure 3.3a).

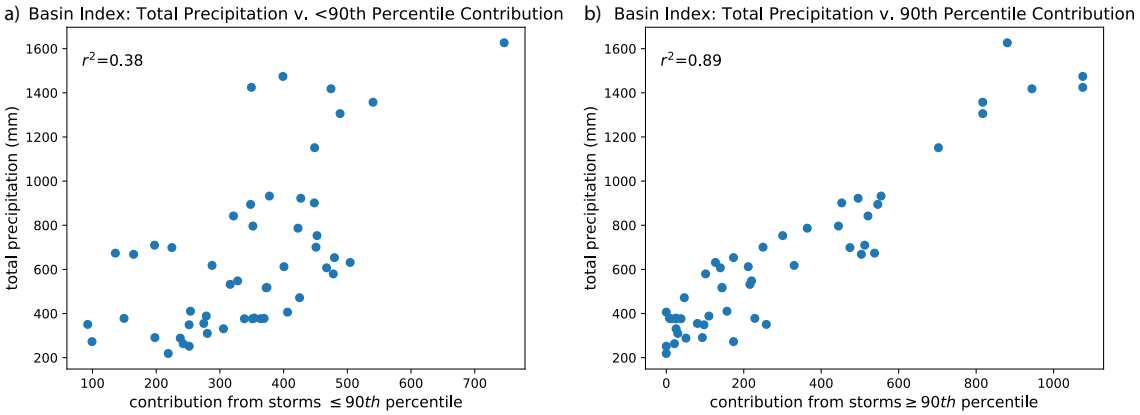

Figure 3.3. *Relationship between a) contribution from all storms <90th percentile and b) all storms ≥90th percentile and total wet season (October to May) precipitation for the Basin Index.*

2.5 Lake Cachuma storage data

Lake Cachuma monthly storage data were obtained from SBCPWD for the period 1955-2017. We selected June 1 of each year as representative of storage associated with a particular wet season. Average June 1 storage was calculated by taking the mean of all June 1 observations and departures from that value were calculated for each year (Figure 3.5). June 1 departures from average storage were very similar to those for March 1, April 1, and May 1; all displayed similar patterns of inter-annual variability. Many factors can affect lake storage, such as water use, downstream releases, and State Water Project deliveries, so this is not an accurate representation of storage due to precipitation only. However, this measure provides useful information on the effects of precipitation variability on lake storage and assists in defining wet and dry years.

2.6. Defining wet and dry years

Wet season precipitation totals in the Santa Ynez Basin are highly variable from year-to-year, positively skewed, and feature outliers (Figure 3.2). To explore differences in the frequency of extreme precipitation events between normal, wetter than normal, and drier than normal years, it is necessary to define these terms in a way that is sensitive to this distribution. The National Centers for Environmental Information's 30-year climate normals (currently 1981-2010; Arguez et al. 2012) are a common definition of typical weather conditions, with precipitation values exceeding the 30-year normal considered "wetter than normal" and amounts falling below, "drier than normal." However, departures from normal may not be the most telling measure of atypical climate conditions in an environment such as the Santa Ynez Basin, where a range of normal precipitation may be more appropriate, with abnormal values lying outside this range (Faiers 1988; Faiers 1989; Null 1990).

Here, a median and quartile approach to defining wet, dry, and normal years (Faiers 1988) is most consistent with observed impacts of precipitation variability in Santa Barbara County (e.g. Yates 1993; County of Santa Barbara 1998; US Drought Monitor 2018). In this approach, wet seasons (dry seasons) occupy the upper (lower) quartile, and normal seasons have totals within the interquartile range (Figure 3.5).

2.7 Comparison with atmospheric river catalog

Extreme events were compared to the Rutz et al. (2014) atmospheric river (AR) catalogue, which is based on NASA's Modern-Era Retrospective Analysis (MERRA; Rienecker et al. 2011). MERRA has a spatial resolution of 0.5° x 0.625° and a temporal resolution of 3 hours covering the period 1980-2017. The catalog requires an AR to have integrated water vapor transport (IVT; a measure combining moisture and wind speed through a vertical column of the atmosphere) exceeding 250 kg m^{-1} s^{-1} and a length exceeding 2000 km (Rutz et al. 2014). The MERRA grid point used to diagnose AR conditions in this analysis is shown in Figure 3.1. Moist, southerly low-level flow is often observed during atmospheric river storms in this area (e.g. Oakley et al. 2017). The selected grid point lies near the crest of the Santa Ynez Mountains south of Cachuma and is representative of conditions slightly upstream (in the atmospheric sense) of the Santa Ynez Basin.

2.8 Evaluating storm characteristics with atmospheric reanalysis data

To evaluate synoptic (large-scale) characteristics of extreme events, we utilize the MERRA reanalysis product (Rienecker et al. 2011). The moderate spatial and temporal resolution is sufficient for revealing synoptic features of interest such as jet placement and moisture transport. This is also complementary to the use of a MERRA-based AR catalog.

Atmospheric conditions are evaluated during the MERRA timestep with the highest IVT value on the wettest day of an extreme event at the Cachuma station. As

the Basin Index is comprised of seasonal averages of event precipitation and characteristics, it does not contain discrete storm events for which such a comparison can be made. The investigated variables include: geopotential heights and winds at several levels, integrated water vapor (IWV; total water vapor in the atmospheric column), and IVT. As the precipitation data generally has an observation time of 8:00-9:00 LST (16-17 UTC), MERRA timestamps from 15 UTC of the previous day to 15 UTC of the observation day are considered.

2.9 Comparison of storm events with ENSO phase

We utilize Oceanic Niño Index (ONI) data for 1950-2017 from the NOAA Climate Prediction Center. A season is considered to be El Niño or La Niña when the threshold of +/- 0.5 ONI is met for a minimum of five overlapping seasons (Climate Prediction Center 2017). Each season is also ascribed as weak-moderate (≥0.5 to <1.5 C anomaly) or strong (≥1.5 C anomaly) based meeting or exceeding the threshold for three consecutive overlapping three-month periods, as performed by Null (2018). The count of 90th percentile storms for each season is then assigned to the corresponding season in the ENSO data.

3. Results and Discussion

3.1 Variability associated with extreme (90th percentile) events

The precipitation contribution from extreme events has a strong relationship with season total precipitation (r^2=0.89; Figure 3.3b), while the relationship with

non-extreme events and total precipitation is much weaker (r^2=0.38; Figure 3.3a). These results are similar to Dettinger (2016), who finds the wettest 5% of wet days have a relationship of approximately r^2=0.8 to 0.9+ with total water year precipitation in the South Coast area. For the Basin Index, the mean seasonal contribution from non-extreme events is 343 mm with a standard deviation of 124 mm. For extreme events, the mean contribution is 305 mm with a standard deviation of 300 mm and there are, on average, 1.3 extreme events per year. The mean of season precipitation totals is 648 mm with a standard deviation of 360 mm. Though the mean precipitation contribution of non-extreme events is slightly higher, the variance among extreme events is much greater and more representative of the considerable variance observed in season precipitation totals.

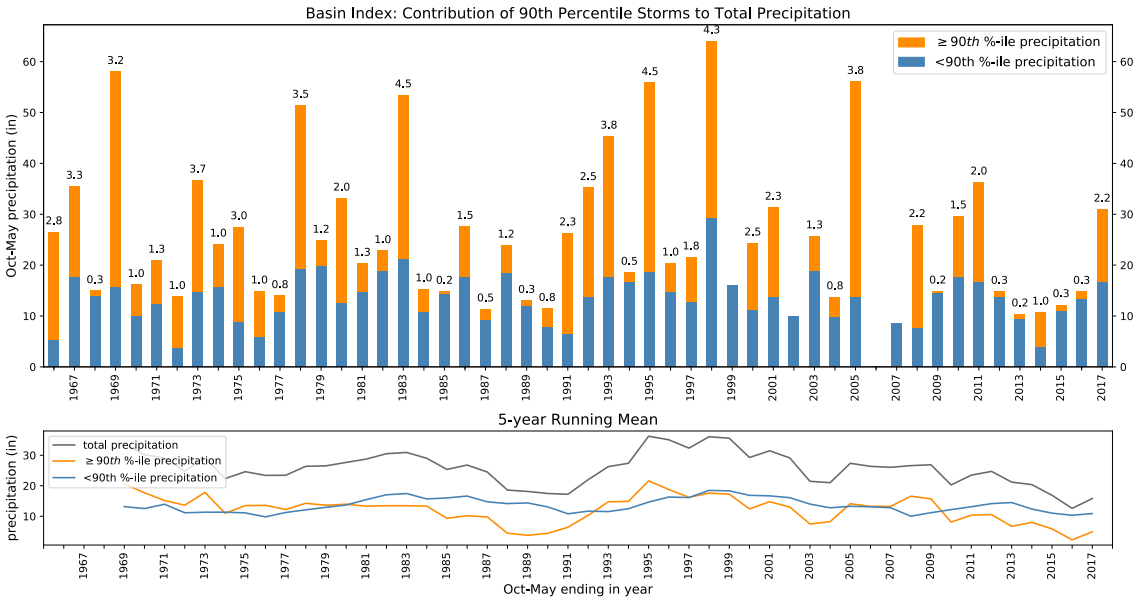

Figure 3.4: *Top panel shows contribution from ≥90th percentile events (orange portion of bars) and all other precipitation (blue bars) averaged across the six Basin*

Index stations for each season. The 90th percentile event count count among the six stations for each season is given at the top of the bar. As storm count and contribution is averaged across the six Basin Index stations by season, fractional contributions and storm counts are present. The bottom panel shows a 5-year running mean for total precipitation (black), precipitation from ≥90th percentile events (orange) and all other precipitation (blue). To provide continuity around the missing season of 2006, the running mean requires a minimum of four years at each point.

Figure 3.4 demonstrates variance by partitioning the contributions of precipitation from extreme (≥90th percentile) events and all other precipitation by season. While non-90th percentile precipitation (blue bars) show minimal change from year-to-year, the orange bars (extreme event contribution) show high inter-annual variability. The bottom portion of Figure 3.4 provides the 5-year running mean to help further illustrate the role of extreme events in precipitation variability. Non-90th percentile (blue line) precipitation stays relatively constant while the orange line, representing extreme precipitation contribution, oscillates around it. The black line, showing total precipitation, most closely follows the variability in the orange line. These results are comparable to Dettinger (2016), who observed a similar pattern in an analysis of the top 5% of wettest days in the Delta Catchment.

3.2 Contribution of 90th percentile storms to wet and dry years

The top panel of Figure 3.5 defines wet (green), dry (yellow) and normal (white) years for the Basin Index based on a median-quartile approach. Using the median-quartile approach yields 14 wet, 14 dry, and 23 normal seasons in the Oct-May 1965-2017 period. The years distinguished as wet and dry agree well with the impacts on water resources and human activities (e.g. Yates 1993; County of Santa Barbara 1998; US Drought Monitor 2018). Persistent, rather than individual, dry years have the greatest impact on Cachuma storage. For example, 2007 stands out as the individual driest year and produces a dip in storage, but the largest storage drops occur during the persistent dry periods of 1987-1991 and 2012-2016 (Figure 3.5).

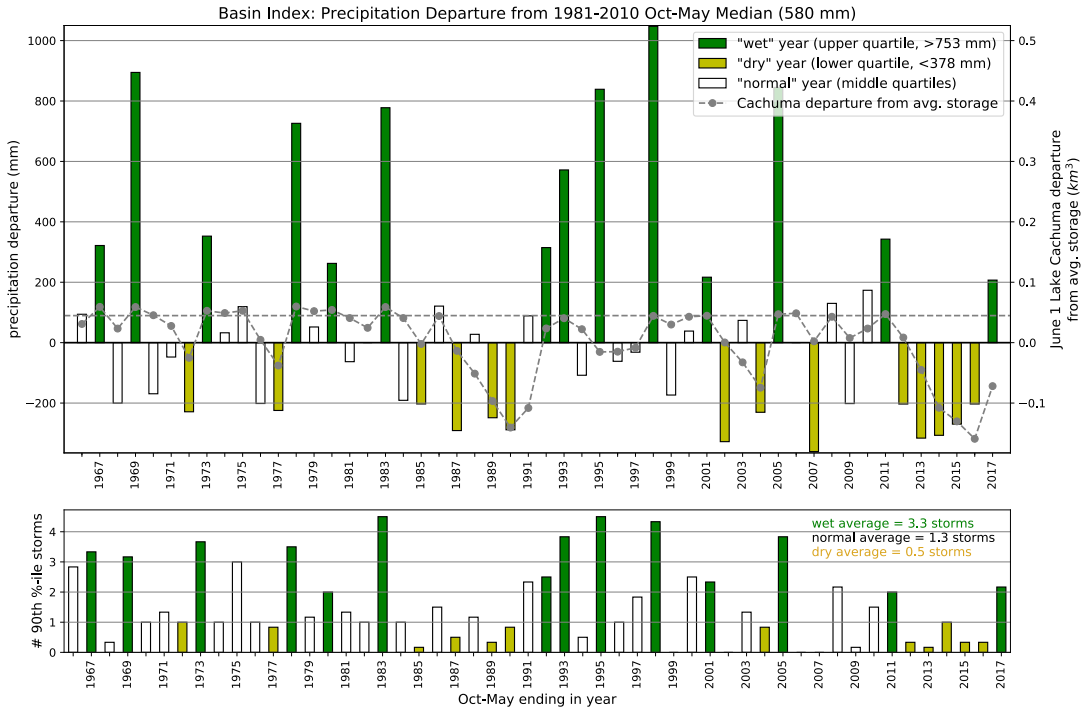

Figure 3.5: *The top panel shows precipitation departure from 1981-2010 median for the Basin Index. Bars are color-coded for years that fall in the wet (green; upper*

quartile), dry (yellow; lower quartile) and normal (white; interquartile range) categories. June 1 departure from average storage is superimposed in grey. The L. Cachuma maximum capacity is indicated by the horizontal grey line. L. Cachuma storage was re-calculated in 2003 due to sedimentation, thus some pre-2003 values are above maximum capacity. The bottom panel shows the number of 90th percentile storms occurring in each year, also color-coded by category (wet, dry, or normal).

The bottom panel of Figure 3.5 provides the frequency of extreme events for each year, and is also color-coded as to whether it was a wet, dry, or normal year. On average, for the Basin Index, there were 3.3 extreme events in a wet year, 1.3 in a normal year, and 0.5 in a dry year. Experiencing a given number of extreme events does not ensure a wet, dry, or normal year. For example, 1975 recorded three extreme events, but its' precipitation total only falls in the normal category. However, the Basin Index does not observe any wet years without at least one extreme event, nor does it experience any dry years with more than one extreme event.

Station	**#90th %-ile events**	**% chance wet**	**% chance normal**	**% chance dry**	**Observed # wet seasons**	**Observed # normal seasons**	**Observed # dry seasons**
Basin Index 51 seasons	≥4	100%	0%	0%	7	0	0
	3	50%	50%	0%	3	3	0
	2	44%	56%	0%	4	5	0
	1	0%	67%	33%	0	12	6
	0	0%	27%	73%	0	3	8

Table 3.1: *Chance of having a wet, dry, or normal October-May season based on number of 90th percentile events at the Basin Index. Percent chance values are computed based on the number of seasons in the station's record achieving a certain 90th percentile event frequency (observed #), and the fraction of those seasons that fall in the wet, dry or normal categories. For example, of the nine seasons with two 90th percentile events, four were "wet" (a 44% chance of wet season if two events occur), five were "normal" (a 56% percent chance for normal season), and zero were "dry" (a 0% chance for dry season).*

Table 3.1 reports the chance of having a wet, dry, normal season based on number of extreme events occurring in the Basin Index. These values are calculated by dividing the count of seasons within each extreme event frequency category (e.g. one, two, three 90th percentile events in a season) by the total number of seasons in each precipitation category (wet, normal, dry). As the number of 90th percentile storms in a particular season may be fractional for the Basin Index, values are rounded to the nearest integer. By this measure, a Basin average of approximately four or more 90th percentile events guarantees a wet season. If three extreme events occur, there is roughly a 50-50 chance of a wet or normal season and no chance of a dry outcome. For two events, there is a 44% chance of a wet year and 56% chance of a normal year. For a single 90th percentile event, there is no chance of achieving a wet year, a 27% chance of a normal year, and a 73% chance of a dry year. In summary, achieving a certain number of extreme events generally does not ensure a

season total places in a certain category (wet, dry, or normal), though influences the likelihood of each category.

3.3 Frequency of 90th Percentile Storms and the El Niño Southern Oscillation (ENSO)

ENSO is known to moderate storm activity on the US West Coast (Cayan et al. 1999). El Niño conditions increase the probability of above average precipitation in southern California, and strong El Niño conditions shift the probability towards well above average precipitation (Hoell et al. 2016). However, there are additional influences beyond the strength of El Niño conditions that influence seasonal precipitation totals in southern California, such as evolution and location of sea surface temperature anomalies and their modulation of atmospheric wave trains. This was the case in 2015-2016, which had strong El Niño conditions, on par with those of 1997-1998, but failed to produce above normal precipitation in southern California (Paek et al. 2017). Using the Oceanic Niño Index (ONI) we examine the role of ENSO as a predictor for frequency of the 90th percentile extreme precipitation events evaluated in this analysis, as well as ENSO relationship to wet and dry years in the Basin Index.

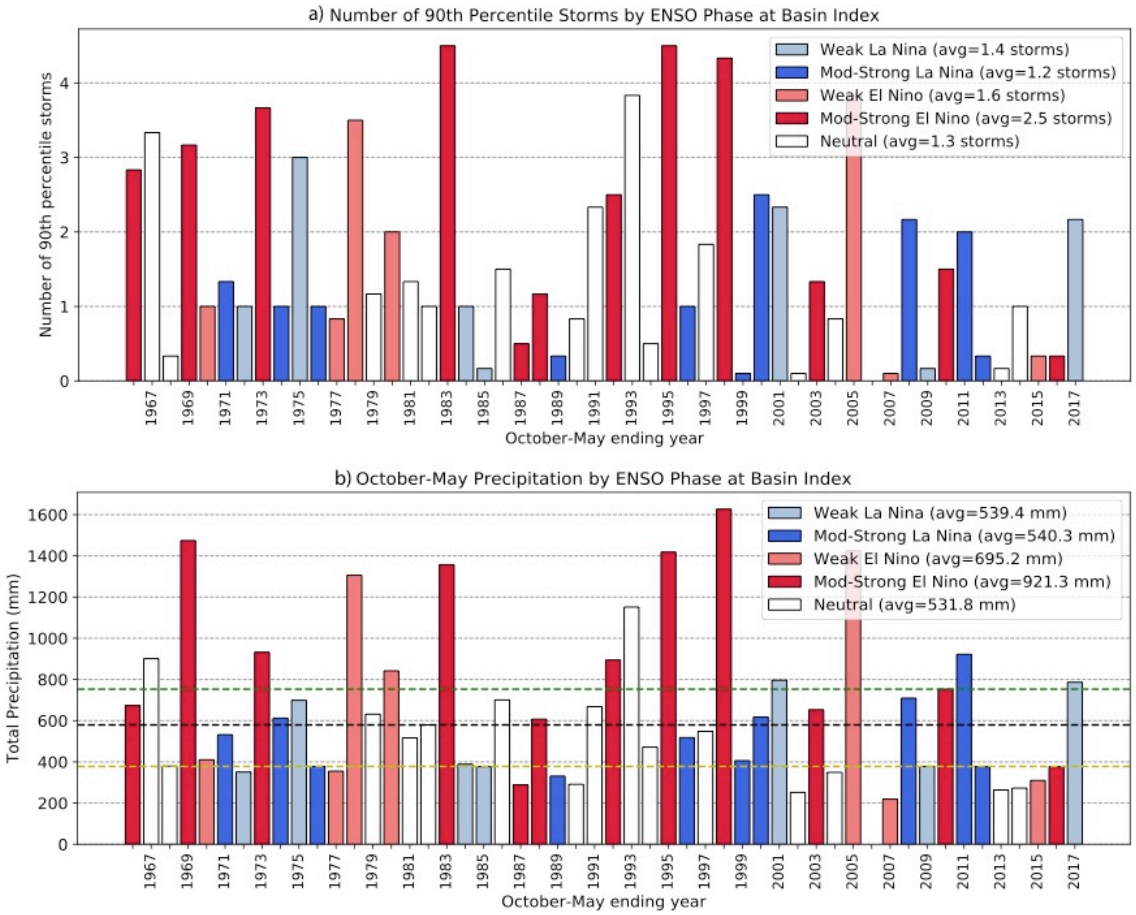

Figure 3.6: *a) Number of 90th percentile storms by ENSO phase and strength for the Basin Index. Smallest bars indicate years with no 90th percentile storms. b) October-May total precipitation by ENSO phase and strength for the Basin Index. Dashed horizontal black line indicates the 1981-2010 median, dashed green line indicates the upper quartile above which wet years lie, and dashed yellow line indicates the lower quartile below which dry years lie (as in Figure 3.5).*

ENSO Category based on ONI	Event Count	Number Wet	Number Dry	Number Normal
Weak El Niño	7	3	3	1

Moderate-Strong El Niño	12	6	2	4
Weak La Niña	7	2	2	3
Moderate-Strong La Niña	10	1	2	7
Neutral	15	2	5	8

Table 3.2*: Count of seasons in each ENSO phase at the Basin Index, and number of seasons falling into each category of wet, dry, and normal as defined in Section 3.2.*

The sample size available is relatively small, though we observe that El Niño years typically experience a greater number of extreme events, ranging from an average of 1.6 during weak episodes to an average of 2.5 during strong episodes (Figure 3.6a). During La Niña events, the average extreme event count is less, ranging from 1.2 events in weak episodes to 1.4 events among strong episodes. Neutral years were very similar to La Niña years, observing an average of 1.3 extreme events. These results are similar to previous work that demonstrates a greater frequency of 90th percentile precipitation days in southern California during El Niño years using the Southern Oscillation Index to categorize ENSO phase (Cayan et al. 1999).

On average, El Niño years exhibit higher October-May precipitation totals than La Niña or Neutral events for the Basin Index (Figure 3.6b; Table 3.2). A much larger fraction of total El Niño events fall in the wet category (47%) than La Niña (18%) or Neutral (13%) years (Table 3.2). However, 26% of El Niño years were dry, among them two strong El Niño events (1986/87 and 2015/16). While a particular

ENSO phase may tilt the odds in favor of a higher or lower frequency of extreme events and precipitation total, it is possible for seasons in all ENSO phases to observe multiple extreme precipitation events and experience a wet year or <1 extreme event and a dry year. On the basis of this historical data analysis, ENSO phase is suggestive, though not predictive, of how many extreme events will occur and season precipitation total. In a warming climate, there is uncertainty about how the existing teleconnection patterns will persist or change (Collins et al. 2010), further complicating the use of ENSO as a predictor for this area.

3.4 Association between atmospheric rivers and 90th percentile storms

ARs are often associated with California's largest storms and floods (Ralph and Dettinger 2012). Whether or not a storm is associated with an atmospheric river may improve forecasting ability and situational awareness, as IVT has been shown to have better predictability than precipitation forecasts for a longer lead-time (Lavers et al. 2016).

We observe the greatest frequency of extreme events in the January-March period (Figure 3.7) and significantly fewer in other months. In all months, ARs make up the majority of extreme events. However, in October, March, and April, we see a larger fraction of non-AR extreme events. In the spring and autumn seasons, the frequency of closed and cutoff low-pressure systems (areas of closed counter-clockwise circulation at mid-to-upper levels in the atmosphere that are partially or completely detached from the mean westerly jet stream, see Figure 3.8 e, h) tends to

peak, and may account for this distinction (Oakley and Redmond 2014). In autumn, remnants of tropical storms occasionally move through the area and can potentially produce heavy rainfall (Corbosiero et al. 2009). Of the 58 storms over the 1980-2017 period for the Basin Index, 43 (74%) are categorized as ARs.

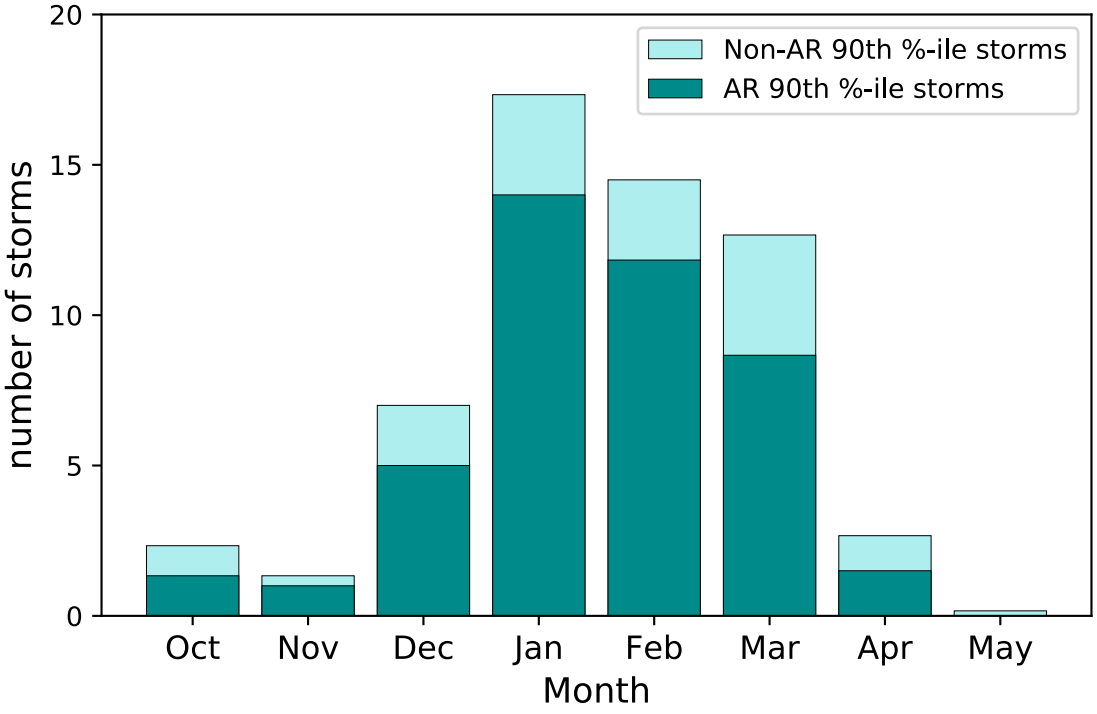

Figure 3.7: *For the Basin Index, frequency of atmospheric river and non-atmospheric river 90th percentile precipitation events by wet season month.*

The forecast or presence of AR conditions provides some indication of the potential for extreme precipitation events in this area. However, only a small fraction of the 412 events meeting AR criteria and persisting a minimum of 12 hours at the relevant MERRA grid point (Figure 3.1) produced 90th percentile precipitation events. Features at finer scales help to explain why most ARs do not produce 90th

percentile precipitation events, and some non-AR events do. Previous studies have found strong low-level winds orthogonal to terrain and the position of the upper level jet to play a key role in significant southern California storms (Tarleton and Kluck 1994; Haynes 2001; Oakley et al. 2017) and orographic precipitation in general (Lin et al. 2001). Stability and blocking also influence precipitation distribution and totals in this region (Hughes et al. 2009). Convective bands are also known to occur in this area (e.g., Griffith et al. 2005), which can produce short duration, high intensity rainfall and may not be related to atmospheric river conditions.

3.5 Synoptic features associated with 90th percentile storms

Composites of the 53 90th percentile events (Figure 3.8 a-c) at the Cachuma precipitation gauge reveal several common characteristics. First, a strong upper level jet positioned such that its' left or curved exit, an area favorable for upward vertical motions, was present in the vicinity of Santa Barbara County (Figure 3.8a). Second, the composite revealed a plume of subtropical moisture into southern California exceeding the common AR criteria of >20 mm IWV and >250 kg m^{-1} s^{-1} IVT (Figure 3.8b). Third, the composite revealed strong (>18 ms^{-1} on average) low-level southerly winds impacting Santa Barbara County (Figure 3.8c). These conditions are consistent with those found in other analyses on impactful storms in southern California (Tarleton and Kluck 1994; Haynes 2001; Oakley et al. 2017), and are also

noted by Lin (2001) as being among common characteristics for heavy orographic (mountain-forced) precipitation.

Several distinct synoptic patterns produce these common conditions in the vicinity of Santa Barbara County. To highlight this variability, we separate the events into four categories based on their synoptic patterns using a qualitative classification similar to Haynes (2001):

- **Class 1**: Closed low with 500 hPa center north of 37.5° N (approximately San Francisco Bay; Figure 3.8 d-f).
- **Class 2**: Closed low with center south of 37.5° N (Figure 3.8 g-i).
- **Class 3**: Straight upper level (300 hPa) jet across northeastern Pacific, south of approximately 35° N (Figure 3.8 j-l).
- **Class 4**: Open-wave trough off West Coast (Figure 3.8 m-o).

A closed low off the West Coast was a common feature, with Class 1 and Class 2 accounting for 53% of events, in agreement with Haynes (2001). The high curvature of closed low features is favorable for southerly winds and moisture transport into the region. The position of the 500 hPa low is only slightly different between Class 1 and Class 2, but there is a notable distinction in the moisture source region. For Class 1 (Figure 3.8e), the main corridor of moisture transport is between approximately 130°-135° W. In Class 2 (Figure 3.8h), the main source region is shifted further east to roughly 118°-120° W.

For Class 3 (Figure 3.8k), the straight jet case, moisture transport occurred over a broad area from 120°-140° W across composite members. The position of the

upper level jet exit just offshore of southern California is favorable for strong low level southerly flow oriented toward Santa Barbara County as part of the low level circulation in the jet exit region (Figure 3.8l).

In the open wave case, Class 4 (Figure 3.8n), over half of the composite members featured long-range moisture transport from the vicinity of Hawai'i or points east. However, several of the cases featured very little moisture transport, diminishing the signal such that there is not a consistent plume across the region in the composite. Class 4 exhibited more variability across composite members than the other categories, but generally featured a somewhat sharp upper level trough off the West Coast (Figure 3.8m), favorable for low-level southerly flow (Figure 3.8o).

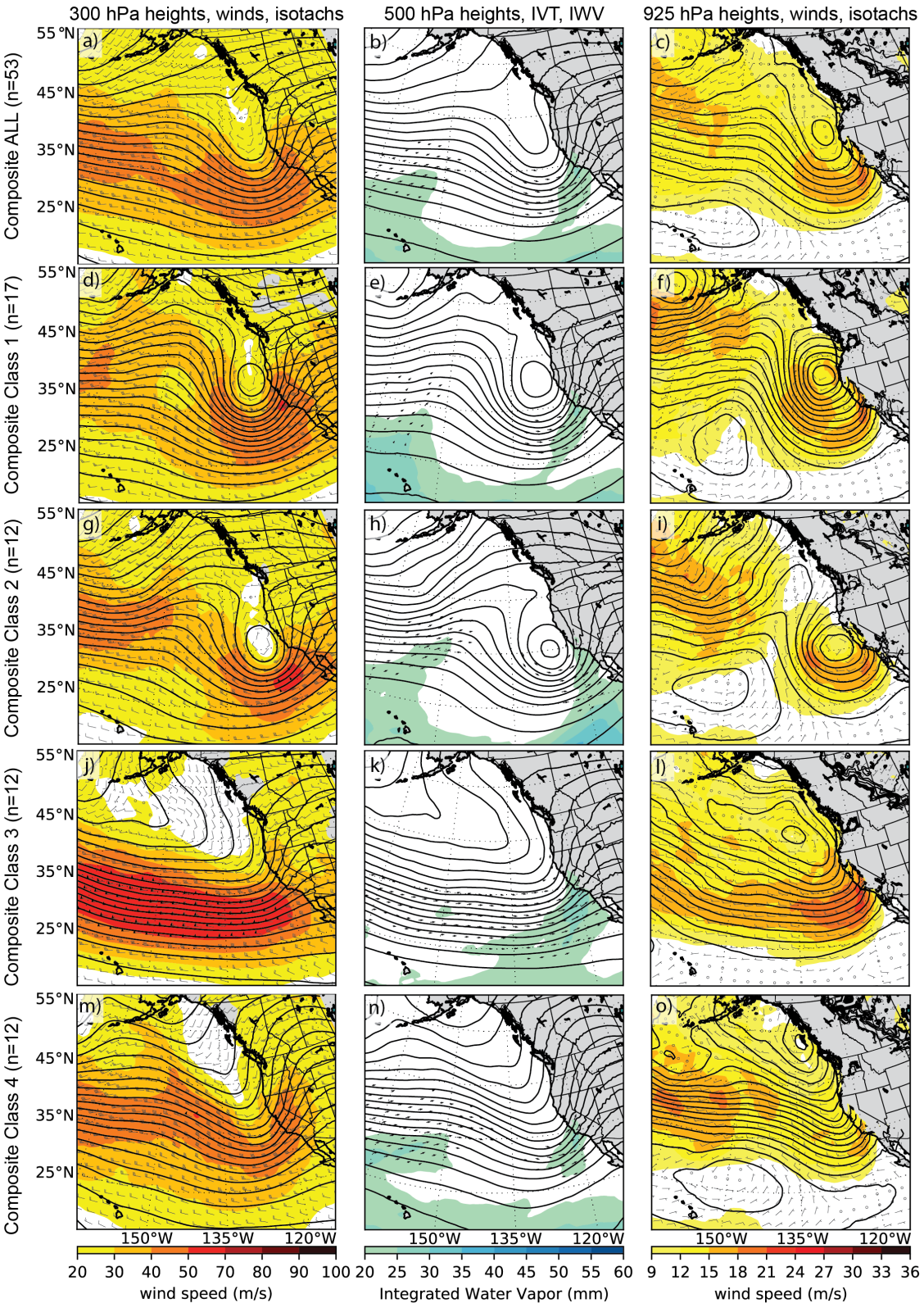
300 hPa heights, winds, isotachs
500 hPa heights, IVT, IWV
925 hPa heights, winds, isotachs
Composite ALL (n=53)
Composite Class 1 (n=17)
Composite Class 2 (n=12)
Composite Class 3 (n=12)
Composite Class 4 (n=12)
a)
b)
c)
d)
e)
f)
g)
h)
i)
j)
k)
l)
m)
n)
o)
55°N
45°N
35°N
25°N
150°W
135°W
120°W
20 30 40 50 70 80 90 100
wind speed (m/s)
20 25 30 35 40 45 50 55 60
Integrated Water Vapor (mm)
9 12 15 18 21 24 27 30 33 36
wind speed (m/s)

Figure 3.8: *Composite synoptic maps constructed from MERRA data for all events (first row) and each class 1-4 (subsequent rows).*

While all four synoptic setups shown produced 90th percentile precipitation events, each configuration and each individual storm has characteristics that may influence the balance of whether the precipitation received will be more hazardous (falling quickly over a short period of time) or beneficial (occurring over a longer duration). For example, the cold upper level cores of closed and cutoff low-pressure systems in Class 1 and Class 2 can destabilize the atmosphere, resulting in intense convective precipitation (Abatzoglou 2016). Closed lows have also been associated with strong winds and tornados in the nearby Los Angeles area (Hales Jr. 1985). Future research can explore in greater detail the role of synoptic and mesoscale features in the balance of creating hazardous and beneficial precipitation.

4. Conclusions

Motivated by the large rise in drought-stricken Lake Cachuma following two large storms in January and February 2017, we quantify a common notion (e.g. Burns 2017) that whether the Santa Ynez River Basin experiences a wet, normal, or dry year hinges upon the presence or absence of a few extreme events. We pose a definition of precipitation event and observe that the contribution from 90th percentile events has a strong relationship with inter-annual precipitation variability (Figures 3.3 and 3.4). Using a quartile approach to define wet, dry, and

normal October-May seasons, the Santa Ynez Basin on average observes 3.3 90th percentile events in wet years, 1.3 in normal years, and 0.5 in dry years (Figure 3.5). Attaining four or more 90th percentile events guarantees a wet year, while observing no 90th percentile events guarantees it will not be a wet year. For other storm counts, the outcomes are mixed (Table 3.1).

For the period 1980-2017 for which reanalysis data were available, 74% of 90th percentile events are associated with atmospheric rivers (Figure 3.7), which may provide insight to extreme event forecasting. El Niño years tend to have greater numbers of 90th percentile events, with 2.2 events on average as compared to 1.3 during La Niña and Neutral years (Figure 3.6), however, there is considerable variability in storm count among years and ENSO phase. Composites of synoptic (large-scale) atmospheric conditions reveal several common features: 1) an upper level jet displaced to south with exit region over the area of interest. 2) Strong low-level southerly winds. 3) Moisture transport reaching or exceeding atmospheric river thresholds. We recognize four distinct synoptic patterns generating these conditions (Figure 3.8).

Images and information from this study can be used in communication strategies by various agencies, such as water purveyors and the National Weather Service. Understanding how a wet or dry year hinges on a couple precipitation events can serve as a motivator for people to conserve water and support awareness of drought risks. Additionally, our results highlight seasonal precipitation forecast challenges in this region. Seasonal to sub-seasonal forecasts

are based on statistical and dynamical models (Goddard et al. 2001). As seasonal rainfall totals are strongly dependent on a few large storms (Figure 3.5), if forecast models do not correctly resolve the strength or occurrence of even one storm, it can greatly affect their skill for this region.

The results of this work support understanding of precipitation variability across a variety of disciplines. Paleoclimatological, geological, and ecological research with a dependence on precipitation variability is commonplace along the South Coast. For example, records of sediment flux into the Santa Barbara Channel in the modern era (e.g. Inman and Jenkins 1999; Warrick and Milliman 2003) as well as historic sediment records in the Santa Barbara Basin (e.g. Hendy et al. 2015) are used to evaluate climate variability and frequency of large rainfall runoff events. Fire occurrence in southern California is tied to prior-year rainfall (e.g., Westerling et al. 2004), and burned area vegetation recovery is strongly controlled by inter-annual rainfall patterns (e.g., Keeley et al. 2005). Our results provide further insights for these types of studies by highlighting the frequency of extreme precipitation events over time and their relationship to wet and dry years and ENSO, as well as noting prominent synoptic patterns and their variations.

Analyses based on paleoclimate records and climate modeling suggests increasing aridity and drought frequency in California in the future (Cook et al. 2015; Cvijanovic et al. 2017), and movement towards fewer, more intense precipitation events (Polade et al. 2014; Dettinger 2016). Our results can serve as a baseline for evaluating future change. Work stemming from this study will evaluate

how observed storm frequency patterns persist or change at the basin scale using downscaled climate model output at a resolution pertinent to the basin scale. Additionally, we can explore changes in the prevalence of various synoptic patterns producing 90th percentile events in climate model output. This basin-scale approach to precipitation variability can be expanded to other dryland regions throughout California and the world.

Conclusion

Post-fire debris flows, shallow landslides, and drought all have significant impacts across the state of California, though this work mainly focuses on the southern portion of the state. These events are precipitation-driven, but across distinct time scales. Post-fire debris flows are generally associated with hourly to sub-hourly rainfall intensities, while shallow landslides require seasonal antecedent precipitation followed by rainfall of a certain intensity and duration that may span a single hour to multiple hours. Drought and water resources are dependent on seasonal and inter-annual precipitation variability. In the preceding three chapters, we explored the spatial and temporal variability of these events and their associated atmospheric conditions. Several conclusions emerge from these studies, providing insight for operational activities in meteorology, geology, and water resource management. This work has also highlighted several avenues for further research to improve understanding of these topics.

Our goal in examining the atmospheric conditions associated with post-fire debris flows in Chapter 1 was to expand understanding of the conditions producing these events beyond the basic concept of "intense convection". We also wanted to assess a variety of historic events and compile information about each to support communication strategies. This would assist the National Weather Service (NWS) in advising their partners and stakeholders that a particular forecast event bared similarity to some historic event. Though NWS is familiar with forecasting high intensity precipitation events, having a summary of conditions producing these

events can help to reduce uncertainty in forecasting. In the Chapter 1 analysis of atmospheric conditions associated with post-fire debris flows, we observed the following:

- Atmospheric rivers (ARs) were present in 13 of 19 PFDF events (9 had AR only, 4 had AR and a closed low)
- All 13 AR events featured IVT >= 90th percentile and 8 had IVT in the 99th percentile (strong events for the location and time of year)
- Closed lows (CL) were present in 5 of 19 PFDF events (1 had CL only, 4 had AR and CL); neither AR nor CL conditions were present in 5 events
- Moderate to strong flow aloft: Upper level (300 hPa) west-southwest flow typically > 40 m s^{-1}
- Upper level jet position in majority of events (13/19) is displaced to south such that the Transverse Ranges lie in divergent jet exit, an area favorable for upward vertical motions
- Presence of moderate speed (5-10+ ms^{-1}) southerly winds below 1 km
- Predominantly moist-neutral stability (AR feature), especially in the 1-2+ km layer; in some cases weakly unstable at low levels
- Median CAPE of 20-40 J kg^{-1} at time of event with a range from 0-1300 J kg^{-1} among events
- High radar returns in all events (>50 dBz); in several cases narrow cold frontal rainbands (NCFR) or other convective rainbands were present

In Chapter 2, we studied the spatial and temporal variability of precipitation intensities with the potential to trigger shallow landslides across California. One of the main goals in this work was to generate information that could be used in the development of a null landslide hazard map based on areas with a general lack of high intensity precipitation events. Additionally, this information improves understanding of the distribution of landslide activity in California and identifies areas where placement of soil moisture sensors may offer the most benefit. Our results include:

- Development of quality-controlled RAWS precipitation data for California in the cool season
- The highest incidence of threshold exceedence occurred at stations located at elevation on coastal prominences or other near-coast locations with exposure to southerly flow
- A high number of over threshold events were also observed in the northwestern Sierra Nevada, associated with San Francisco Bay Area terrain gap
- Approximately 70-90% of over threshold precipitation events are associated with atmospheric rivers depending on threshold and location
- The greatest frequency of over threshold events tends to coincide with the wettest month of the season in a given geomorphic province

- Areas experiencing frequent over threshold events generally match those areas known to have the greatest landslide incidence or hazard, with the exception of the northern Sierra Nevada

In Chapter 3, our goal was to quantify the anecdotal statement that the difference between a wet or dry year in the Santa Ynez River Basin is just a few big storms. We also sought to identify the synoptic conditions associated with such storms and explore the association with the El Niño Southern Oscillation, which has been shown to modulate inter-annual precipitation in this region (e.g., Cayan et al. 1999). In our analysis of data from a variety of sources, we observed that:

- The contribution from 90th percentile precipitation events has a strong relationship with inter-annual precipitation variability
- A median and quartile approach is useful to define wet, dry, and normal seasons
- Santa Ynez Basin on average observes 3.3 90th percentile events in wet years, 1.3 in normal years, and 0.5 in dry years
- Attaining four or more 90th percentile events guarantees a wet year, while observing no 90th percentile events guarantees it will not be a wet year
- 74% of 90th percentile events are associated with atmospheric rivers
- El Niño years tend to have greater numbers of 90th percentile events, with 2.2 events on average as compared to 1.3 during La Niña and Neutral years

however, there is considerable variability in storm count related to ENSO phase

- Composites of synoptic (large-scale) atmospheric conditions reveal several common features: 1) an upper level jet displaced to south with exit region over the area of interest. 2) Strong low-level southerly winds. 3) Water vapor transport reaching or exceeding atmospheric river thresholds
- At least four distinct synoptic patterns generating the conditions favorable for extreme precipitation events

The conclusions from analysis of the synoptic conditions associated with post-fire debris flow events and those associated with extreme precipitation events in the Santa Ynez River Basin were quite similar. For example, the presence of an atmospheric river in ~70% of cases, a strong upper level jet, and strong low-level southerly winds. However, not all the 90th percentile events likely produce high intensity rainfall sufficient for debris flows, and some 90th percentile events are relatively short duration (2 days or less), while others are much longer. Additionally, there are many high intensity events in chapter 2 that, especially in the Transverse Ranges, were not associated with atmospheric rivers. This leads to the conclusion that conditions beyond atmospheric rivers and associated strong orographic ascent contribute to precipitation extremes, both at the short duration and storm total timescales. The observation of convective rainbands producing post-fire debris flows and the assertion that such bands are prevalent in the area

(e.g. Griffith et al. 2005) suggests that mesoscale features are key to understanding intense precipitation, debris flows, and shallow landslides in southern California as well as other parts of the state.

Future work addressing this topic would begin with developing a climatological understanding of the location, frequency, and movement of convective bands in the Southern California Bight or other areas of interest. This may reveal patterns on their development and what coastal or terrain features impact their movement and lifespan. Additionally, identifying and quantifying favorable convergence zones from a climatological perspective would be valuable. From a forecasting perspective, developing an operational model that provided an ensemble forecast of convective bands would be a valuable tool. Some of this work is underway at the Center for Western Weather and Water Extremes at Scripps Institution of Oceanography..

Currently, no operational products exist for use by the National Weather Service that provide rainfall at sub-hourly rates that are typically associated with post-fire debris flows or act as shallow landslide triggers. Future work related to the findings of this research could seek to evaluate the value and feasibility of developing such products and explore how to make them operational. Building such products would also require enhanced understanding of the convective features producing high intensity precipitation in this area.

The role of sea surface temperatures (SSTs) in the southern California Bight may also play a role in the frequency or intensity of convective rain bands. As the

bottom of the atmospheric column is warmed, one would anticipate a greater lapse rate, creating more unstable conditions. Additionally, warmer SSTs may allow for greater evaporation and higher precipitation totals, as noted in a field campaign in the Bight (Neiman et al. 2004). Anecdotal reports from NWS San Diego hypothesize that warmer than normal sea surface temperatures over the last couple years have been related to more frequent periods of instability and convective bands. High resolution modeling studies that evaluate the role of SSTs in controlling atmospheric stability in the Bight as well as how precipitation intensities vary under different SST conditions would be useful in addressing this question.

With the hourly RAWS data assessed in Chapter 2, one useful application may be to examine changes in extremes over time. People interested in flood and landslide risk are interested in knowing whether we are already seeing the impacts of climate change and more extreme precipitation. A cursory analysis of several stations did not reveal a change in number of >10 mm h^{-1} events per number of wet hours, but looking at other statistics such as the number of extreme events may be useful. Incorporating other networks, such as the ALERT network, and finer temporal resolutions may also be useful.

In exploring precipitation variability in the Santa Ynez River Basin in Chapter 3, we focus on only a small basin impacting a few hundred thousand people. It would be an interesting exercise to compare these findings to several small basins in Mediterranean climates around the world (e.g., southern Australia, South Africa, central Chile, portions of Europe) and assess whether the dependence on a few large

cool season storms is typical of these regions. A broad comparison such as this could expand the usefulness of the work to other parts of the world.

A final recommendation for the application of this work and future avenues of study relates to education. A recent meeting to evaluate the events following the January 9 2018 Montecito post-fire debris flow event (County of Santa Barbara 2018) that killed 23 people suggested that more education of the public and elected officials is needed on what a post-fire debris flow is and the role of short duration-high intensity precipitation in producing such events. Education on these topics would help to overcome evacuation fatigue and give people a better understanding of the potential destruction that can be caused by debris flows. Water agencies can benefit from materials presented in Chapter 2 of this research as they can use to educate their boards and rate-payers on precipitation variability in southern California. This can help water users understand why we see such high inter-annual variability with low predictability in this region and susceptibility of the area to drought. We will continue to work with the agencies engaged in this research to continue outreach and communication and seek future projects and partnerships to further support education related to these topics.

Climate modeling studies suggest a movement towards fewer, more intense precipitation events (Pierce et al. 2013; Polade et al. 2014; Dettinger 2016). The frequency of the most extreme (top 0.05%) hourly precipitation intensities is suggested to increase roughly threefold in southern California (Prein et al. 2017). These findings suggest that the potential for post-fire debris flows and more

variable precipitation will increase for southern California in a future climate. It is probable that the threat of landslides could decrease if conditions are no longer favorable to reach the antecedent moisture conditions necessary for landsliding (Bennett et al. 2016). We will continue to build off the material presented in the three preceding chapters to understand these hazards in southern California and educate the public, policy makers, water resource agencies, and emergency managers to improve awareness, preparedness, and resilience.

References

Abatzoglou, J. T. (2016). Contribution of cutoff lows to precipitation across the United States. *Journal of Applied Meteorology and Climatology*, *55*(4), 893-899.

Abatzoglou, J. T., 2013: Development of gridded surface meteorological data for ecological applications and modeling. *International Journal of Climatology*, **33**(1), 121-131.

ABC7 News (2014) Nov 2 2014: Camarillo Springs evacuation order lifted after debris flow. http://abc7.com/weather/1-rescued-residents-evacuated-after-camarillo-mudslide/376277/. Accessed 10 February 2016

American Meteorological Society (AMS; 2017a). Glossary of Meteorology. Atmospheric River. Accessed online 12 November 2017 at http://glossary.ametsoc.org/wiki/Atmospheric_river

American Meteorological Society (AMS; 2017b). Glossary of Meteorology: Storm. Accessed online 12 November 2017 at http://glossary.ametsoc.org/wiki/Storm

Arguez, A., Durre, I., Applequist, S., Vose, R. S., Squires, M. F., Yin, X., and coauthors (2012). NOAA's 1981–2010 US Climate normals: an overview. *Bulletin of the American Meteorological Society*, *93*(11), 1687-1697.

Baum, R. L., J. W. Godt, 2010: Early warning of rainfall-induced shallow landslides and debris flows in the USA. *Landslides*, **7**(3), 259-272.

Baum, R. L., J. W. Godt, W. Z. Savage, 2010: Estimating the timing and location of shallow rainfall-induced landslides using a model for transient, unsaturated infiltration. *Journal of Geophysical Research: Earth Surface*, **115**(F3).

Bedrossian, T.L., 1996: 1995 Storm Events: An Overview of the Department of Conservation, Division of Mines and Geology's Emergency Landslide Response. *California Geology*, **49**(5), 111-119.

Bennett, G. L., J. J. Roering, B. H. Mackey, A. L. Handwerger, D. A. Schmidt, and B. P. Guillod (2016), Historic drought puts the brakes on earthflows in Northern California, Geophys. Res. Lett., 43, doi:10.1002/2016GL068378.

Bogaard, T., R. Greco, 2018: Invited perspectives: Hydrological perspectives on precipitation intensity-duration thresholds for landslide initiation: proposing hydro-meteorological thresholds. *Natural Hazards and Earth System Sciences*, *18*(1), 31-39.

Biasutti, M., R. Seager, D. B. Kirschbaum, 2016: Landslides in West Coast metropolitan areas: The role of extreme weather events. *Weather and Climate Extremes*, **14**, 67-79.

Brabb, E.E., J. P. Colgan, T. C. Best, 1999: Map showing inventory and regional susceptibility for Holocene debris flows, and related fast-moving landslides in the conterminous United States. Miscellaneous Field Studies Map *MF-2329*, scale 1:2,500,000, U.S. Geological Survey.

Brooks, H.E. and D.J. Stensrud, 2000: Climatology of Heavy Rain Events in the United States from Hourly Precipitation Observations. *Mon. Wea. Rev.,* **128**, 1194–1201.

Brown, T. J., J. D. Horel, G. D. McCurdy, *M. G. Fearon,* 2011: What is the Appropriate RAWS Network? *CEFA Report 11-01,* 97pp*. Center for Climate, Ecosystem, and Fire Applications, Desert Research Institute, Reno, Nevada. Accessed 10 January 2017,* https://cefa.dri.edu/Publications/RAWS%20Network%20Analysis%20final%20report.pdf

Browning KA and Pardoe CW (1973) Structure of low-level jet streams ahead of mid-latitude cold fronts. Q.J.R. Meteorol. Soc., 99(422):619–638

Burns, M. (2017). Fifty more inches of rain needed to fill Cachuma. *Santa Barbara Independent.* Accessed online 10 October 2017 at https://www.independent.com/news/2017/jan/20/fifty-more-inches-rain-needed-fill-cachuma/

Caine, N. (1980). The rainfall intensity: duration control of shallow landslides and debris flows. *Geografiska Annaler. Series A. Physical Geography*, 23-27.

California Department of Forestry and Fire Protection (CALFIRE), 2014, Fire Perimeters, Version14_2. http://frap.cdf.ca.gov/data/frapgisdata-sw-fireperimeters_download. Accessed 12 March 2016

California Geological Survey (CGS), 2002: California Geomorphic Provinces, *California Geological Survey Note 36,* pp. 4. Accessed 10 October 2016,

http://www.conservation.ca.gov/cgs/information/publications/cgs_notes/note_36/Documents/note_36.pdf

California Office of Emergency Services (2010) 2010 January statewide winter storms after action/corrective action report. http://www.caloes.ca.gov/PlanningPreparednessSite/Documents/08%20January2010%20Statdewide%20Rains%20Exec%20Summary%20and%20report2.pdf. Accessed 10 February 2016

California Department of Water Resources (2017). Daily Reservoir Storage Summary. Accessed online 1 March 2017. http://cdec.water.ca.gov/cgi-progs/current/RES

Campbell, R. H. (1975). *Soil slips, debris flows, and rainstorms in the Santa Monica Mountains and vicinity, southern California*. US Geological Survey Professional Paper 851.

Cannon, S. H., S. D. Ellen, 1985: Rainfall conditions for abundant debris avalanches, San Francisco Bay region, California. *California Geology*, **38**(12), 267-272.

Cannon, S. H., S. D. Ellen, 1988: Rainfall that resulted in abundant debris flow activity during the storm, *in* Ellen, S. D. and Wieczorek, G. F., eds., Landslides, floods, and marine effects of the storm of January 3-5, 1982, in the San Francisco Bat region, California. *U.S. Geological Survey Professional Paper 1434*, p. 27-33.

Cannon SH, Gartner JE (2005) Wildfire-related debris flows from a hazards perspective. Chapter 15 in: Jakob M, Hungr O, Jakob, DM (2005) Debris-flow hazards and related phenomena. Berlin, Springer, pp 411-443

Cannon SH, Gartner JE, Wilson RC, Bowers JC, Laber JL (2008) Storm rainfall conditions for floods and debris flows from recently burned areas in southwestern Colorado and southern California. Geomorphology 96(3):250-269

Cannon SH, Boldt EM, Kean JW, Laber JL, Staley DM (2010) Relations between rainfall and postfire debris-flow and flood magnitudes for emergency-response planning, San Gabriel Mountains, southern California. U.S. Geological Survey Open–File Report 2010-1039, pp. 31

Casadei, M., W. E. Dietrich, N. L. Miller, 2003: Testing a model for predicting the timing and location of shallow landslide initiation in soil-mantled landscapes: *Earth Surface Processes and Landforms*, **28**(9), 925-950

CBS Los Angeles (2014) Nov 1 2014: Major debris flow forces evacuation of 11 Camarillo Springs Homes. http://losangeles.cbslocal.com/2014/11/01/major-debris-flow-forces-evacuation-of-11-camarillo-springs-homes/. Accessed 12 March 2016

Carlson TN (1998) Mid-Latitude Weather Systems. American Meteorological Society, Boston, pp 507

Carpinteria Valley Water District (2017). Supply and sources. Accessed online 27 December 2017. http://www.cvwd.net/water_info/sources.htm

Cayan, D. R., Redmond, K. T., & Riddle, L. G. (1999). ENSO and hydrologic extremes in the western United States. *Journal of Climate*, *12*(9), 2881-2893.

Chawner WD (1935) Alluvial Fan Flooding: The Montrose, California, Flood of 1934. Geographical Review 25(2):255-263.

CIMSS (2016). Morphed integrated microwave imagery at CIMSS- Total precipitable water (MIMIC-TPW). http://tropic.ssec.wisc.edu/real-time/mimic-tpw/epac/main.html . Accessed 20 March 2016.

City of Sierra Madre Blog (2009) February 2009 Emergency Information by Sierra Madre PIO http://sierramadrepio.blogspot.com/2009_02_01_archive.html. Accessed 10 February 2016

Clark AJ, Schaffer CJ, Gallus Jr. WA, Johnson-O'Mara K (2009) Climatology of storm reports relative to upper-level jet streaks. Weather and Forecasting 24(4):1032-1051

Climate Prediction Center (2017). Cold and warm episodes by season. Accessed online 3 December 2017 at http://www.cpc.ncep.noaa.gov/products/analysis_monitoring/ensostuff/ONI_v5.php

Collins, M., An, S. I., Cai, W., Ganachaud, A., Guilyardi, E., Jin, F. F., ... & Vecchi, G. (2010). The impact of global warming on the tropical Pacific Ocean and El Niño. *Nature Geoscience*, *3*(6), 391.

Cook, B. I., Ault, T. R., & Smerdon, J. E. (2015). Unprecedented 21st century drought risk in the American Southwest and Central Plains. *Science Advances*, *1*(1), e1400082.

Corbosiero, K. L., Dickinson, M. J., & Bosart, L. F. (2009). The contribution of eastern North Pacific tropical cyclones to the rainfall climatology of the southwest United States. *Monthly Weather Review*, *137*(8), 2415-2435.

County of Santa Barbara (1998). 1998 Flood Report. Accessed online October 5 2017 at https://www.countyofsb.org/uploadedFiles/pwd/Content/Water/1998FloodRpt.pdf

County of Santa Barbara (2018, January 10) 2018 January Storm Incident Update. Accessed January 11, 2018. https://www.countyofsb.org/asset.c/3681

County of Ventura (2015) Multi-hazard Mitigation Plan: September 2015, pp. 718 http://www.vcfloodinfo.com/pdf/2015%20Ventura%20County%20MultiHazard% 20Mitigation%20Plan%20and%20Appendices.pdf. Accessed 12 January 2017.

Cvijanovic, I., Santer, B. D., Bonfils, C., Lucas, D. D., Chiang, J. C., & Zimmerman, S. (2017). Future loss of Arctic sea-ice cover could drive a substantial decrease in California's rainfall. *Nature communications*, *8*(1), 1947.

Daly, C., M. Halbleib, J. I. Smith, W. P. Gibson, M. K. Doggett, and coauthors, 2008: Physiographically sensitive mapping of climatological temperature and precipitation across the conterminous United States. *International Journal of Climatology*, **28**(15), 2031-2064.

Daily Mail UK (2014) 14 Dec 2014: The street that was buried by a mudslide. http://www.dailymail.co.uk/news/article-2873433/Devastation-California-mudslide-seen-air-boulder-strewn-rivers-mud-swept-hillsides-submerged-homes.html. Accessed 12 January 2016.

DeBano LF (1981) Water repellent soils; a state-of-the-art. Forest Service; General Technical Report No. PSW-46. Pacific Southwest Forest and Range Experiment Station.

DeBano LF (2000) The role of fire and soil heating on water repellency in wildland environments: a review. Journal of Hydrology, v. 231-232, pp.195-206.

Dettinger MD, Ralph FM, Das T, Neiman PJ, Cayan DR (2011) Atmospheric rivers, floods and the water resources of California. Water 3(2):445-478

Dettinger, M. D. (2016). Historical and future relations between large storms and droughts in California. *San Francisco Estuary and Watershed Science*, *14*(2).

Dorman, C. E., & Winant, C. D. (2000). The structure and variability of the marine atmosphere around the Santa Barbara Channel. *Monthly Weather Review*, *128* (2), 261-282.

Duchon, C. E. and C. J. Biddle, 2010: Undercatch of tipping-bucket gauges in high rain rate events. *Advances in Geosciences*, 25, 11-15, doi:10.5194/adgeo-25-11-2010.

Duchon, C. E. *and* G. R. Essenberg, 2001: Comparative rainfall observations from pit and aboveground rain gauges with and without wind shields*, Water Resour. Res.,* **37**(12)*,* 3253– 3263*, doi:*10.1029/2001WR000541*.*

Eaton EC (1936) Flood and erosion control problems and their solution. Transactions of the American Society of Civil Engineers 101(1):1302-1330

Faiers, G.E. 1988: "Defining Normal Precipitation," *National Weather Digest,* Vol 13, No. 1, 20-21.

Faiers, G. E. (1989). Normality and Variability of Seasonal Snowfall in the Eastern Two-Thirds of the United States. *Nat. Wea. Dig*, *14*(23.25).

Gartner JE, Bigio ER, Cannon SH (2004) Compilation of Post Wildfire Runoff-Event Data from the Western United States. US Geological Survey Open-file Report 04-1085.

Gartner JE, Cannon SH, Santi PM, Dewolfe VG (2008) Empirical models to predict the volumes of debris flows generated by recently burned basins in the western U.S. Geomorphology 96:339-354

Gartner, JE, Cannon SH, Santi PM (2014) Empirical models for predicting volumes of sediment deposited by debris flows and sediment-laden floods in the Transverse Ranges of southern California. Engineering Geology 176:45-56

Goddard, L., Mason, S.J., Zebiak, S.E., Ropelewski, C.F., Basher, R. and Cane, M.A. (2001), Current approaches to seasonal to interannual climate predictions. Int. J. Climatol., 21: 1111–1152. doi:10.1002/joc.636

Godt, J. W., R. L. Baum, A. F. Chleborad, 2006: Rainfall characteristics for shallow landsliding in Seattle, Washington, USA. *Earth Surface Processes and Landforms*, **31**(1), 97-110.

Godt, J. W., Schulz, W. H., Baum, R. L., & Savage, W. Z. (2008). Modeling rainfall conditions for shallow landsliding in Seattle, Washington. *Reviews in Engineering Geology*, *20*, 137-152.

Goleta Water District (2017). Lake Cachuma: Our biggest water supply source. Accessed online 12 August 2017. http://www.goletawater.com/water-supply/lake-cachuma

Griffith, D. A., Solak, M. E., Almy, R. B., & Gibbs, D. (2005). The Santa Barbara Cloud Seeding Project in Coastal Southern California, Summary of Results and Their Implications. *The Journal of Weather Modification*, *37*(1), 21-27.

Gutierrez, C., W. Bryant, G. Saucedo, C. Wills, 2010: Geologic Map of California. *California Geologic Data Map Series Map No. 2*, scale 1:750,000, California Department of Conservation. Accessed 8 March 2017, http://www.conservation.ca.gov/cgs/cgs_history/PublishingImages/GMC_750k_MapRelease_page.jpg

Guzzetti F., S. Peruccacci, M. Rossi, C. P. Stark, 2007: Rainfall thresholds for the initiation of landslides in central and southern Europe. *Meteorology and Atmospheric Physics*, ***98***(3-4), 239-267.

Guzzetti F, Peruccacci S, Rossi M, Stark CP (2008) The rainfall intensity–duration control of shallow landslides and debris flows: an update. Landslides 5(1):3-17

Hales Jr, J. E. (1985). Synoptic features associated with Los Angeles tornado occurrences. *Bulletin of the American Meteorological Society*, 657-662.

Hansch, S., L. Locklin, C. Willis, L. Ewing, 1998: Coastal Impacts of the 1997-98 El Nino and Predictions for La Nina. California Coastal Commission report to Coastal Commissioners and Interested Parties File Tu-11. Accessed 8 March 2017, https://documents.coastal.ca.gov/reports/1998/9/T11-9-1998.pdf

Harris, H. (2017). Oakland: Landslides leave hills homes in peril. 7 April 2017. Accessed online: https://www.eastbaytimes.com/2017/04/07/landslide-leaves-six-oakland-hills-homes-in-peril/

Haynes, A. (2001). Synoptic pattern typing for historical heavy precipitation events in southern California. NOAA NWS Western Region Technical Attachment No. 01-15. Accessed online 12 October 2016 https://www.weather.gov/wrh/wrh_ta

Hendy, I. L., Napier, T. J., & Schimmelmann, A. (2015). From extreme rainfall to drought: 250 years of annually resolved sediment deposition in Santa Barbara Basin, California. *Quaternary International*, *387*, 3-12.

Herhold, S. (2017). Highway 17's treacherous bargain. *San Jose Mercury News.* 18 February 2017. Accessed online: https://www.mercurynews.com/2017/02/18/herhold-highway-17s-treacherous-bargain/

Hobbs PV (1978) Organization and structure of clouds and precipitation on the mesoscale and microscale in cyclonic storms. Reviews of Geophysics 16(4):741-755

Hobbs PV, Persson POG (1982). The mesoscale and microscale structure and organization of clouds and precipitation in midlatitude cyclones. Part V: The substructure of narrow cold-frontal rainbands. Journal of the Atmospheric Sciences 39(2):280-295

Hoell, A., Hoerling, M., Eischeid, J., Wolter, K., Dole, R., Perlwitz, J., and coauthors. (2016). Does El Niño intensity matter for California precipitation? *Geophysical Research Letters*, *43*(2), 819-825.

Hughes M, Hall A, Fovell RG (2009). Blocking in areas of complex topography, and its influence on rainfall distribution. Journal of the Atmospheric Sciences 66(2):508-518

Hughes M*,* Neiman PJ*,* Sukovich E, Ralph M *(*2012*)* Representation of the Sierra Barrier Jet in 11 years of a high-resolution dynamical reanalysis downscaling compared with long-term wind profiler observations*.* J. Geophys. Res. 117 *D18116, doi:*10.1029/2012JD017869

Inman, D. L., & Jenkins, S. A. (1999). Climate change and the episodicity of sediment flux of small California rivers. *The Journal of Geology*, *107*(3), 251-270.

Irvine, P.J., 1996: Debris flows resulting from January 1995 rainstorms. *California Geology.* **49** (5) 129-134.

Iverson, R. M., 2000: Landslide triggering by rain infiltration. *Water Resources Research*, *36*(7), 1897-1910.

Jakob, M. and O. Hungr, 2005: *Debris-flow Hazards and Related Phenomena*, Springer, Berlin.

Jennings, A. H., 1963: Maximum recorded United States point rainfall for 5 minutes to 24 hours at 296 first order stations, *Technical Paper No. 2*., U.S. Department of Commerce, Washington D.C.

Jibson, R. W. (2006). The 2005 La Conchita, California, landslide. *Landslides*, *3*(1), 73-78.

Jorgensen DP, Pu Z, Persson POG, Tao WK (2003) Variations associated with cores and gaps of a Pacific narrow cold frontal rainband. Monthly Weather Review 131(11):2705-2729

Jorgensen DP, Hanshaw MN, Schmidt KM, Laber JL, Staley DM, Kean JW, Restrepo PJ (2011). Value of a dual-polarized gap-filling radar in support of southern California post-fire debris-flow warnings. Journal of Hydrometeorology. 12 (6):1581-95.

Kalnay E, Kanamitsu M, Kistler R, Collins W, Deaven D, Gandin L, and authors (1996) The NCEP/NCAR 40-year reanalysis project. Bulletin of the American Meteorological Society 77(3):437-471

Kean JW, Staley DM, Cannon SH (2011) In situ measurements of post-fire debris flows in southern California: Comparisons of the timing and magnitude of 24 debris-flow events with rainfall and soil moisture conditions. Journal of Geophysical Research: Earth Surface 116(F4)

Keeley JE, Fotheringham CJ, Moritz MA (2004) Lessons from the October 2003 wildfires in southern California. Journal of Forestry 102(7):26-31

Keeley, J. E., Fotheringham, C. J., Baer-Keeley, M. (2005). Determinants of post-fire recovery and succession in Mediterranean-climate shrublands of California. *Ecological Applications*, 15: 1515–1534. doi:10.1890/04-1005

Kim, D., B. Nelson, D. J. Seo, 2009: Characteristics of reprocessed Hydrometeorological Automated Data System (HADS) hourly precipitation data. *Weather and Forecasting*, **24**(5), 1287-1296.

Kondragunta, C. R., K. Shrestha, 2006: Automated real-time operational rain gauge quality-control tools in NWS hydrologic operations. In *Proc. 20th American Meteorological Society Conf. on Hydrology*, Vol. 29, Atlanta, GA.

Lamjiri, M. A., M. D. Dettinger, F. M. Ralph, B. Guan, 2017: Hourly storm characteristics along the U.S. West Coast: Role of atmospheric rivers in extreme precipitation, *Geophys. Res. Lett.,* 44, *7020-7028, doi:*10.1002/2017GL074193.

Larsen, M. C., and A. Simon, 1993: A rainfall intensity-duration threshold for landslides in a humid-tropical environment, Puerto Rico. *Geografiska Annaler,* Series A. Physical Geography, 13-23.

Latousek, T. (1995). Cachuma Project. *Bureau of Reclamation.* Accessed online 27 December 2017 at https://www.usbr.gov/projects/pdf.php?id=91

Lavers DA, Waliser DE, Ralph FM, Dettinger MD (2016) Predictability of horizontal water vapor transport relative to precipitation: Enhancing situational awareness for forecasting Western US extreme precipitation and flooding. Geophysical Research Letters 43(5):2275-2282

Lin YL, Chiao S, Wang TA, Kaplan ML, Weglarz RP (2001) Some common ingredients for heavy orographic rainfall. Weather and forecasting 16(6):633-660

Loáiciga, H. (2001). History of water in Santa Barbara, California. *Pacifica, Association of Pacific Coast Geographers.* Accessed online 10 October 2017 http://apcgweb.org/sites/default/files/editor_uploads/files/pacificas01.pdf

Los Angeles Times Blog, Groves M (2009) 06 February 2009 Mud mucks up streets in Sylmar. http://latimesblogs.latimes.com/.m/lanow/2009/02/mud-flow-mucks.html. Accessed 6 January 2016.

Los Angeles Times, Lin II RG, Kim V, Vives R (2010) 07 February 2010: Niagara of mud hits homes. http://articles.latimes.com/2010/feb/07/local/la-me-rain7-2010feb07. Accessed 20 January 2016

Lundquist, J.D., P.J. Neiman, B. Martner, A.B. White, D.J. Gottas, F.M. Ralph, 2008: Rain versus snow in the Sierra Nevada, California: Comparing Doppler profiling radar and surface observations of melting level. *J. Hydrometeor.,* **9**, 194–211, doi: https://doi.org/10.1175/2007JHM853.1.

Lundquist, J.D., J.R. Minder, P.J. Neiman, E. Sukovich, 2010: Relationships between barrier jet heights, orographic precipitation gradients, and streamflow in the northern Sierra Nevada. *J. Hydrometeor.,* **11**, 1141–1156, https://doi.org/10.1175/2010JHM1264.1

MacDonald NJ (1976) On the apparent relationship between convective activity and the shape of 500 mb troughs. Monthly Weather Review 104(12):1618-1622

Marshall JS, Palmer WMK (1948) The distribution of raindrops with size. Journal of Meteorology 5(4):165-166.

Menne, M. J., Durre, I., Vose, R. S., Gleason, B. E., & Houston, T. G. (2012). An overview of the global historical climatology network-daily database. *Journal of Atmospheric and Oceanic Technology*, *29*(7), 897-910.

Mesinger F, DiMego G, Kalnay E, Mitchell K, Shafran PC, Ebisuzaki W, and authors (2006) North American regional reanalysis. Bulletin of the American Meteorological Society 87(3):343-360

Modrick, T. M., K. P. Georgakakos, 2015: The character and causes of flash flood occurrence changes in mountainous small basins of Southern California under projected climatic change. *Journal of Hydrology: Regional Studies*, *3*, 312-336.

Montecito Water District (2017). History and Background. Accessed online 27 December 2017. http://www.montecitowater.com/general.htm

Monteverdi JP (1995) Overview of the meteorology of rain events in California. California Extreme Precipitation Symposium proceedings. http://cepsym.org/Sympro1995/monteverdi.pdf. Accessed 14 March 2016

Moody JA, Shakesby RA, Robichaud PR, Cannon SH, Martin DA (2013) Current research issues related to post-wildfire runoff and erosion processes. Earth Science Reviews 122:10-37

Moore BJ, Neiman PJ, Ralph FM, Barthold F (2012) Physical processes associated with heavy flooding rainfall in Nashville, Tennessee and vicinity during 1-2 May 2010: The role of an atmospheric river and mesoscale convective systems. Monthly Weather Review, 140, 358-378.

Morton, D.M., R. M. Alvarez, and R. H. Campbell, 2003: Preliminary soil-slip susceptibility maps, southwestern California, *U.S. Geological Survey Open-File Report* 03-17, pp. 14. Accessed 8 March 2017, https://pubs.usgs.gov/of/2003/0017/

Myrick, D. T. and J. D. Horel, 2008: Sensitivity of surface analyses over the western United States to RAWS observations. *Weather and Forecasting*, **23**(1), 145-158.

NASA Earth Observatory (2003). Fires in southern California. http://earthobservatory.nasa.gov/NaturalHazards/view.php?id=12373&eocn=image&eoci=morenh Accessed 1 May 2016

National Centers for Environmental Information (2016) Radar Data Map, National Reflectivity Mosaic. https://gis.ncdc.noaa.gov/maps/ncei/radar. Accessed 20 January 2016

National Research Council (NRC), 2004: *Partnerships for reducing landslide risk—assessment of the national landslide hazards mitigation strategy*, National Academies Press, Washington, D.C.

Neary DG, Klopatek CC, DeBano LF, Folliott PF (1999) Fire effects on belowground sustainability: a review and synthesis. Journal of Forest and Ecological Management 122:51–71

Neiman PJ, Ralph FM, White AB, Kingsmill DE, Persson POG (2002) The statistical relationship between upslope flow and rainfall in California's coastal mountains: Observations during CALJET. Monthly Weather Review 130(6): 1468-1492.

Neiman PJ, Ralph FM, Persson POG, White AB, Jorgensen DP, Kingsmill DE (2004) Modification of fronts and precipitation by coastal blocking during an intense landfalling winter storm in southern California: Observations during CALJET. Monthly Weather Review 132(1):242-273

Neiman PJ, Ralph FM, Wick GA, Lundquist JD, Dettinger MD (2008) Meteorological characteristics and overland precipitation impacts of atmospheric rivers affecting the West Coast of North America based on eight years of SSM/I satellite observations. Journal of Hydrometeorology 9(1): 22-47

NOAA Earth System Research Laboratory (ESRL; 2016) NOAA ESRL GSD-MADIS CAP profiler real time data display. https://madis-data.noaa.gov/cap/profiler.jsp?view=swus. Accessed 10 January 2016

NOAA Hydrometeorological Design Studies Center (HDSC; 2017) NOAA Atlas 14 Point Precipitation Frequency Estimates. http://hdsc.nws.noaa.gov/hdsc/pfds/. Accessed 24 January 2017

NOAA-USGS Debris Flow Task Force (2005) NOAA-USGS debris-f low warning system: Final report. U.S. Geological Survey Circular 1283, 47 pp. http://pubs.usgs.gov/circ/2005/1283/pdf/Circular1283.pdf Accessed 20 August 2016

Null, J. (1990). Some thoughts on drought, precipitation climatology, and methodology. NOAA NWS Western Region Technical Attachment No. 90-11. Accessed online 12 October 2017 at https://www.weather.gov/wrh/wrh_ta

Null J (2018) El Nino and La Nina years and intensities based on Oceanic Niño index (ONI). Accessed online 8 November 2017 at http://ggweather.com/enso/oni.htm

Oakley NS, Redmond KT (2014) A climatology of 500-hPa closed lows in the Northeastern Pacific Ocean, 1948–2011. Journal of Applied Meteorology and Climatology 53(6):1578-1592

Oakley, N. S., Lancaster, J. T., Kaplan, M. L., & Ralph, F. M. (2017). Synoptic conditions associated with cool season post-fire debris flows in the Transverse Ranges of southern California. *Natural Hazards*, *88*(1), 327-354. doi: 10.1007/s11069-017-2867-6.

O'Hara BF, Kaplan ML, Underwood SJ (2009) Synoptic climatological analyses of extreme snowfalls in the Sierra Nevada. Weather and Forecasting 24(6):1610-1624

Palecki, M. A., J. R. Angel, S. E. Hollinger, 2005: Storm precipitation in the United States. Part I: meteorological characteristics. *Journal of Applied Meteorology*, **44**(6), 933-946.

Papathoma-Köhle, M., A. Zischg, S. Fuchs, T. Glade, M. Keiler, 2015: Loss estimation for landslides in mountain areas – An integrated toolbox for vulnerability assessment and damage documentation. *Environmental Modelling & Software*. **63**, 156-169 https://doi.org/10.1016/j.envsoft.2014.10.003.

Paek, H., Yu, J. Y., & Qian, C. (2017). Why were the 2015/2016 and 1997/1998 extreme El Niños different? *Geophysical Research Letters*, *44*(4), 1848-1856.

Parise M, Cannon SH (2012) Wildfire impacts on the processes that generate debris flows in burned watersheds. Natural Hazards, 61(1):217-227

Perica, S., Dietz, S. Heim, S. and coauthors, 2014: *Precipitation frequency atlas of the United States Volume 6 Version 2.3: California*, US Department of Commerce, NOAA, Silver Spring Maryland.

Pierce, D. W., Cayan, D. R., Das, T., Maurer, E. P., Miller, N. L., Bao, Y., ... & Franco, G. (2013). The key role of heavy precipitation events in climate model disagreements of future annual precipitation changes in California. *Journal of Climate*, *26*(16), 5879-5896.

Plymouth State University (2016) Plymouth State Weather Center. http://vortex.plymouth.edu/. Accessed 12 March 2016

Polade, S. D., Pierce, D. W., Cayan, D. R., Gershunov, A., & Dettinger, M. D. (2014). The key role of dry days in changing regional climate and precipitation regimes. *Scientific Reports*, *4*, 4364.

Prein, A. F., R. M. Rasmussen, K. Ikeda, C. Liu, M. P. Clark, G. J. Holland, 2017: The future intensification of hourly precipitation extremes. *Nature Climate Change*, **7**(1), 48-52.

PRISM Climate Group, 2015: 30 Year Normals. Accessed 10 February 2017, http://prism.nacse.org/normals/

Radbruch, D. H. and Crowther, K.C. (1973). Map showing areas of estimated relative amounts of landslides in California. USGS Map I-747. Accessed online August 21 2016 at: http://pubs.usgs.gov/imap/0747/plate-1.pdf

Radbruch-Hall, D. Colton, R., Davies, W. and co-authors. (1982). USGS Open Fire Report 97-289 (1982) Digital compilation of landslide overview map of the conterminous United States. Accesssed Aug 16 2016 https://pubs.er.usgs.gov/publication/ofr97289

Ralph, F.M., P.J. Neiman, D.E. Kingsmill, P.O. Persson, A.B. White, E.T. Strem, E.D. Andrews, and R.C. Antweiler, 2003: The Impact of a Prominent Rain Shadow on Flooding in California's Santa Cruz Mountains: A CALJET Case Study and Sensitivity to the ENSO Cycle. *J. Hydrometeor,* **4**, 1243-1264, https://doi.org/10.1175/1525-7541(2003)004<1243:TIOAPR>2.0.CO;2

Ralph FM, Neiman PJ, Wick GA (2004) Satellite and CALJET aircraft observations of atmospheric rivers over the eastern North Pacific Ocean during the winter of 1997/98. Monthly Weather Review 132(7):1721-1745

Ralph FM, Neiman PJ, Rotunno R (2005) Dropsonde observations in low-level jets over the northeastern Pacific Ocean from CALJET-1998 and PACJET-2001: Mean vertical-profile and atmospheric-river characteristics. Monthly Weather Review 133(4):889-910

Ralph FM, Neiman, PJ, Wick GA, Gutman SI, Dettinger MD, Cayan DR, White AB (2006) Flooding on California's Russian River: Role of atmospheric rivers. Geophysical Research Letters 33(13)

Ralph FM, Dettinger MD (2012) Historical and national perspectives on extreme West Coast precipitation associated with atmospheric rivers during December 2010. Bulletin of the American Meteorological Society 93(6):783-790

Ralph, F. M., T. Coleman, P.J. Neiman, R. Zamora, and M.D. Dettinger (2013) Observed impacts of duration and seasonality of atmospheric-river landfalls on soil moisture and runoff in coastal northern California. *J. Hydrometeor.*, **14**, 443-459.

Ralph, F.M, K. A. Prather, D. Cayan, J.R. Spackman, P. DeMott, M. Dettinger, C. Fairall, R. Leung, D. Rosenfeld, S. Rutledge, D. Waliser, A. B. White, J. Cordeira, A. Martin, J. Helly, and J. Intrieri, (2016) CalWater Field Studies Designed to Quantify the Roles of Atmospheric Rivers and Aerosols in Modulating U.S. West Coast Precipitation in a Changing Climate. *Bull. Amer. Meteorol. Soc*. **97**, 1209–1228

Raphael MN (2003) The Santa Ana winds of California. Earth Interactions 7(8):1-13

Reid, M. E., 1997: Slope instability caused by small variations in hydraulic conductivity. *Journal of Geotechnical and Geoenvironmental Engineering*, **123**(8), 717-725.

Ricciardulli, L. and F. J. Wentz, 2016: Remote Sensing Systems ASCAT C-2015 Daily Ocean Vector Winds on 0.25 deg grid, Version 02.1, Remote Sensing Systems, Santa Rosa, CA. Accessed 15 July 2017, www.remss.com/missions/ascat

Rienecker, M. M., Suarez, M. J., Gelaro, R., Todling, R., Bacmeister, J., Liu, E., ... & Bloom, S. (2011). MERRA: NASA's modern-era retrospective analysis for research and applications. *Journal of climate*, *24*(14), 3624-3648.

Riggan PJ, Lockwood RN, Lopez EN (1985) Deposition and processing of airborne nitrogen pollutants in Mediterranean-type ecosystems of southern California. Environmental Science and Technology 19(9):781-789

Ritter, D. F., Kochel, R. C., & Miller, J. R. (1995). Process geomorphology. Wm. C. Brown Publishers, Dubuque, IA

Russo, T. A., A. T. Fisher, D. M. Winslow, 2013: Regional and local increases in storm intensity in the San Francisco Bay Area, USA, between 1890 and 2010, *J. Geophys. Res. Atmos.,* 118, 3392–3401, *doi:*10.1002/jgrd.50225.

Rutz JJ, Steenburgh WJ, Ralph FM (2014) Climatological characteristics of atmospheric rivers and their inland penetration over the western United States. Monthly Weather Review 142(2):905-921

Rutz, J. J., W. J. Steenburgh, F. M. Ralph, 2015: The inland penetration of atmospheric rivers over western North America: A Lagrangian analysis. *Monthly Weather Review*, **143**(5), 1924-1944.

San Bernardino Sun (1980a) 10 January 1980: Heavy rain causes havoc. https://www.newspapers.com/newspage/62887387/. Accessed 20 January 2016

San Bernardino Sun (1980b) 06 April 1980:The storms of winter: an overview. https://www.newspapers.com/newspage/62867758/. Accessed 20 January 2016

San Bernardino Sun (1980c) 29 January 1980: Mud threatens S.B. homes again https://www.newspapers.com/newspage/62881718/. Accessed 20 January 2016

San Bernardino Sun (1980d) 17 February 1980: Downpours force more evacuations. https://www.newspapers.com/newspage/62648829/. Accessed 20 January 2016

Santa Barbara County Public Works Department (SBCPWD; 2017). Rainfall and Reservoir Summary. Accessed online 10 November 10 2017 at http://www.countyofsb.org/uploadedFiles/pwd/Content/Water/Documents/rainfallreport.pdf

Santi, P. M., Higgins, J. D., Cannon, S. H., & Gartner, J. E. (2008). Sources of debris flow material in burned areas. *Geomorphology*, *96*(3), 310-321.

Santi, P. M., K. Hewitt, D. F. VanDine, E. Barillas Cruz, 2011: Debris-flow impact, vulnerability, and response. *Natural Hazards*, **56**(1), 371-402.

Santi PM, Morandi L (2012) Comparison of debris-flow volumes from burned and unburned areas. Landslides 10(6):757-769

Schleiss AJ, de Cesare G, Franca MJ, Pfister M (2014) Reservoir Sedimentation. CRC Press, London pp. 300

Serna, J. (2017). How a 'rain shadow' left this reservoir parched even after all those storms. *Los Angeles Times*. Accessed online 26 January 2017 at http://www.latimes.com/local/lanow/la-me-ln-lake-cachuma-rain-shadow-20170123-story.html

Shakesby RA, Moody JA, Martin DA, Robichaud PR (2016) Synthesising empirical results to improve predictions of post-wildfire runoff and erosion response. International Journal of Wildland Fire 25(3):257-261

Slosson JE, Havens GW, Shuirman G, Slosson TL (1991) Harrison Canyon debris flows of 1980. Environmental Geology and Water Sciences 18(1):27-38

Shuirman G, Slosson JE (1992) Forensic engineering: Environmental case histories for civil engineers and geologists. Academic Press.

Sidman, G., Guertin, D. P., Goodrich, D. C., Unkrich, C. L., & Burns, I. S. (2016). Risk assessment of post-wildfire hydrological response in semiarid basins: the effects of varying rainfall representations in the KINEROS2/AGWA model. *International Journal of Wildland Fire*, *25*(3), 268-278.

Small, IJ (1999) An observational study of a California Bight coastal convergence zone produced by flow interaction with mainland topography: precipitation producer in southern California. NOAA Technical Attachment No. 99-19. http://www.wrh.noaa.gov/media/wrh/online_publications/TAs/ta9919.pdf. Accessed 15 April 2016

Staley DM, Kean JW, Cannon SH, Schmidt KM, Laber JL (2013) Objective definition of rainfall intensity–duration thresholds for the initiation of post-fire debris flows in southern California. Landslides 10(5):547-562

Staley DM, Negri JA, Kean JW, Laber JL, Tillery AC, Youberg AM, (2016) Prediction of spatially explicit rainfall intensity-duration thresholds for post-fire debris-flow generation in the western Unites States: Geomophology 278(2017):149-162

Stock, J. D. and D. Bellugi, 2011: An empirical method to forecast the effect of storm intensity on shallow landslide abundance. *Italian Journal of Engineering Geology and Environment*, Casa Editrice Universita La Sapienza, 1013–1022, doi:10.4408/IJEGE.2011-03.B-110

Sukup SJ, Laber J, Sweet D, Thompson R (2016) Analysis of an Intense Narrow Cold Frontal Rainband and the Springs Fire Debris Flow of 12 December 2014. NWS. Technical Attachment 1601. http://www.wrh.noaa.gov/media/wrh/online_publications/TAs/TA1601.pdf. Accessed 15 January 2016

Tarleton LF, Kluck DR (1994) Analysis of major storms in southern California. California Extreme Precipitation Symposium proceedings. http://cepsym.org/Sympro1994/tarleton.pdf . Accessed 14 March 2016

Taylor DB (1982) Floodflows in Major Streams in Ventura County. In Brooks NH, ed., Storms, floods, and debris flows in southern California and Arizona 1978 and 1980: Proceedings of a Symposium, September 17-18, 1980. National Academy Press pp. 487

Troxell HC, Petersen JQ (1937) Flood in La Canada Valley, California January 1, 1934: U.S. Geological Survey Water-Supply Paper 796-C, pp. 98

United States Drought Monitor (2018). Time Series. Accessed online 3 October 2017 at http://droughtmonitor.unl.edu/Data/Timeseries.aspx

United States Geological Survey (2005) Southern California- wildfires and debris flows. USGS Fact Sheet 2005-3106. http://pubs.usgs.gov/fs/2005/3106/. Accessed 10 January 2016

Upson, J. E. and Thomas, Jr., H. G. (1951). Geology and water resources of the Santa Ynez River Basin, Santa Barbara County, California. *Geological Survey Water Supply Paper 1107*. United States Government Printing Office, Washington ,D.C. Accessed online 10 August 2017 https://pubs.usgs.gov/wsp/1107/report.pdf

URS Corporation (2005) Flood Mitigation Plan for Ventura County, California: URS Corporation. pp. 128 http://www.ventura.org/wcvc/documents/PDF/floodmitigationplan2005.pdf. Accessed 12 January 2016

Vose, R. S., S. Applequist, M. Squires, I. Durre, M. J. Menne, and coauthors, 2014: Improved historical temperature and precipitation time series for US climate divisions. *Journal of Applied Meteorology and Climatology*, **53**(5), 1232-1251.

Warrick, J. A., & Milliman, J. D. (2003). Hyperpycnal sediment discharge from semiarid southern California rivers: Implications for coastal sediment budgets. *Geology*, *31*(9), 781-784.

Weaver RL (1962) Meteorology of hydrologically critical storms in California. Hydrometeorological Report 37. US Dept. of Commerce

Wells WG II, (1981) Some effect of brushfires on erosion processes in coastal southern California. In: Davies TRH, Pearce AJ (Eds.), Erosion and Sediment Transport in Pacific Rim Steeplands, January 1981, Chirst Church, New Zealand. Sponsored jointly by the Royal Society of New Zealand, New Zealand Hydrological Society, IAHS, and the National Water and Soil Conservation Authority of New Zealand. International Association of Hydrologic Sciences Publication, vol. 132 pp. 305–342.

Wells II WG (1987) The effects of fire on the generation of debris flows in southern California, *in* Costa JE, Wieczorek GF, eds. Debris flows/avalanches - process, recognition, and mitigation: Geological Society of America, Reviews in Engineering Geology VII. pp. 105-114

Westerling, A. L., Cayan, D. R., Brown, T. J., Hall, B. L., & Riddle, L. G. (2004). Climate, Santa Ana winds and autumn wildfires in southern California. *Eos, Transactions American Geophysical Union*, *85*(31), 289-296.

Western Regional Climate Center (WRCC), 2017: Cooperative Climatological Data Summaries. Accessed 6 March 2017, https://wrcc.dri.edu/Climate/west_coop_summaries.php

White, A. B., P. J. Neiman, J. M. Creamean, T. Coleman, F. M. Ralph, K. A. Prather, 2015: The impacts of California's San Francisco Bay Area gap on precipitation observed in the Sierra Nevada during HMT and CalWater. *J. Hydrometeorology,* **16**, 1048–1069, doi: https://doi.org/10.1175/JHM-D-14-0160.1.

Wieczorek, G. F., 1987: Effect of rainfall intensity and duration on debris flows in central Santa Cruz Mountains, California. *Reviews in Engineering Geology*, **7**, 93-104.

Wieczorek, G. F., J. Sarmiento, 1988: Rainfall, piezometric levels, and debris flows near La Honda, California, in storms between 1975 and 1983, *in* Ellen, S. D. and Wieczorek, G. F., eds., Landslides, floods, and marine effects of the storm of January 3-5, 1982, in the San Francisco Bay region, California. *U.S. Geological Survey Professional Paper 1434*, p. 27-33.

Wieczorek, G. F., 2002: Catastrophic rockfalls and rockslides in the Sierra Nevada, USA. *Reviews in Engineering Geology*, **15**, 165-190.

Wills, C. J., F. G. Perez, C. I. Gutierrez, 2011: Susceptibility to deep-seated landslides in California. *California Geological Survey Map Sheet 58*. Accessed 10 February 2017, http://www.conservation.ca.gov/cgs/information/publications/ms/Documents/MS58.pdf

Wills, C.J., N. E. Roth, T. P. McCrink, W. R. Short, 2017: The California Landslide Inventory Database, *Proceedings for the 3rd North American Symposium on Landslides*, 666-674.

Wilson, R. C., and Wieczorek, G. F., 1995: Rainfall thresholds for the initiation of debris flows at La Honda, California. *Environmental & Engineering Geoscience*, **1**(1), 11-27.

Wilson, R. C., 1997a: Operation of a landslide warning system during the California storm sequence of January and February 1993. *Reviews in Engineering Geology*, **11**, 61-70.

Wilson, R. C., 1997b: Broad-scale climatic influences on rainfall thresholds for debris flows: adapting thresholds for northern California to southern California. *Reviews in Engineering Geology*, **11**, 71-80.

Wilson, R. C. and A. S. Jayko, 1997: Preliminary maps showing rainfall thresholds for debris-flow activity, San Francisco Bay Region, California, *No. 97-745-F*, US Dept. of the Interior, US Geological Survey.

Yates, N. (1993). The Water Picture: 1986-1993. *Los Angeles Times*. Accessed online 3 October 2017 at http://articles.latimes.com/1993-02-25/news/mn-776_1_water-picture

Young, A. M., K. T. Skelly, J. M Cordeira, 2017: High-impact hydrologic events and atmospheric rivers in California: An investigation using the NCEI Storm Events Database. *Geophysical Research Letters*, **44**(7), 3393-3401.

Zhu Y, Newell RE (1998) A proposed algorithm for moisture fluxes from atmospheric rivers. Monthly Weather Review. 126(3): 725-735

Zachariassen, J., K. F. Zeller, N. Nikolov, and T. McClelland, 2003: A review of the Forest Service Remote Automated Weather Station (RAWS) network**,** *Gen. Tech. Rep. RMRS-GTR-119.* U.S. Department of Agriculture, Forest Service, Rocky Mountain Research Station, Fort Collins, CO, pp. 153 + CD. Accessed 18 April 2017, https://www.fs.fed.us/rm/pubs/rmrs_gtr119

Appendix A

1	2	3	4	5	6	7	8
PFDF Date (LST) and burn area	NARR event time (LST)	Trough tilt	Avg 300 hPa wind dir., speed	300 hPa jet S of region?	Rainfall rate or range, mm h^{-1}	Approx. radar return (dBZ)	IVT kg m^{-1} s^{-1} p-tile
1980-01-09 Daley	1000 (18 UTC)	NEU	189° 25.3 ms^{-1}	Yes	5-13	NA	361 96th
1980-01-13 Daley	1900 (03 UTC 1/14)	NEU	260° 41.1 ms^{-1}	Over	5-13	NA	507.9 99th
1980-01-28 Daley	2200 (06 UTC)	POS	226° 24 ms^{-1}	No	3-13	NA	271 93rd
1980-02-16 Daley	1600 (00 UTC 2/17)	NEG	261° 37.8 ms^{-1}	Yes	5-23	NA	576 99th
1980-02-16 Creek Road	1000 (18 UTC)	NEG	246° 39.3 ms^{-1}	Yes	8-23	NA	451 98th
1984-12-19 San Dimas	1600 (00 UTC 12/20)	POS/ CL	230° 57.4 ms^{-1}	Yes	12-13	NA	222 87th
1995-01-10 Steckel	0400 (12 UTC)	NEU/ CL	244° 41.6 ms^{-1}	Yes	17-32	>50	705 99th
1998-02-02 Grand	04:00 (12 UTC)	NEG	265° 48.9 ms^{-1}	Over	9-15	>50	409 99th
1998-02-06 Hopper/ Grand	1000 (18 UTC)	NEG	229° 57.4 ms^{-1}	Yes	14-19	>60	637 99th
2003-12-25 Simi	1300 (21 UTC)	NEU	256° 57.9 ms^{-1}	Over	6-14	>50	551 99th
2003-12-25 Grand Prix/Old	1000 (18 UTC)	NEU	260° 51.1 ms^{-1}	Over	5-33	>50	534 99th
2009-02-05 Sayre	1900 (03 UTC 2/6)	NEU	265° 35.8 ms^{-1}	Yes	5-13	>60	251 92nd
2009-02-13 Sayre	1300 (21 UTC)	NEG/ CL	263° 47.8 ms^{-1}	Over	2-6	>50	277 90th
2009-02-16 Sayre	0700 (15 UTC)	NEU	222° 58.3 ms^{-1}	Yes	5-8	>50	357 94th
2009-11-12 Station	2200 (06 UTC 11/13)	POS	236° 44.1 ms^{-1}	Yes	0-4	>60	165 74th
2009-12-12 Station	1600 (00 UTC 12/13)	POS	277° 53.2 ms^{-1}	Over	5-7	>50	433 99th
2010-01-18 Station	1000 (18 UTC)	NEG	257° 41.5 ms^{-1}	Yes	6-15	>50	413 96th
2010-02-06 Station	0400 (12 UTC)	NEG	243° 33.5 ms^{-1}	Yes	6-26	>60	221 88th
2010-02-27 Station	0700 (15 UTC)	NEU	228° 34 ms^{-1}	Yes	6-9	>50	331 95th
2014-10-31 Springs	2200 (06 UTC 11/1)	NEU	226° 55.8 ms^{-1}	Yes	7-13	>60	257 94th
2014-12-12 Springs	0100 (09 UTC)	NEG	216° 49.5 ms^{-1}	Yes	15-24* *15 min	>60	709 99th

1	9	10	11	12	13	14	15
PFDF Date (LST) and burn area	IWV mm p-tile	Event type	Stability	Max CAPE J kg^{-1} p-tile	VBG CAPE J kg^{-1}	Avg 925 hPa wind dir., speed	Low level jet?
1980-01-09 Daley	32.1 98th	AR	NEU	20 75th	79	194° 5.3 ms^{-1}	NA
1980-01-13 Daley	39.1 99th	AR	NEU	80 85th	110	230° 5.2 ms^{-1}	NA
1980-01-28 Daley	26.1 94th	OTH	WUN	90 80th	8	219° 3.6 ms^{-1}	NA
1980-02-16 Daley	37.1 99th	AR	NEU	30 65th	463	180° 9.2 ms^{-1}	NA
1980-02-16 Creek Road	32.6 98th	AR	NEU	10 50th	463	148° 10.7 ms^{-1}	NA
1984-12-19 San Dimas	16.6 67th	CL	WUN	220 92nd	52	183° 7.9 ms^{-1}	NA
1995-01-10 Steckel	31.8 98th	ARCL	WUN	50 94th	40	196° 14.6 ms^{-1}	NA
1998-02-02 Grand	32.6 99th	AR	NEU	100 84th	15	129° 7.7 ms^{-1}	NA
1998-02-06 Hopper/ Grand	28.7 97th	AR NCFR	NEU	470 97th	158	161° 15.2 ms^{-1}	NA
2003-12-25 Simi	28.8 96th	AR	UN-NEU	120 88th	18	213° 8.3 ms^{-1}	NA
2003-12-25 Grand Prix/Old	29.7 97th	AR	UN-NEU	70 82nd	18	211° 8.4 ms^{-1}	NA
2009-02-05 Sayre	25.4 92nd	OTH NCFR	NEU	80 82nd	84	203° 4.2 ms^{-1}	Y
2009-02-13 Sayre	18.5 68th	ARCL NCFR	UN-NEU	170 90th	18	202° 8.2 ms^{-1}	Y
2009-02-16 Sayre	22.9 84th	ARCL	NEU	280 93rd	0	165° 10.8 ms^{-1}	Y
2009-11-12 Station	21.1 74th	OTH	UN-NEU	210 93rd	10	235° 3.9 ms^{-1}	N
2009-12-12 Station	26.4 95th	AR	NEU	150 88th	212	188° 10.5 ms^{-1}	Y
2010-01-18 Station	27 94th	AR	UN-NEU	30 76th	20	159° 10.4 ms^{-1}	Y
2010-02-06 Station	25.4 92nd	OTH	UN-NEU	30 68th	1	160° 4.1 ms^{-1}	N
2010-02-27 Station	25.0 94th	ARCL NCFR	NEU	270 89th	75	192° 7.5 ms^{-1}	Y
2014-10-31 Springs	28.5 94th	OTH	UN-NEU	1330 99th	135	238° 6.2 ms^{-1}	N
2014-12-12 Springs	36.1 99th	AR NCFR	UN-NEU	520 97th	3	192° 15.6 ms^{-1}	Y

Table A1: Summary of characteristics of each PFDF event. Values from NARR data were taken at the NARR event time. *Column 1* provides date and burn area in which the debris flow occurred.
Column 2 provides the NARR time assigned to the event in both LST and UTC time.
Column 3 describes the tilt of the synoptic scale trough associated with the event, either positive (axis northeast to southwest), negative (axis northwest to southeast, or neutral (axis north-south). Several events have an embedded closed low but parent trough still has a sense of orientation.
Column 4 gives the average 300 hPa wind speed and direction among 12 NARR gridpoints overlying the burn area.
Column 5 describes the position of the main 300 hPa jet relative to the Transverse Range area.
Column 6 provides range of hourly rainfall rates associated with the event.
Column 7 provides approximate radar returns associated with events for which radar was available (NA indicates unavailable). *Column 8* gives the maximum integrated water vapor transport (IVT) value among 12 NARR gridpoints overlying the burn area and the percentile of this value.
Column 9 gives the maximum integrated water vapor (IWV) value among 12 NARR gridpoints overlying the burn area and the percentile of this value.
Column 10 advises whether the event was an atmospheric river (AR), closed low (CL), or other (OTH), as well as if a narrow cold frontal rainband appears to be present in radar imagery (NCFR).
Column 11 describes whether the event had moist-neutral (NEU) stability, was unstable in low levels becoming moist-neutral (UN-NEU), or was weakly unstable to 700 hPa or higher (WUN).
Column 12 gives the maximum convective available potential energy (CAPE) value among 12 NARR gridpoints overlying the burn area and its percentile.
Column 13 gives the CAPE value from rawinsonde observations at Vandenberg at the time closest to PFDF event.
Column 14 gives the average 925 hPa wind speed and direction among 12 NARR gridpoints overlying the burn area.
Column 15 describes whether a low-level jet was identified in wind profiler data at the time of event (NA = not available)

Appendix B

This study utilizes data from the Remote Automated Weather Station (RAWS) network (Zachariassen et al., 2003; Brown et al., 2011), operated by the National Interagency Fire Center (NIFC) and its partners. To utilize the RAWS dataset, we performed quality control (QC) on the RAWS precipitation data with a goal of optimization; developing a QC method that minimizes bad precipitation values and maximizes valid values. Our method explores several QC approaches and compares the results of each to a set of "known" values to quantify performance. Results of the best performing QC method were used as the study dataset.

B1.1 RAWS network selection

The RAWS network was chosen for this analysis because its stations are situated in complex terrain- foothills and lower slopes of mountain ranges where landslides most often occur. RAWS augment areas that typically have sparse data in the mountainous regions of the West and fill in a mid-elevation gap observation gap that is not covered by other networks like the SNOwpack TELemetry network (high elevation), and the majority of mesonets that tend towards population centers or transportation corridors (Myrick and Horel, 2008).

Several factors may contribute to erroneous precipitation records at RAWS stations, including:

1. Tipping bucket gauges are not heated, therefore do not measure frozen precipitation well and are subject to freezing (Daly et al., 2008; Vose et al., 2014).
2. Frozen precipitation collects on gauges and melts when temperatures increase, registering erroneous hourly measurements; however, these values that are typically smaller in magnitude than the thresholds pertinent to this study.
3. Local RAWS owners/operators may enter accumulated precipitation from a period of missing data as an hourly value, resulting in an erroneous hourly precipitation record (G. McCurdy, *personal communication,* 18 November 2017).
4. Wire exposure/malfunction may cause one or a series of incorrect precipitation observations, as will transmission or data coding errors (G. McCurdy, *personal communication,* 18 November 2017).

Data for 455 RAWS stations in California were obtained from the Western Regional Climate Center (WRCC; http://raws.dri.edu). QC for the gauge operational limits had been applied prior to our acquisition of the data. The following QC methods work to remove issues associated with the errors described above.

B1.2 Development of a "truth" dataset to evaluate QC methods

To quantify the performance of each QC attempt, a "truth" dataset was developed, with the term "truth" indicating that values had been examined through

various means and documented as "valid" (should appear in the final QC dataset) or "bad" (should not appear in the final QC dataset).

The "truth" dataset consists of precipitation values ≥25 mm h^{-1}. We focus on this subset of observations for several reasons. 1) In explorations of the data, values that clearly stood out as being erroneous (e.g., a single hour of precipitation in the cool season on a day when there was otherwise no precipitation) were generally ≥25 mm h^{-1}. These errors were typically associated with error types 3 or 4 above. 2) When using radar imagery to validate precipitation, it is more feasible to validate the presence or lack of very high intensity rainfall than moderate or light rainfall due to a stronger signal. 3) Values ≥25 mm h^{-1} are relevant to all four landslide-triggering thresholds assessed.

The validity of precipitation values in the "truth" dataset was determined using archive radar imagery from the National Centers for Environmental Information (https://gis.ncdc.noaa.gov/maps/ncei/radar) and data from other fields (solar radiation, relative humidity) from the RAWS station in question as well as neighboring stations within both within and outside the RAWS network, obtained from WRCC (https://wrcc.dri.edu/). If these various resources indicated that it was likely that a particular value occurred, that value was considered "valid". If the sources consulted suggested the value was unlikely (e.g., no radar returns on the specified date/time, other instruments on the station and surrounding stations show no precipitation, low relative humidity, or lack cloudiness) then the value is considered "bad." There are inherent limitations in the development of the "truth"

dataset, though it provides a qualitative means to evaluate QC methods, which offers a great benefit.

The resultant "truth" dataset consists of 62 "valid" and 62 "bad" values (total of 124 values) for the period 1995-2016. The results comparing each QC trial to the "truth" dataset are described in Table S1 and Figure S1.

B1.3. Quality control process

The method used to QC RAWS precipitation data follows the framework of a four-level process for rain gauge quality control proposed by Kondragunta and Shrestha (2006) and applied by Kim et al. (2009) in reprocessing of Hydrometeorological Automated Data System (HADS) hourly precipitation data.

Level 1 QC: Performed on a single observation and include transmission or coding errors, or meaningless values like negative precipitation (Kondragunta and Shrestha, 2006).

In this step, we calculate incremental values from the native accumulating values. If two consecutive data points are not consecutive hours, the incremental value is set as missing and the check begins at the next value. This step also looks for station resets to 0 or negative accumulations, which are set to incremental values of missing for the hour in which they occurred.

Level 2 QC: Performed on a single observation and checked against some boundaries for validity; referred to as a climatological range check by Kondragunta and Shrestha (2006).

2a. At this level, we first remove all values >130 mm h^{-1}. This is based on the greatest 1000-year return intervals for hourly precipitation in California according to the NOAA Atlas 14 (Perica et al., 2014) and exceeds all maximum hourly values at first order California stations presented in Jennings (1963). This check helps address errors associated with challenges 3 and 4 given above.

2b. As a secondary Level 2 QC check, we tested removing cases where the incremental precipitation value was ≥25 mm h^{-1} and no precipitation was observed in the prior or following hour for the September-May season. This check was introduced to help remove erroneous isolated values of high precipitation such as those introduced by error types 2 and 3 above. We tested this check all year versus September-May only, (S1) and found the most favorable results using September-May only. We reason this check performs best during the cool-season as this is when synoptic-scale storms are most prevalent in California and it is unlikely that a burst of rain confined to a single hour would occur in these storms. In contrast, high intensity and very localized thunderstorms are possible in many areas of California in the summertime. This check, though not ideal as there are valid meteorological events that violate this criteria, serves to remove many invalid data points

associated with error types 3 and 4 that proved difficult to remove by other means.

Level 3 QC: This level includes more advanced checks including a spatial consistency check ("buddy check") and a multi-sensor check (Kondragunta and Shrestha, 2006).

At this level, we implement a "buddy check" to address errors from challenges 2 and 4, and to a lesser extent, type 2. All stations within a 0.5-degree box around the station are examined as "buddies." This resulted in an average of 13 buddies per station. The buddy check was conducted on all values ≥5 mm h^{-1}, the minimum hourly value of interest to this project. We tested variants of applying the buddy check to the various parts of the season and also whether better results were achieved looking for a buddy with >0 precipitation or a buddy with >10% of the observed value at the station in question (Table S1). The best performing option was performing a buddy check all year where a buddy must have at least 10% of what was observed at the station in question.

To validate a station's observation, at least 1 buddy had to meet the precipitation value criteria within ±2 h of the observed time. For a value to be considered "bad", a station had to have at least 3 buddies reporting <10% when the station in question reported ≥5 mm h^{-1}. Therefore, a station with less than 3 buddies reporting at that time would not be subject to this check.

Sensitivity tests revealed that requiring only 1-2 buddies was too lax (in some cases, a nearby station was reporting erroneously as well) allowed and requiring >3 buddies left many values/stations not evaluated due to the lack of nearby stations. Of the 455 stations examined, only 19 had <3 buddies.

We found this check very beneficial for removing erroneous cool season values, but due to the isolated nature of summertime thunderstorms, the buddy check removed some valid values in the summertime. However, we do not utilize the summer season in the final analysis.

Level 4 QC: Corrections at this level are based on human expert judgment such as knowledge of the gauge history or ancillary information on a particular weather event (Kondragunta and Shrestha, 2006).

At level 4, we have now performed QC on the full year for all stations. For the purpose of investigating precipitation intensities that may trigger shallow landslides, we create a subset of stations at this QC level.

We maintain all stations that have >80% of data for the October-May period across the 22-year period 1995-2016, resulting in 166 stations across California. Setting the threshold of missing data at 80-85% is common practice in climatological analyses (Daly et al., 2008; Abatzoglou, 2013; Perica et al., 2014). We also remove all stations at an elevation of ≤1700 m. This is intended to remove stations that are typically situated above the

approximate climatological median snow level in the Sierra. This reduces the final station count to 147.

Lastly, all values where the temperature is ≤ 0°C are removed to account for RAWS data challenge 1 stated above. There is uncertainty and variability around the temperature at which frozen precipitation occurs (e.g., Lundquist et al., 2008) and we cannot ensure the station temperature sensor is functioning correctly. However, we present this check as a rough approximation to eliminate erroneous values associated with frozen precipitation.

The best performing QC method (that which maximized exclusion of bad values while minimizing exclusion of valid values) was Round 9 (14.5% valid excluded, 17.7% bad included; Table S1 and Figure S1). While the amount of error is not ideal, it shows a marked improvement from Round 1 where nearly all of the bad values were accepted. For the October-May period only, when resultant data were compared to the "truth" dataset values for that date range, no valid values were excluded (0/30) and 20% of bad values were included (8/40). Following the evaluation process, the "truth" values were inserted into or removed from the final dataset.

B1.4. Summary of selected QC approach

The selected QC process (Round 9) had the following checks applied, as shown in Table S1:

- Remove station resets, negative accumulations, transmission errors
- Remove values >130 mm h^{-1}
- For Sept-May, remove all cases where ≥25 mm h^{-1} and no precipitation in preceding or following hour
- Throughout the year, perform buddy check and require at least 1 buddy to have >10% of precipitation value in question
- Retain stations with >80% of Oct-May data, remove stations with elevation >1700 m, and remove precipitation when temperature < 0°C

B1.5. Discussion and limitations

We present an approach to QC RAWS precipitation data, using a set of validated extreme (≥ 25 mm h^{-1}) observations as a "known" dataset for comparison. This approach, like any QC approach, results in some subset of true precipitation at a location and has error associated with it. There are several limitations to this approach to be considered, however we find the resulting analysis to capture the spatial and temporal patterns of precipitation exceeding various thresholds that we would expect from previous literature. The limitations and our rationale for accepting them are as follows:

1. RAWS do not have wind shields and are typically located in exposed areas. In this study, we do not account for gauge undercatch due to wind (Duchon and

Biddle, 2010) or due to lack of a shield (Duchon and Essenburg, 2001). Winds over 5 to 6 m s^{-1} can produce undercatch on the order of 6%, and correcting for these errors can be very problematic (Duchon and Biddle, 2010). Undercatch associated with unshielded tipping bucket gauges was 4% relative to a tipping bucket pit gauge (Duchon and Essenburg, 2001). This study focuses on frequency of over-threshold precipitation events rather than precise magnitude of the events. This may cause frequency of events to be biased low.

2. RAWS are unheated and any snow that collects on the gauge will melt and run through the gauge when temperatures warm. While it is unlikely that the melt-off of will exceed the precipitation thresholds evaluated in this study, it may be possible and can potentially introduce an invalid value into the dataset in areas that experience snowfall. Removal of stations >1700 m and the "buddy check" helps to reduce these instances, but cannot control all of them.
3. The "known" dataset consists of a small sample population within the data. The samples chosen may influence the outcome of proportions of valid excluded and bad included and thus the chosen QC method. It was not feasible to manually check all values in the dataset, so we had to accept this limitation.
4. There are hourly precipitation datasets available for California beyond the RAWS. We chose to focus research efforts on QC and implementation of one

network (RAWS) that had stations in the most favorable locations. Future work could incorporate more datasets to both validate RAWS observations and increase spatial density of precipitation data.

5. We do not recommend use of this dataset for the evaluation of climatological precipitation. QC is applied with a focus on verifying extremes and, with the many errors removed in this dataset as well as missing values, we do not believe it accurately represents precipitation over climatological periods (daily, monthly summaries) and is best utilized for event-based examinations, particularly hourly extremes.
6. This QC method does not remove errors in the warm season (June-August) well and thus may not be not suitable for analysis during this period. As described above it was extremely challenging to remove temporally and spatially isolated erroneous precipitation events while preserving similarly isolated valid events.

QC Round	+/- 1 h		Buddy Check				% Valid Excluded	% Bad Included
	All year	Sep-May	All year	Nov-Apr	>0	>10%		
1							0%	98%
2	X			X	X		8.1%	30.7%
3	X		X		X		14.5%	24.2%
4	X		X			X	19.4%	14.5%
5	X			X		X	8.1 %	24.2%
6			X		X		8.1%	53.2%
7			X			X	14.5%	30.7 %
8				X	X		0%	85.5%
9		**X**	**X**			**X**	**14.5%**	**17.7%**
10		X	X		X		8.1 %	29 %
11		X		Sep-May X		X	1.6%	41.9%

Table B1. Quality control (QC) trials and their outcomes as compared to a "truth" dataset. The selected QC method is shown in bold. Each column is as follows:

+/- 1 h: If the observed precipitation value was ≥ 25 mm h^{-1}, requires precipitation in hour prior or following. This column indicates if this check was applied to the whole year, Sep-May only, or not at all.

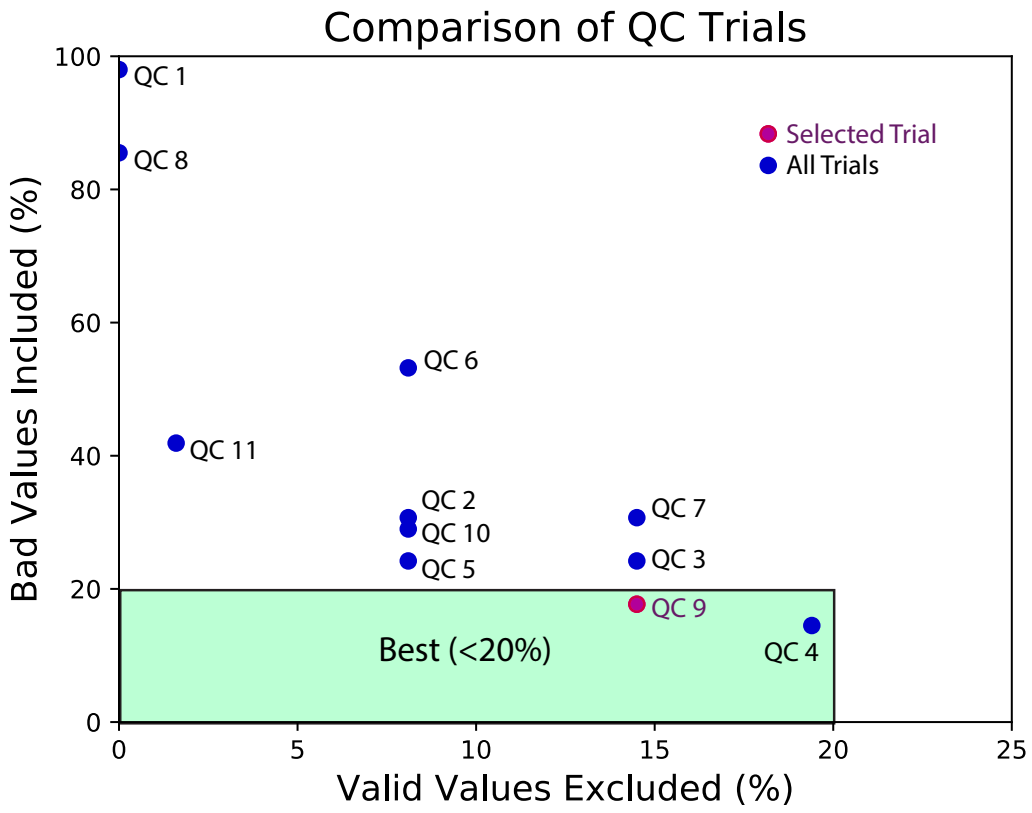

Figure B1. Comparison of QC trials and their performance with respect to excluding bad values and including valid values from the "truth" dataset. The best performing trials were Round 4 and Round 9. Round 9 was selected as the final QC method for its better performance at incorporating valid values in the known dataset.